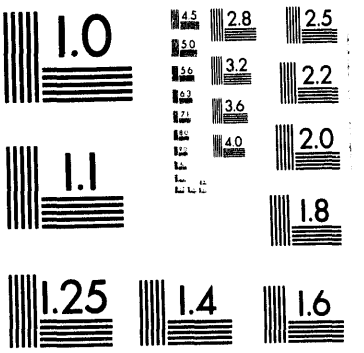
1.0
1.1
1.25
1.4
1.6
1.8
2.0
2.2
2.5
2.8
3.2
3.6
4.0
4.5
5.0
5.6
6.3
7.1

1 of 1

Distribution
Category UC-610

SAND93-3808
Unlimited Release
Printed January 1994

Air Ingression Calculations for Selected Plant Transients using MELCOR

L. N. Kmetyk
Thermal/Hydraulic Analysis Department
Sandia National Laboratories
Albuquerque, NM 87185-5800

Abstract

Two sets of MELCOR calculations have been completed studying the effects of air ingression on the consequences of various severe accident scenarios. One set of calculations analyzed a station blackout with surge line failure prior to vessel breach, starting from nominal operating conditions; the other set of calculations analyzed a station blackout occurring during shutdown (refueling) conditions. Both sets of analyses were for the Surry plant, a three-loop Westinghouse PWR. For both accident scenarios, a basecase calculation was done, and then repeated with air ingression from containment into the core region following core degradation and vessel failure.

In addition to the two sets of analyses done for this program, a similar air-ingression sensitivity study was done as part of a low-power/shutdown PRA, with results summarized here; that PRA study also analyzed a station blackout occurring during shutdown (refueling) conditions, but for the Grand Gulf plant, a BWR/6 with Mark III containment.

These studies help quantify the amount of air that would have to enter the core region to have a significant impact on the severe accident scenario, and demonstrate that one effect of air ingression is substantial enhancement of ruthenium release. These calculations also show that, while the core clad temperatures rise more quickly due to oxidation with air rather than steam, the core also degrades and relocates more quickly, so that no sustained, enhanced core heatup is predicted to occur with air ingression.

Contents

List of Figures

List of Tables

1 Introduction

Most modelling of core degradation during severe nuclear reactor accidents has considered only steam oxidation of metals (Zircaloy, stainless steel and Inconel) in the core. There are, however, opportunities for air also to enter the core and oxidize metals. Air oxidation is quite clearly possible in accidents under shutdown conditions when the reactor coolant system is open to the containment atmosphere. Air ingression into the reactor vessel also may occur during operational accidents once some portion of the degrading core penetrates the reactor vessel. A natural circulation of air through the reactor core can develop if there are breaks in the reactor coolant system as well as the vessel. [1]

The effects of air on the course of core degradation have not been extensively studied. It is known that the air oxidation of zirconium cladding on the fuel obeys different kinetics than does steam oxidation [2]. The reaction of oxygen with zirconium yields about 85% more heat than does steam oxidation. Given the important role chemically-generated heat plays in the progression of core damage in an accident, the ingression of air might be expected to profoundly accelerate core degradation.

Canadian researchers [3, 4] and others [5] have shown that air can greatly enhance the release of radioactive ruthenium from fuel. In the absence of strong oxidants like air, ruthenium is usually predicted to be released to a very small ($\ll$1%) extent in reactor accidents [6, 7]. Experimental studies have shown that in air there is essentially quantitative, significant release of ruthenium from hot fuel. These experimental studies, however, have not considered competitive processes. Clad oxidation might consume oxygen from the air before it could react with the fuel. Or, clad oxidation could cause such rapid heating of the core that there would be little time for ruthenium release to take place before the core slumped into the lower plenum of the reactor vessel.

To explore the system-wide implications of air ingression during severe reactor accidents, two series of reactor accident calculations have been conducted using the MELCOR computer code [8]. These calculations have been of limited scope, to assess the magnitude of air ingression that would be necessary to produce any significant alteration of core degradation or radionuclide release. These calculations constitute initial steps toward the definition of experimental conditions that might be employed in the planned fifth test of the Phebus-FP program [9] which is to involve air ingression [10]. Because so little is known about air oxidation during severe reactor accidents, only limited modifications to the MELCOR code could be made to treat the effects of air ingression. The changes in reaction kinetics of air and Zircaloy, and the enhanced heat of Zircaloy-air reaction, were available in the standard MELCOR 1.8.2 code version. Modifications made for these calculations treated only the enhanced release of ruthenium from fuel in air; effects air could have on the release and transport characteristics of other radionuclides were not modelled for these initial calculations.

Section 2 briefly describes the models in the MELCOR code of particular application for these air-ingression analyses.

Section 3 presents results from a set of calculations studying the effect of various amounts of air ingression into the core region during core degradation, beginning immediately after vessel breach, in the Surry PWR for a station blackout accident under mid-loop operation (*i.e.*, plant operational states in which the reactor coolant system level is lowered to the mid-plane of the hot leg) during refueling outages at low-power and shutdown conditions. Section 4 gives results from a set of MELCOR calculations examining the impact from interaction of air with residual fuel following vessel rupture in the Surry PWR for a station blackout at full power in which a surge line rupture has occurred during the in-core damage phase of the accident.

Section 5 describes results from calculations done to address concerns about air oxidation and the associated enhanced release of ruthenium expected to occur when irradiated reactor fuel is heated in air; those calculations were done as part of a separate, ongoing program providing MELCOR support calculations for the Grand Gulf low-power/shutdown PRA [11]. While these Grand Gulf MELCOR calculations were not done as part of the air ingression analysis effort reported on in this report, they investigated the same issues and evaluated the same accident consequences, and came to the same basic conclusions. Because those calculations will not be formally documented until the completion of that PRA program, the NRC contract monitor for that program has graciously agreed to allow us to include a brief summary of those calculations and results in this report.

Section 6 summarizes the conclusions of these various air-ingression studies.

2 MELCOR Code and Models

MELCOR [8] is a fully integrated, engineering-level computer code which is being developed at Sandia National Laboratories for the U. S. Nuclear Regulatory Commission (USNRC). The progression of severe accidents in light water reactor (LWR) nuclear power plants, including reactor coolant system and containment thermal/hydraulic response, core heatup, degradation and relocation, and fission product release and transport, is treated in MELCOR in a unified framework for both boiling water reactors (BWRs) and pressurized water reactors (PWRs). The MELCOR computer code has been developed to the point that it is now being successfully applied in severe accident analyses, particularly in probabilistic risk assessment (PRA) studies (*e.g.*, [6]).

The MELCOR code does not currently include all the phenomenological models that would be needed to calculate the potential for, and magnitude of, air ingression into the vessel and core region during various accident scenarios. A model for in-vessel natural circulation would be needed to model air ingression during refueling or other shutdown accidents, to calculate hot steam upflow from the core to the upper plenum, probably in the center of the core, and simultaneous downflow of air from the upper plenum into the core region, probably around the periphery of the core region. Such a model is currently under development, but is not yet ready for use. A similar model is needed to predict air ingression in accidents such as the station blackout with surge line break; while MELCOR can calculate the inflow of gases from the cavity up though the core and out the surge line break in such a situation, it predicts little or no oxygen present in the cavity source region during this period as the original cavity atmosphere is all displaced by steam and noncondensables generated in core-concrete interactions. Either a specific code model for single-phase countercurrent flow or a noding with multiple subdivided flow paths with different elevation differences, flow areas and loss coefficients would be needed to calculate hot cavity gases flowing up into the dome (or out into the basement) simultaneously with colder containment atmosphere flowing down into the cavity; that noding modification was not tried for the calculations in this study.

However, MELCOR does include those models needed to calculate the consequences of various amounts of air ingression, if the air ingression is assumed and specified explicitly. In particular, these air-ingression calculations require models for the oxidation of Zircaloy by air, and for the enhanced release of ruthenium from heated fuel in an air environment.

The MELCOR code currently includes models for oxidation of Zircaloy by both H_2O and O_2, and of steel by steam only, calculated using parabolic kinetics, with appropriate rate constant expressions and limited by gaseous diffusion considerations if necessary [12]. In general, solid-state diffusion of oxygen through an oxide layer to unoxidized metal is represented by the parabolic rate equation

$$\frac{d(W^2)}{dt} = K(T) \tag{2.1}$$

where W is the mass of metal oxidized per unit surface area and $K(T)$ is a rate constant expressed as an exponential function of surface temperature T; for the Zircaloy-O_2

reaction, the rate constant is evaluated using constants from [2] to yield

$$K(T) = 50.4exp\left(\frac{-14630.0}{T}\right) \tag{2.2}$$

For oxidation of Zircaloy in environments containing both H_2O and O_2, the maximum oxidation rate calculated for the two gases is used. There are two options for partitioning the oxidant consumption between the oxygen and the steam. The default option (used in all these air-ingression calculations) does not permit any consumption of steam until all of the available oxygen has been consumed. This model is available in the released version of MELCOR 1.8.2.

Three options are currently available in MELCOR [13] for modelling the release of fission products from core materials: the CORSOR, CORSOR-M [14] or CORSOR-Booth [15] models may be specified. For these air-ingression analyses, the fission product release model in MELCOR was recently expanded to include an enhanced ruthenium (Class 6) release rate explicitly dependent on the oxygen potential, using as the rate expression

$$\frac{dF}{dt} = 7956P(O_2)^{1.75}exp\left[\frac{-17400}{T}\right](1-F)s^{-1} \tag{2.3}$$

where $P(O_2)$ is the oxygen partial pressure in atmospheres [16]. This modification will enhance ruthenium release when air is present, and was used for all the MELCOR analyses done in this air-ingression study. (Note that, if O_2 in equilibrium with a mixture of H_2 and H_2O were used in this expression, the release predicted would be similar to that calculated using the standard CORSOR-M expression.) This enhanced ruthenium release model was implemented in the production code with version 1.8NX, and is therefore not available in the released version of MELCOR 1.8.2 (MELCOR 1.8NM). Releases of all other classes were calculated using the standard CORSOR-M coefficients available in the code for in-vessel release, and ex-vessel releases were calculated using the standard VANESA expressions for all radionuclide classes.

Note that one of the sensitivity study calculations described in Section 5 used an alternate form of the Class 6 ruthenium release rate expression (also given in [16]), which is not explicitly dependent on the oxygen potential:

$$\frac{dF}{dt} = 518exp\left[\frac{-17400}{T}\right](1-F)s^{-1} \tag{2.4}$$

3 MELCOR Surry Midloop Calculations with Air Ingression

A set of calculations has been completed studying the effect of various amounts of air ingression into the core region during core degradation, beginning immediately after vessel breach, in the Surry PWR for a station blackout accident under mid-loop operation during low-power and shutdown conditions. The intent of the calculation effort is to scope the effects air intrusion might have on the core degradation and radionuclide release under shutdown conditions.

A mid-loop configuration Surry deck used was obtained from Brian Holmes, BNL [17]. That deck was based upon our Surry TMLB' high-pressure short-term station blackout deck [18], but modified by BNL for mid-loop conditions in plant operating state 6 (POS6) as part of a low-power/shutdown PRA study underway at Brookhaven. POS6 is a condition occurring during the early portion of the refueling mode of operation, in which the reactor coolant system level is lowered to the mid-plane of the hot leg during refueling. This state is the PWR analogue of the POS6 configuration modelled for the Grand Gulf low-power and shutdown air ingression analyses discussed in Section 5. The plant configuration during the low-power/shutdown period can vary widely depending on the purpose of the outage. It was assumed that all the loops were isolated and that the safety valves were removed for maintenance, which provides a vent path from the reactor coolant system to the containment. Containment spray availability was one of the uncertainty parameters in the PRA study, with no sprays available in the base case. Containment, while "closed" during mid-loop operation at Surry, was assumed to leak during POS6, because a temporary restraining plug in the escape tunnel in the containment equipment hatch has no overpressure capability. [19, 20, 21]

We made two changes to the Surry mid-loop configuration deck as received from BNL: the decay heat was set to 24 hours after shutdown (the earliest the plant could possibly be in POS6), and gravity feed from the refueling water storage tank (RWST) to the cold legs (being evaluated as a long-term cooling mechanism) was set to zero. These changes were made to get to core damage as quickly as possible.

A reference calculation was done with no air ingression forced. A series of additional calculations was done, with various amounts of air ingression. A flow path was defined going from the containment dome to the core, and a constant velocity flow was specified to start immediately at vessel failure. The containment dome was used as the air source volume instead of the cavity because the cavity air was quickly displaced by steam and/or hydrogen, while the containment dome atmosphere remained mostly ~80%-N_2/~20%-O_2 with less dilution by steam, hydrogen and other noncondensables generated by core-concrete interaction. The velocity needed to obtain desired molar flows was estimated based upon STP conditions, not adjusted for containment pressurization; since the air ingression considered covered many orders of magnitude, the ~20% increase between the actual flow obtained using a velocity estimated based on STP conditions and the desired air flow was considered negligible.

The MELCOR Surry core model [18] consists of 39 core cells divided into 3 radial rings and 13 axial levels; Figure 3.1 illustrates the reactor core nodalization used. Axial levels 4 through 13 make up the active core region, while levels 1 through 3 model the lower plenum, including the core support plate in level 3. Equal-height axial levels were used in the active fuel region, above the core support plate. The three radial rings were not equally subdivided in either radius or area; the innermost, high-powered ring includes ~15% of the core, the middle ring contains ~60% of the core, and the outermost, low-power ring includes the remaining ~25% of the core.

Table 3.1 summarizes the state of the various materials in the core active fuel region, core plate and lower plenum at the time a lower head penetration first fails (*i.e.*, at vessel breach); this state is common to all the air ingression sensitivity study calculations done, because the air ingression is specified to start at vessel breach. Masses of intact components and of debris components are given for each region, together with average temperatures for the debris in the lower plenum, and fractions of Zircaloy and steel oxidized by the time of vessel breach. The fraction of debris molten in each region is estimated from the average debris temperature, which in this case resulted in assuming that Zircaloy, steel, steel oxide and control rod poison in the active fuel region and lower plenum debris are molten and that UO_2 and ZrO_2 in the debris are solid (*i.e.*, neglecting eutectics mixtures; this assumption is forced by the MELCOR output available to the analyst). Also given is the fraction of material relocated. This is generally larger than the fraction molten because material can melt and relocate, and then subsequently refreeze or quench; also, UO_2 fuel usually relocates as a solid, after clad collapse but before fuel melt.

The various materials in the MELCOR "fuel/clad" component just prior to vessel failure, both any intact materials remaining in their original position and candled, refrozen conglomerate debris materials, are shown in Figures 3.2 through 3.4 for the three radial rings in the MELCOR Surry core model. Figures 3.5 through 3.7 show the materials calculated to be in the "particulate debris" component in the three core rings at the same time, while the various materials in the MELCOR "other-structure" component just prior to vessel failure, both any intact materials remaining in their original position and candled, refrozen conglomerate debris materials, are shown in Figures 3.8 through 3.10 for the three core rings in the MELCOR Surry core model. (Refer to [8] for an explanation of these MELCOR components, if necessary.) The "elevation" used as the ordinate in Figures 3.2 through 3.10 is the same as the core level elevations shown in Figure 3.1, with the core support plate at $\geq$3m, the lower plenum between 0 and ~3m, and the active fuel region from $\geq$3m to ~6.722m. The fraction of each core cell occupied by any given material is shown. However, recall that the core cells are not equal in the three rings; the innermost, high-powered ring includes ~15% of the core, the middle ring contains ~60% of the core, and the outermost, low-power ring includes the remaining ~25% of the core.

The innermost ring has no intact structure in the active fuel region at all at the time of vessel failure (Figure 3.2), but there is a substantial debris bed both in the lower plenum and in the active fuel region above the core support plate in that first ring (Figure 3.5).

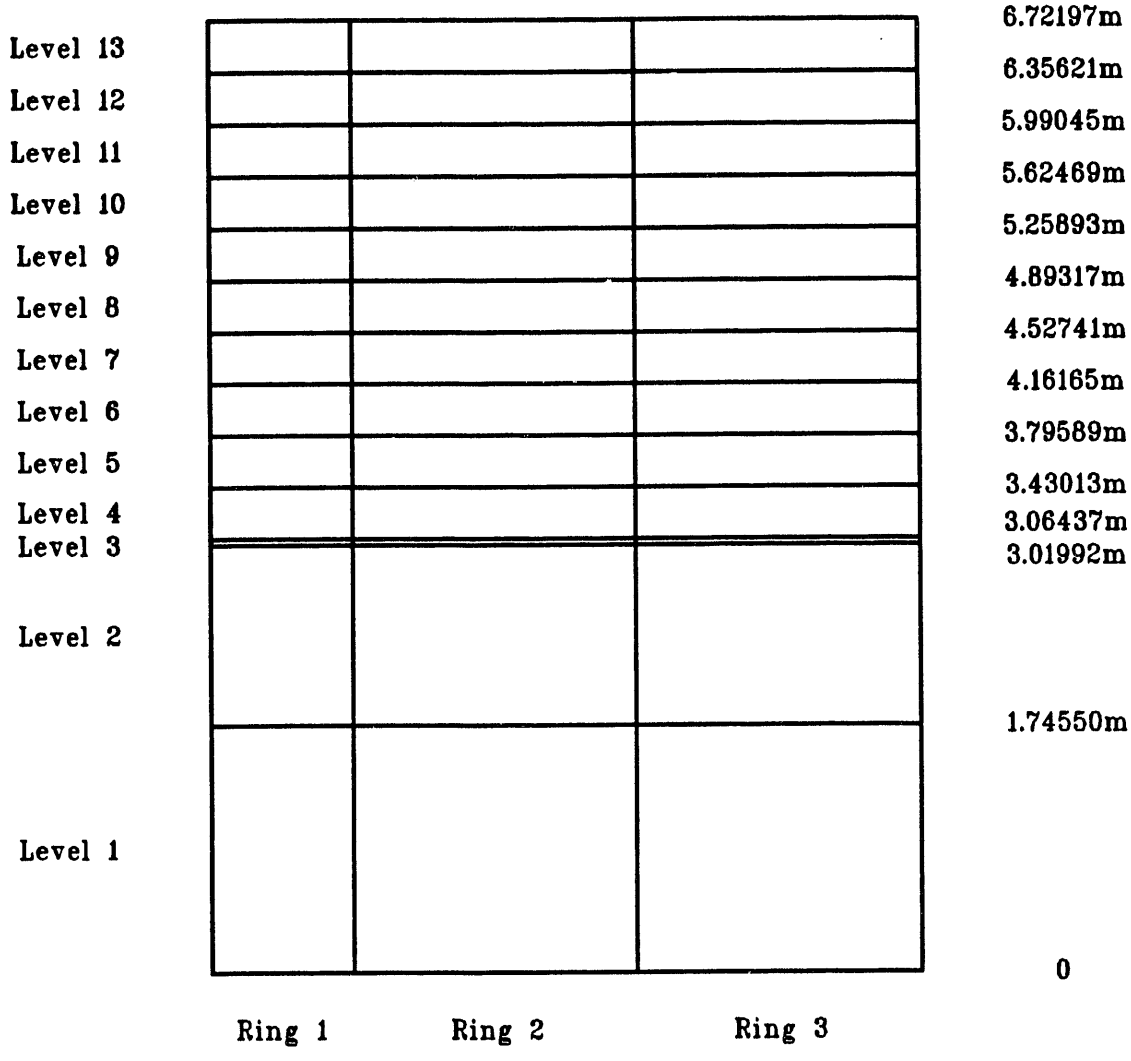

Figure 3.1. Reference MELCOR COR Input Model for Surry Core

Table 3.1. Core State at Vessel Failure in MELCOR Surry Midloop Calculations with Air Ingression

	Intact	Debris
Active Fuel Region Masses (kg)		
UO_2	14,347	34,615
Zircaloy	6,559	1,947
Zirc Oxide	3,096	835
Steel	178	21
Steel Oxide	112	8
CRP	808	1,084
Total	25,100	38,510
Core Plate Masses (kg)		
UO_2		94
Zircaloy		37
Zirc Oxide		13
Steel	225	54
Steel Oxide		9
CRP		15
Total	225	222
Lower Plenum Masses (kg)		
UO_2		31,656
Zircaloy		3,334
Zirc Oxide		1,721
Steel	0	87
Steel Oxide	0	51
CRP		92
Total	0	36,941
Average Debris Temperature (K)		
Active Fuel Region		~2300
Core Plate		~1000
Lower Plenum		~2350
Fraction Debris Molten		
Active Fuel Region		~8%
Core Plate		~0%
Lower Plenum		~10%
Fraction Material Relocated	~75%	
Fraction Oxidized	Zircaloy	Steel
	~35.25%	~25.67%

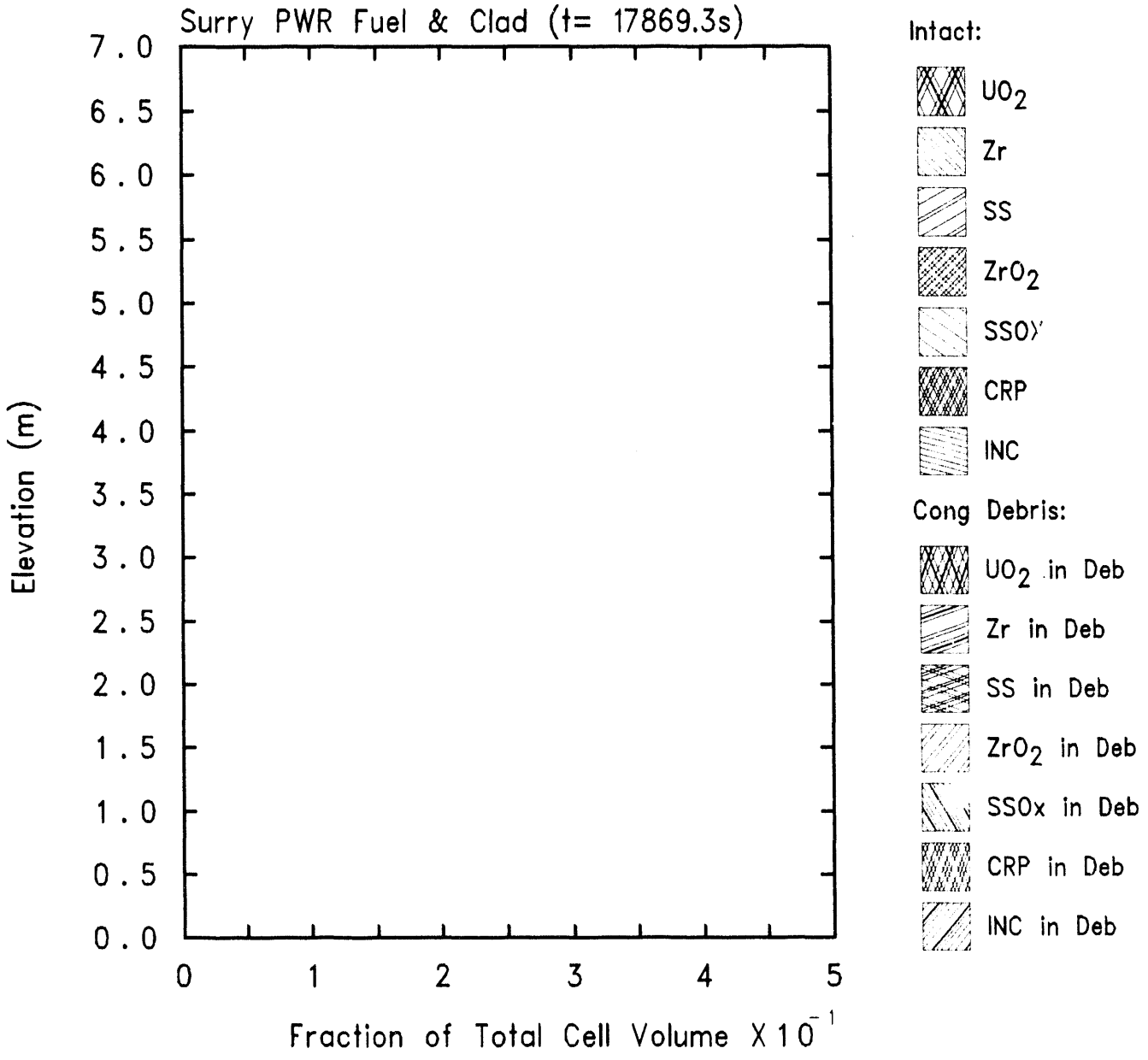

Figure 3.2. Core Ring 1 Fuel/Clad Component Materials at Vessel Failure in MELCOR Surry Midloop Calculations with Air Ingression

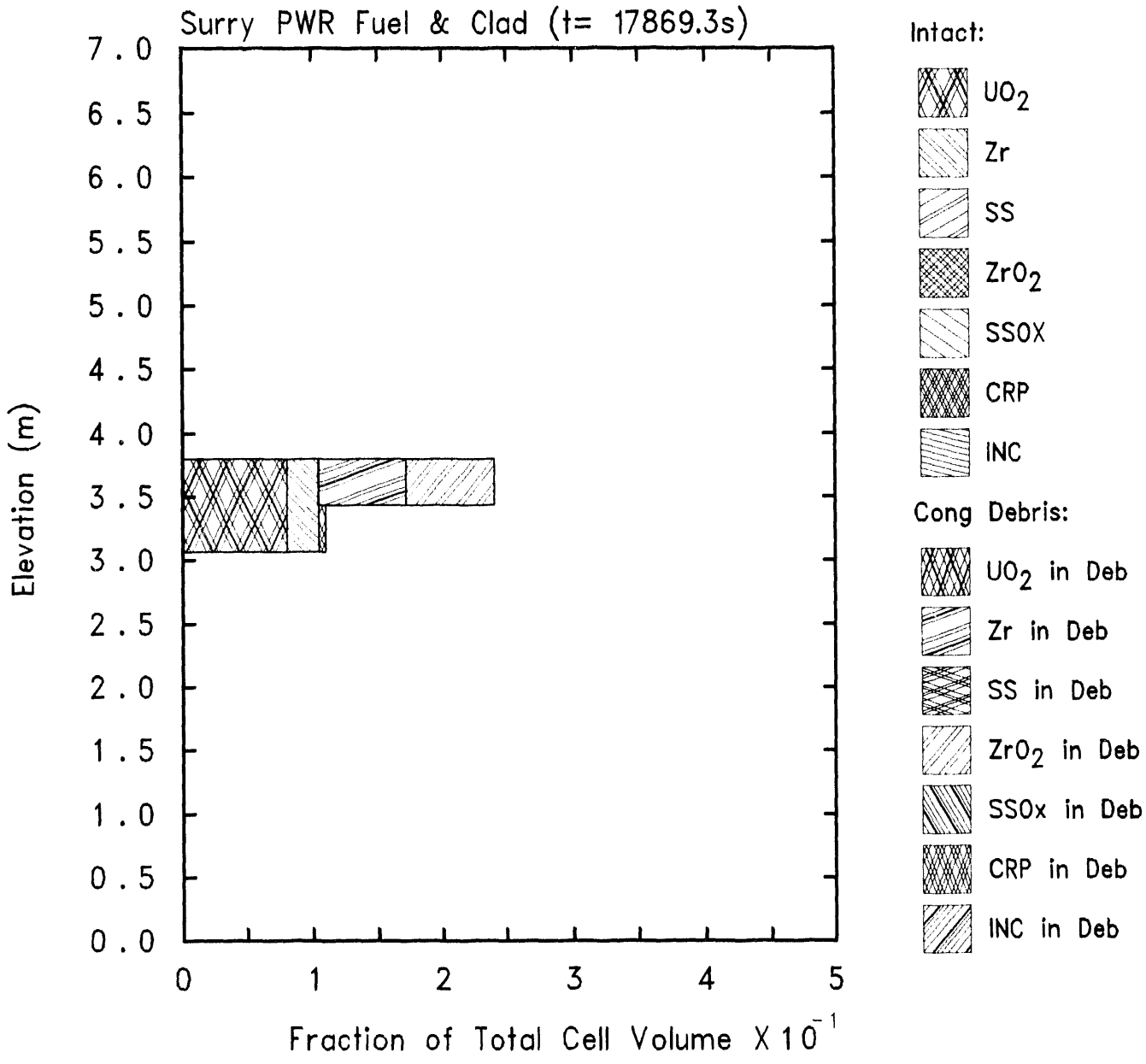

Figure 3.3. Core Ring 2 Fuel/Clad Component Materials at Vessel Failure in MELCOR Surry Midloop Calculations with Air Ingression

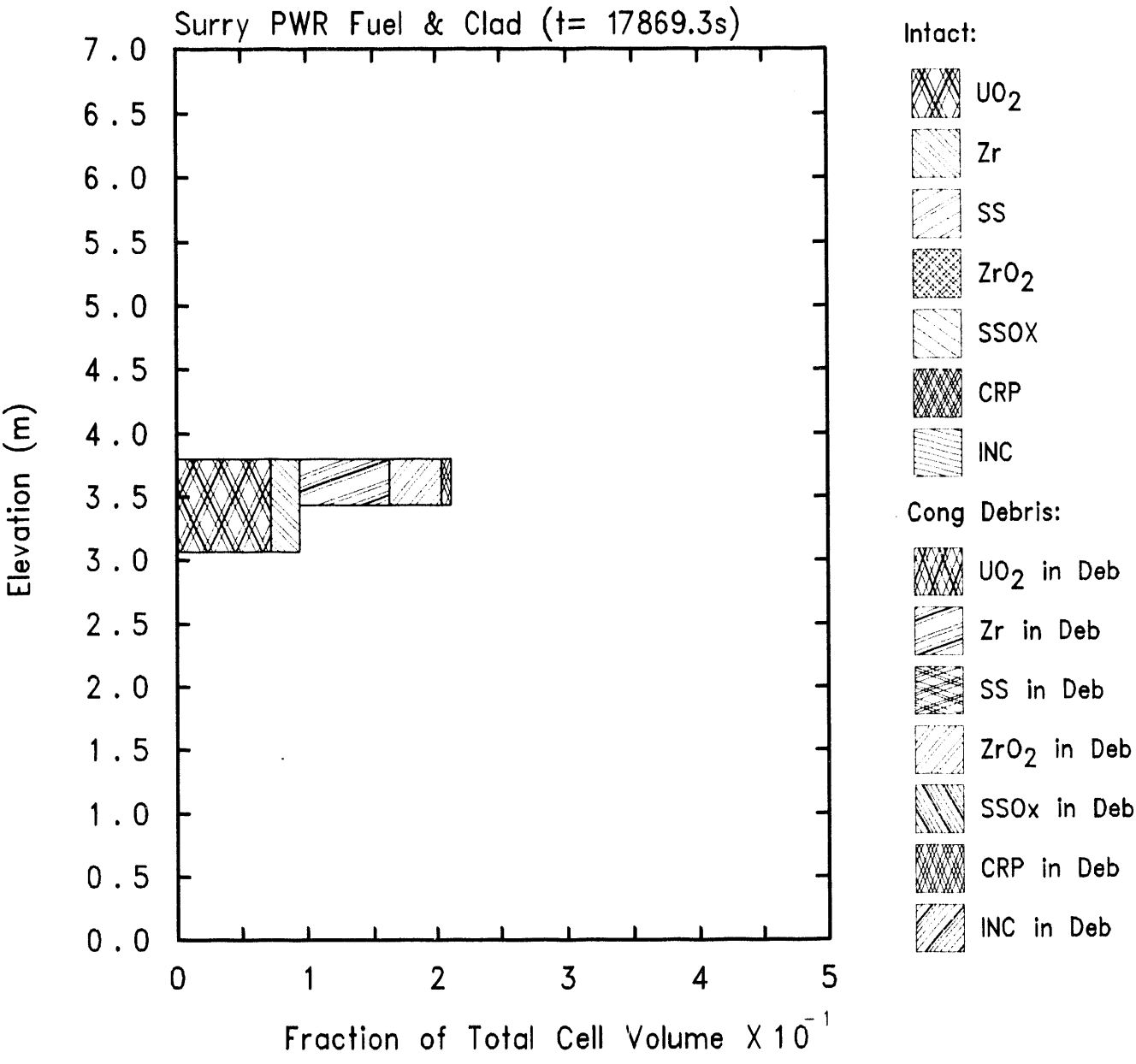

Figure 3.4. Core Ring 3 Fuel/Clad Component Materials at Vessel Failure in MELCOR Surry Midloop Calculations with Air Ingression

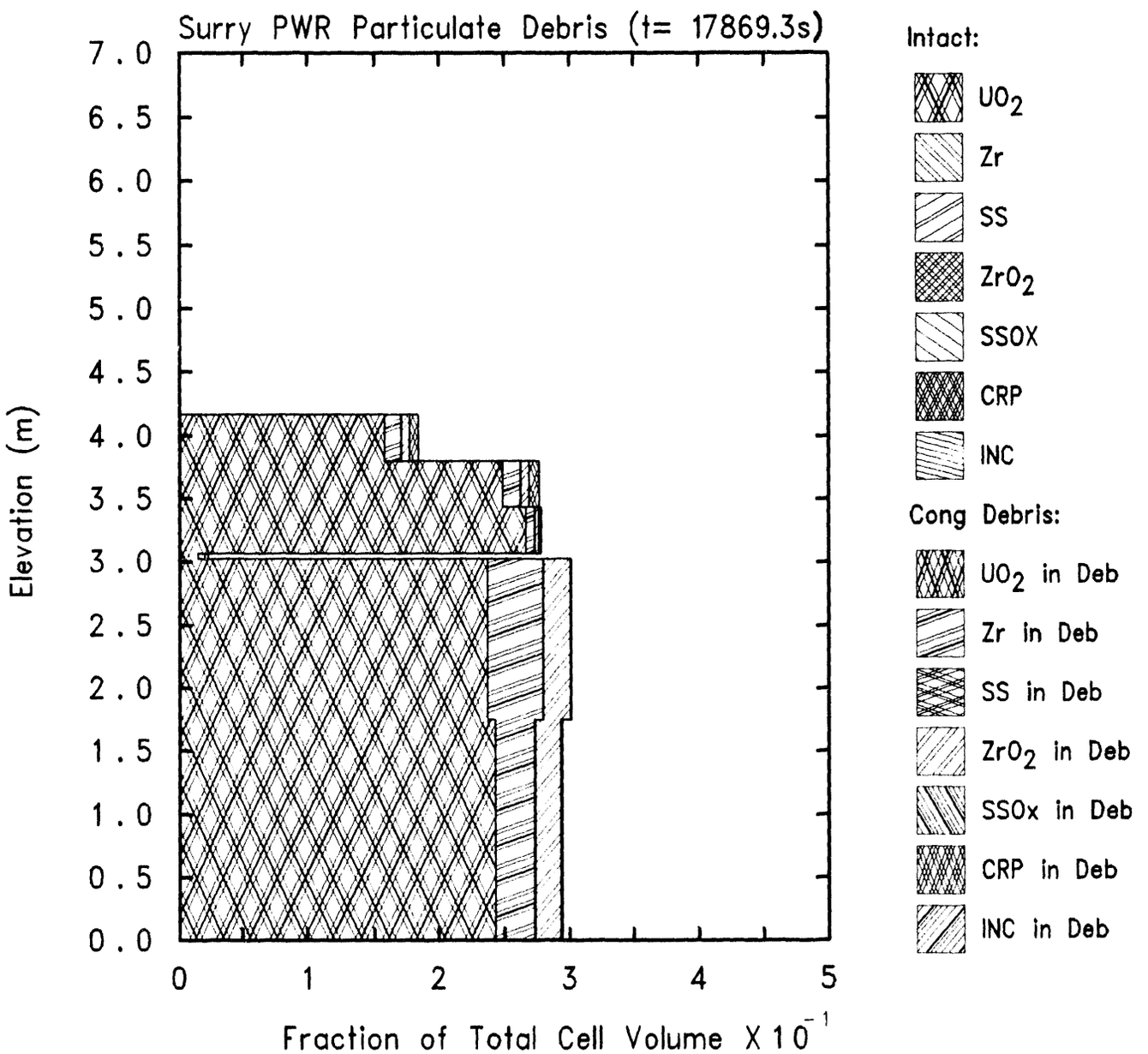

Figure 3.5. Core Ring 1 Particulate Debris Component Materials at Vessel Failure in MELCOR Surry Midloop Calculations with Air Ingression

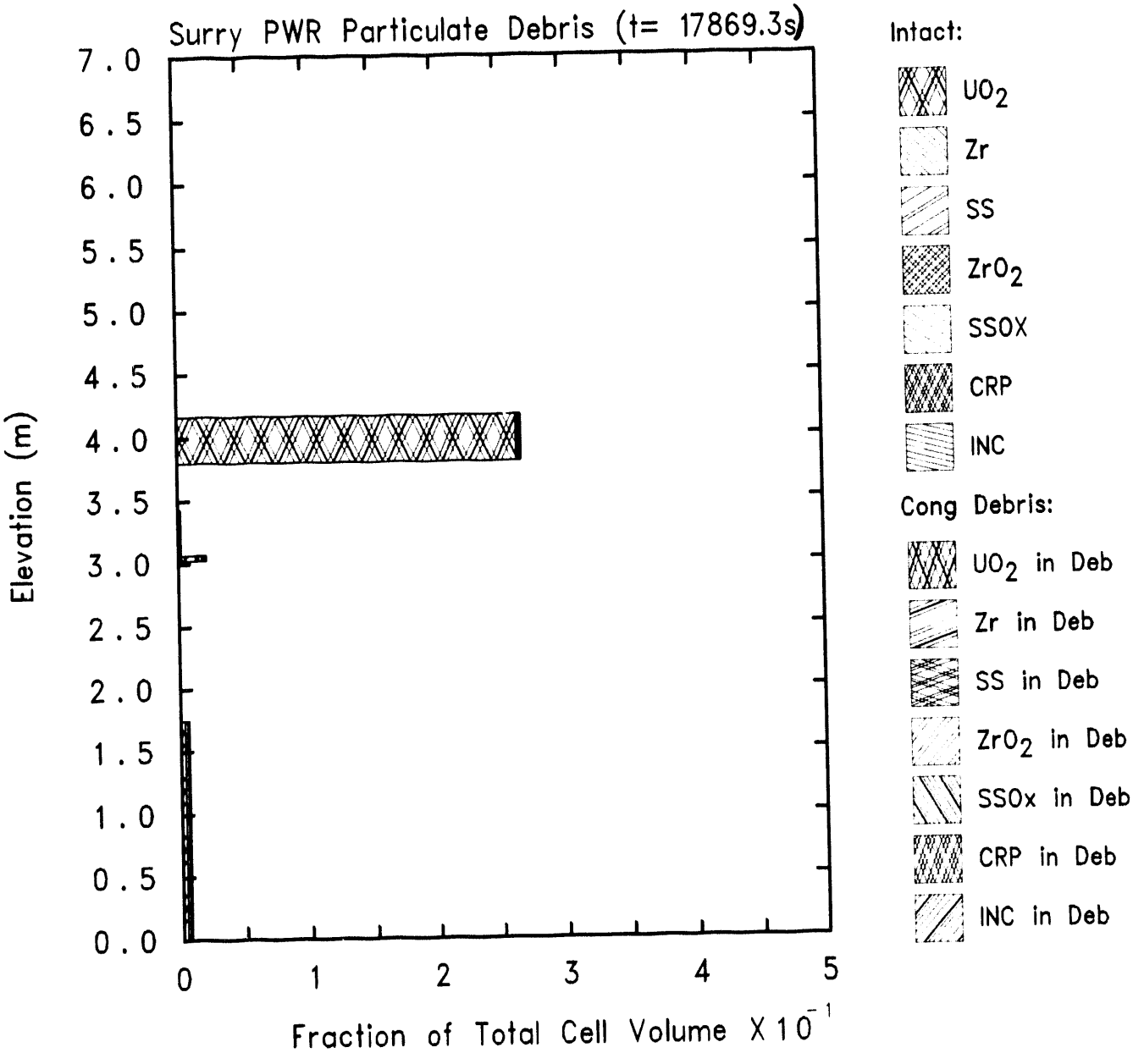

Figure 3.6. Core Ring 2 Particulate Debris Component Materials at Vessel Failure in MELCOR Surry Midloop Calculations with Air Ingression

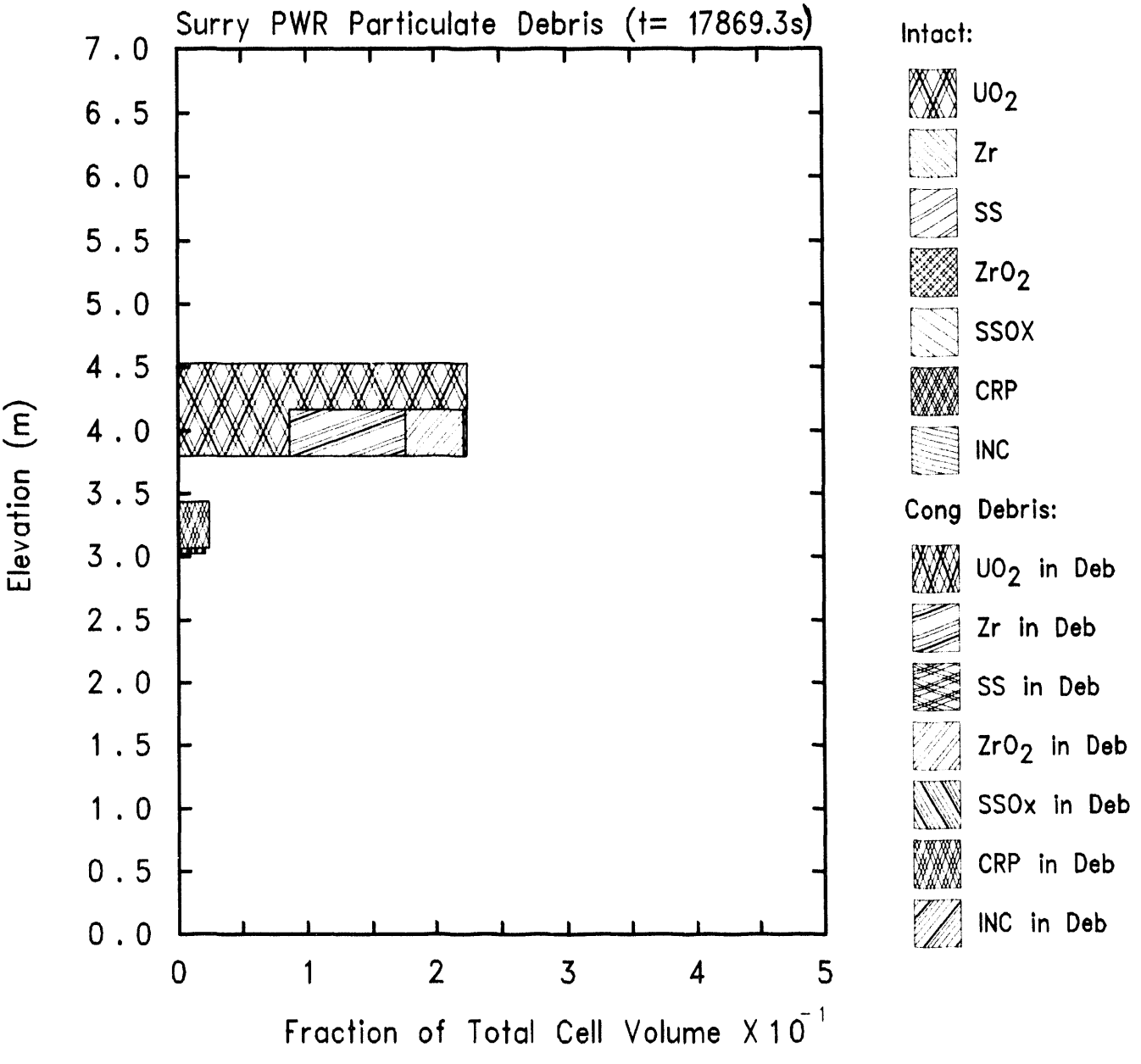

Figure 3.7. Core Ring 3 Particulate Debris Component Materials at Vessel Failure in MELCOR Surry Midloop Calculations with Air Ingression

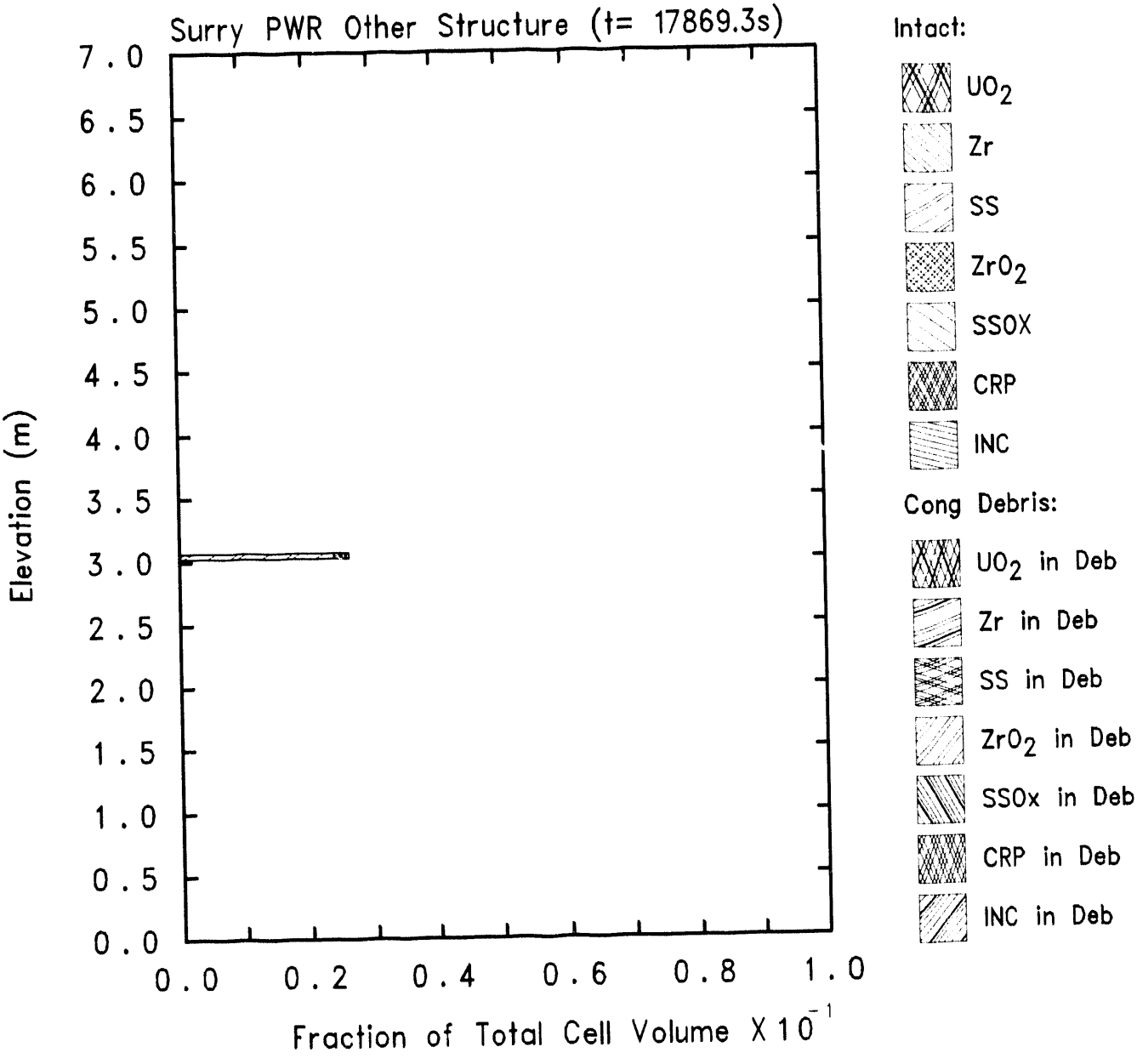

Figure 3.8. Core Ring 1 Other Structure Component Materials at Vessel Failure in MELCOR Surry Midloop Calculations with Air Ingression

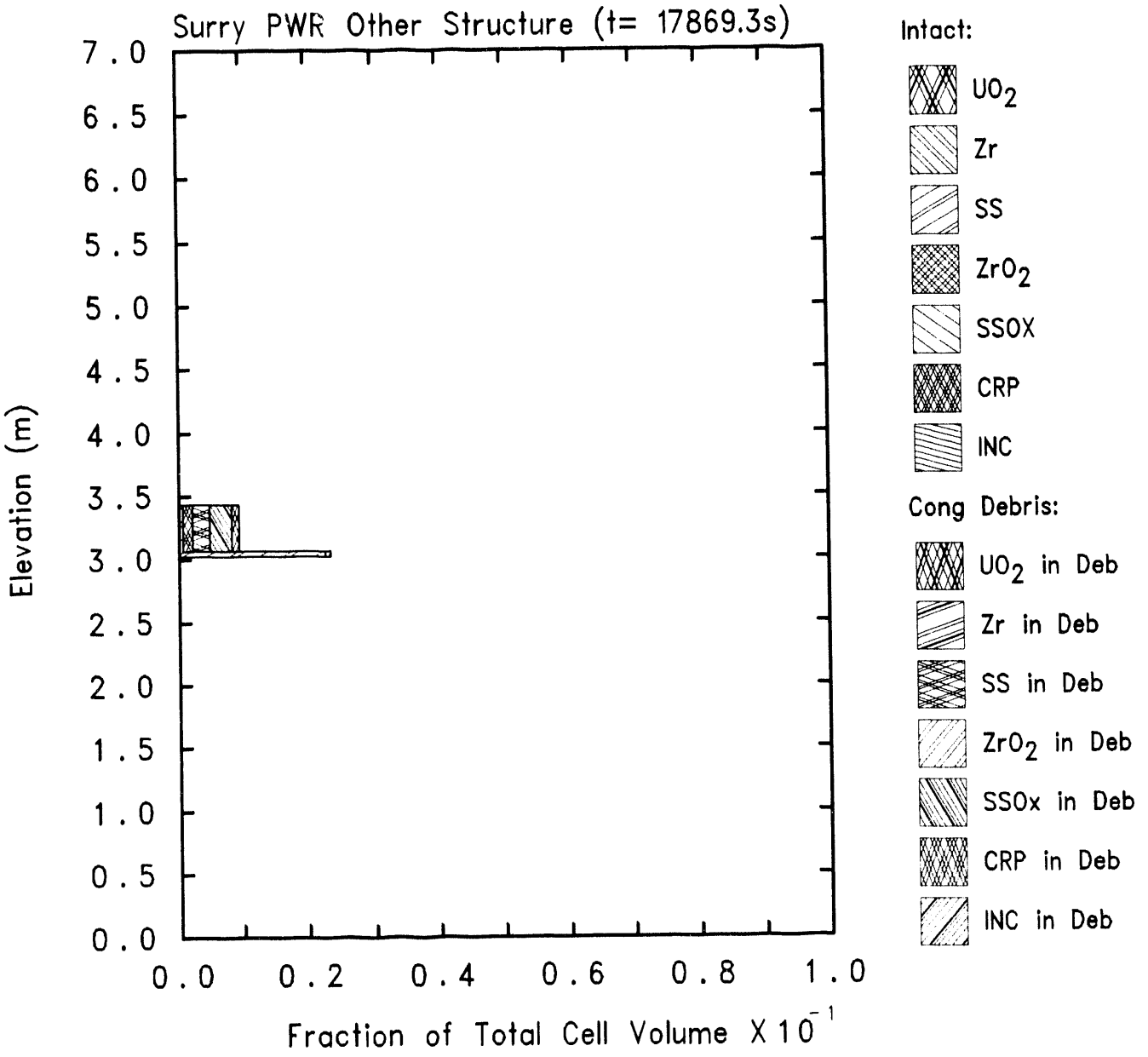

Figure 3.9. Core Ring 2 Other Structure Component Materials at Vessel Failure in MELCOR Surry Midloop Calculations with Air Ingression

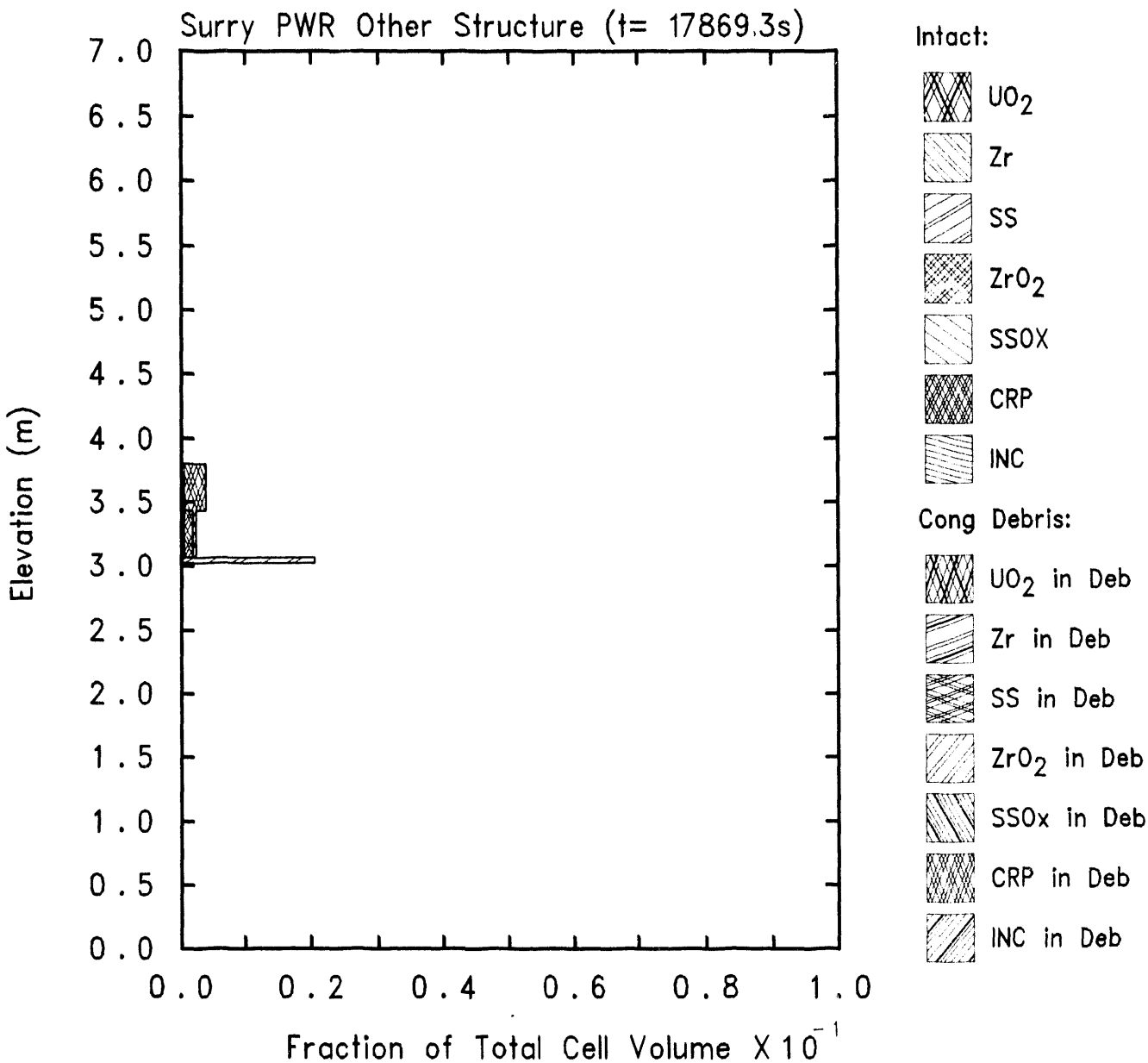

Figure 3.10. Core Ring 3 Other Structure Component Materials at Vessel Failure in MELCOR Surry Midloop Calculations with Air Ingression

Some intact material remains in the lower core levels in the active fuel region in both the second and third rings (Figures 3.3 and 3.4), with those intact materials together with the core plate supporting one or more levels of particulate debris held in the active fuel region in both the second and third rings (Figures 3.6 and 3.7). The core plate itself is clearly visible in Figures 3.8 through 3.10 as the very thin structure at $\geq$3m elevation; in Figures 3.9 and 3.10 the core plate is seen to be supporting some candled, refrozen other structure, such as control rod poison and the control rod guide tube material. Note that only ~35% of the Zircaloy (and 25-30% of the steel) has been oxidized up to this time, either in the intact clad or in the debris bed; most of the Zircaloy remains unoxidized in both the remaining intact clad and in the debris bed at the time of vessel failure and at the specified start of the assumed air ingression.

Figure 3.11 through 3.14 present the steam, nitrogen, oxygen and hydrogen mole fractions in the core active fuel region control volume, respectively, resulting from various amount of air ingression. In all cases, prior to vessel breach, the core atmosphere oscillates between mostly steam and mostly hydrogen. After vessel breach, the results with $\simeq$1mole/s air ingression are generally similar to the results with no prescribed air ingression; the core atmosphere is mostly steam, with some small amount of N_2 and O_2 appearing some time after vessel breach. The results with higher air ingression rates ($\simeq$10mole/s and up) are all similar after vessel failure, and qualitatively different from the results with $\simeq$1mole/s air ingression and with no prescribed air ingression; the core atmosphere is mostly air, as soon as air ingression is specified to begin, with some small amount ($\leq$20%) of steam. In all cases, very little ($\leq$5%) hydrogen is present after vessel rupture.

Mass-weighted average core clad temperatures in these calculations with various air ingression rates are presented in Figure 3.15. In all cases with any amount of air ingression, the average clad temperatures after oxidation runaway are similar and are visibly higher than the basecase analysis with no air ingression; however, in all cases with any amount of air ingression, the clad subsequently fails sooner (indicated by the temperature going to zero) than predicted in the basecase analysis with no air ingression. This is because the higher late-time temperatures in the analyses with air ingression (due to the higher energy of reaction for Zircaloy oxidation with air rather than with steam) cause the core material to melt, relocate and be lost to the cavity sooner than predicted with no air ingression into the core. Figure 3.16 gives the maximum clad temperatures for these Surry midloop calculations, with and without air ingression, showing that the maximum clad temperature does not increase significantly as the average clad temperature increases; the intact Zircaloy clad always fails and relocates when it reaches its melt point of 2098K. (The intact fuel average and maximum temperature comparisons are very similar to these intact clad average and maximum temperature comparisons.)

Typical clad temperatures predicted in these calculations are given in Figures 3.17 and 3.18 for cells in the middle core ring, in the lower core active fuel region (about 0.6m above the core support plate), and in the upper core active fuel region (about 2.0m above the core support plate), respectively. The higher clad temperatures after oxidation runaway with air ingression and air oxidation are clearly visible in the lower core, but

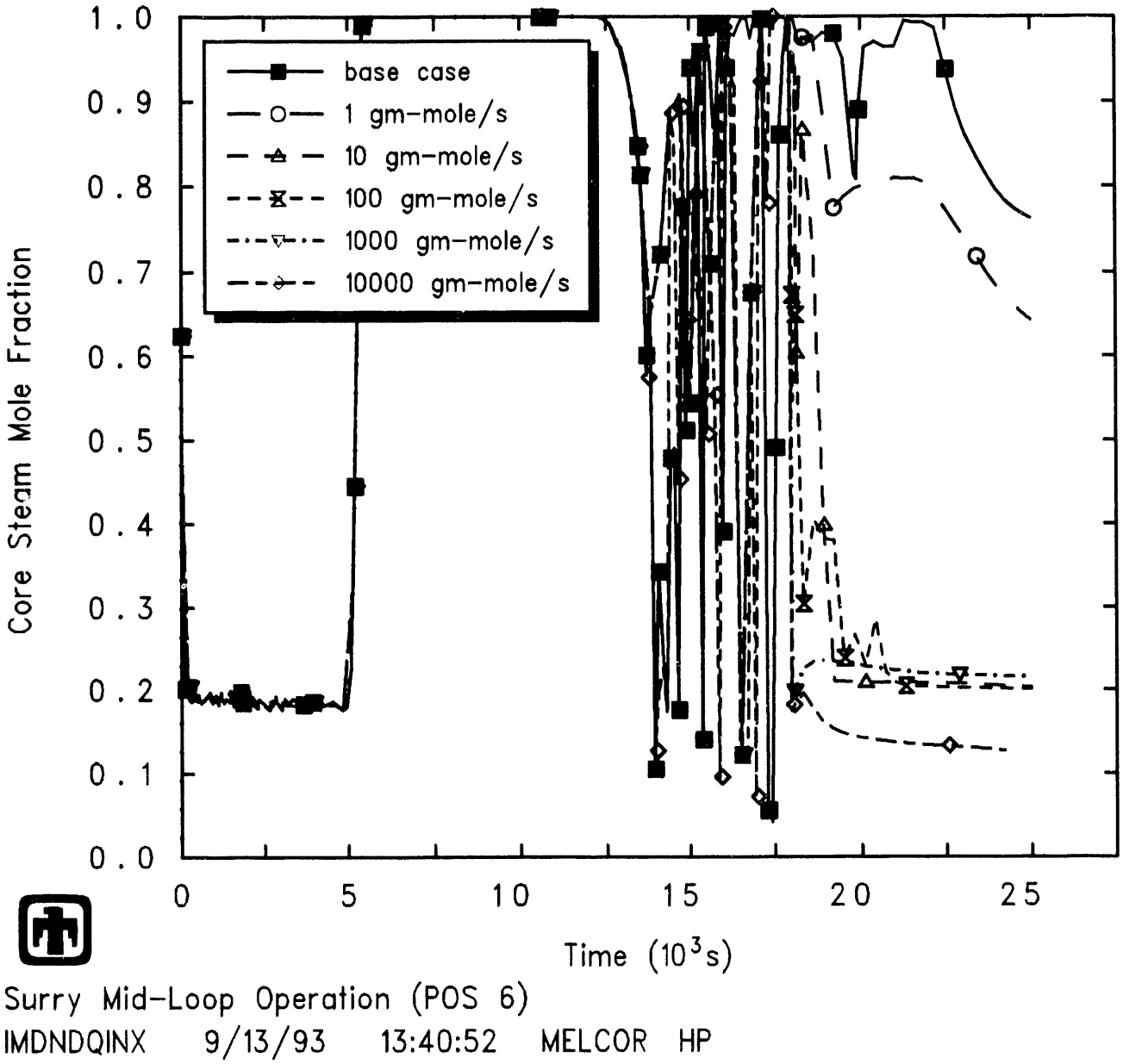

Figure 3.11. Core Active Fuel Region Steam Mole Fractions in MELCOR Surry Midloop Calculations with Air Ingression

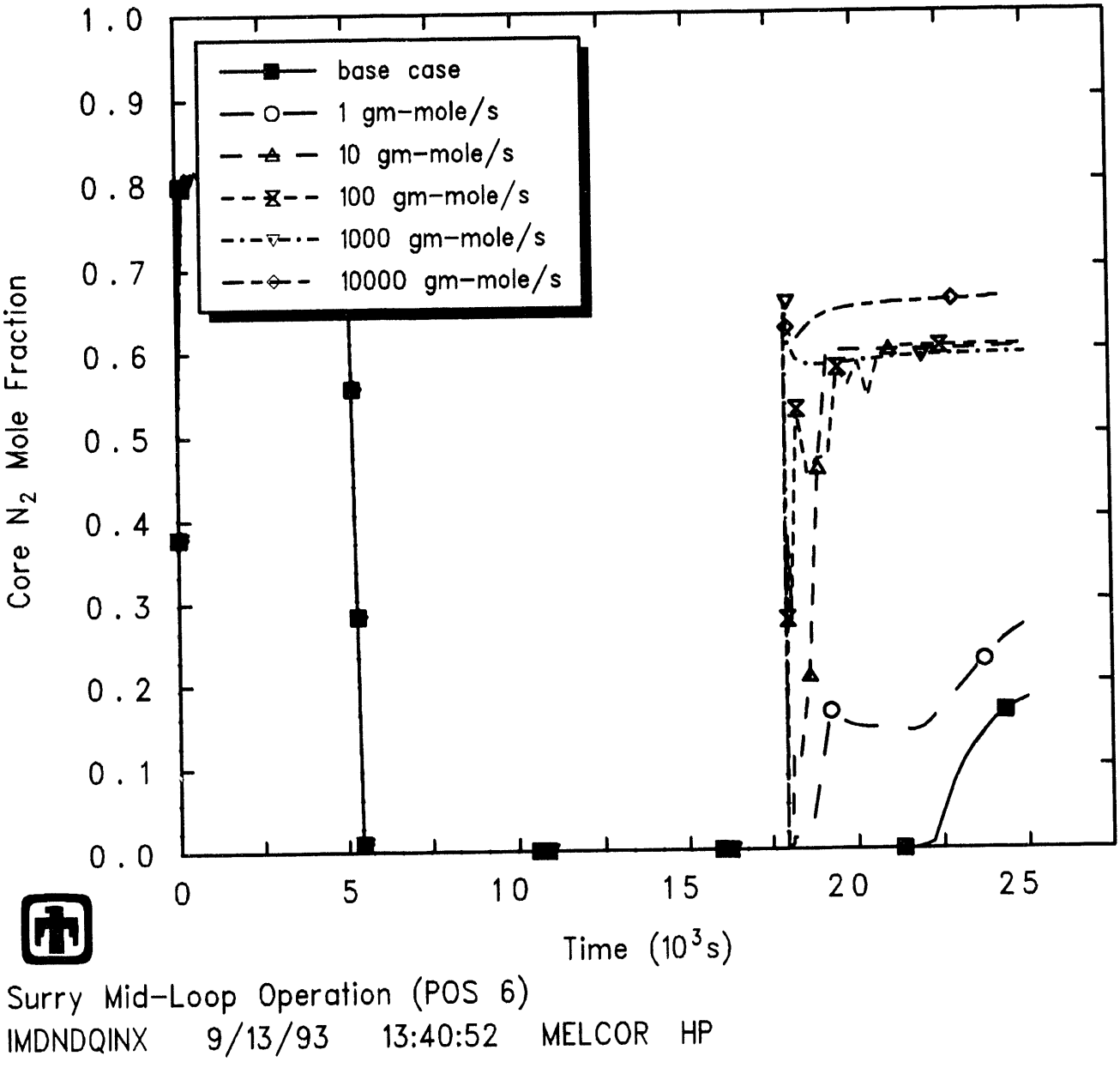

Figure 3.12. Core Active Fuel Region Nitrogen Mole Fractions in MELCOR Surry Midloop Calculations with Air Ingression

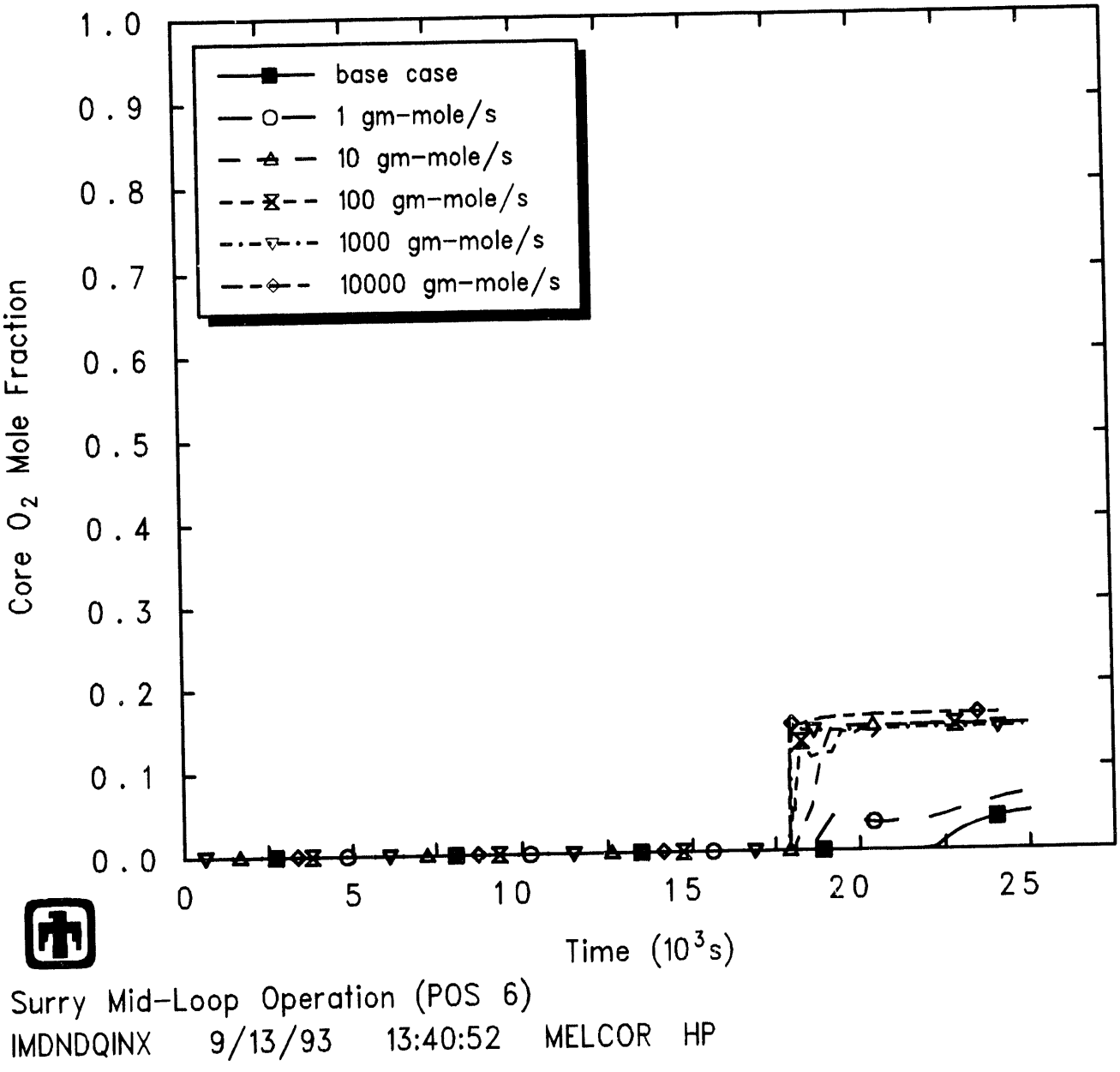

Figure 3.13. Core Active Fuel Region Oxygen Mole Fractions in MELCOR Surry Midloop Calculations with Air Ingression

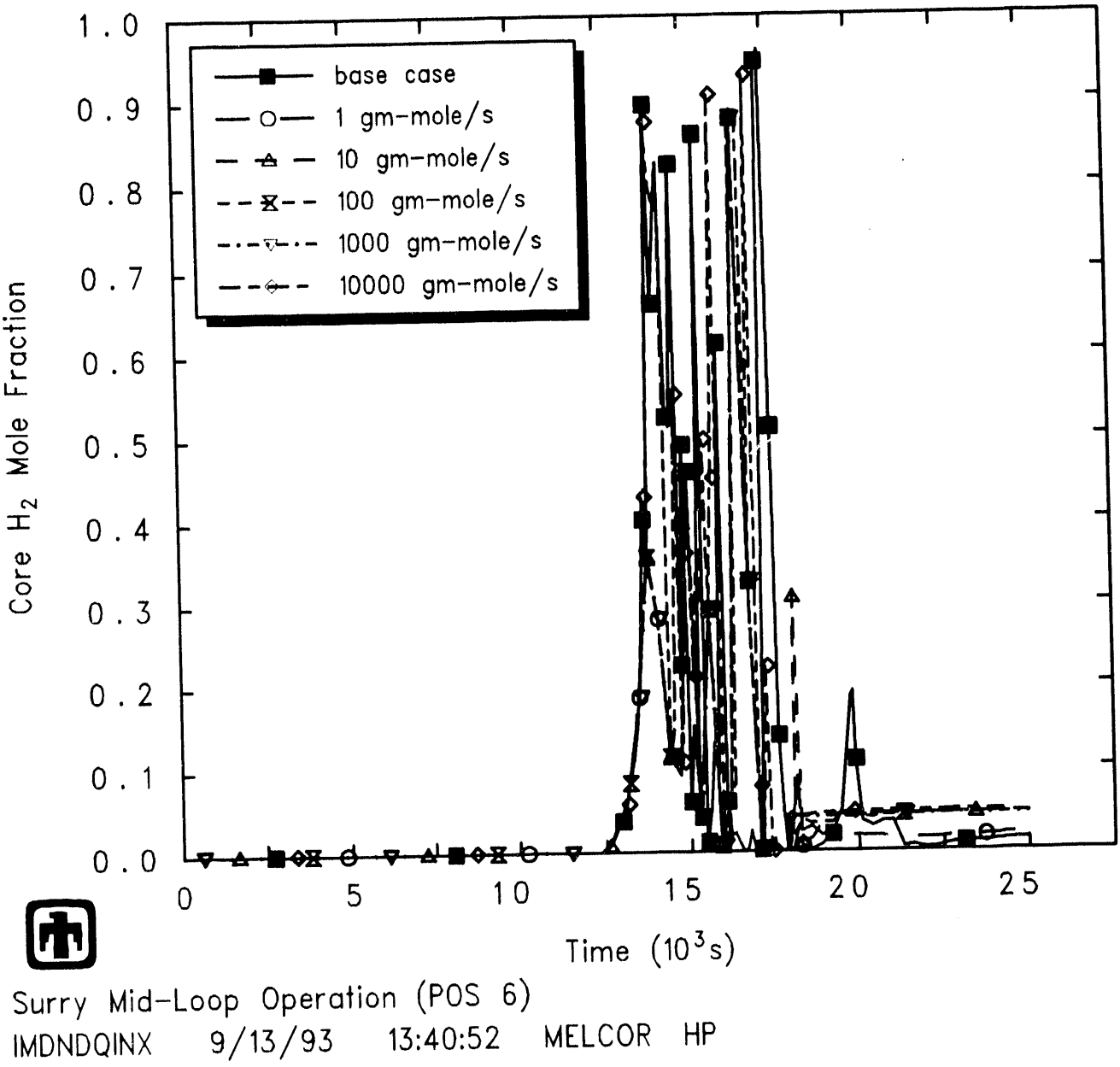

Figure 3.14. Core Active Fuel Region Hydrogen Mole Fractions in MELCOR Surry Midloop Calculations with Air Ingression

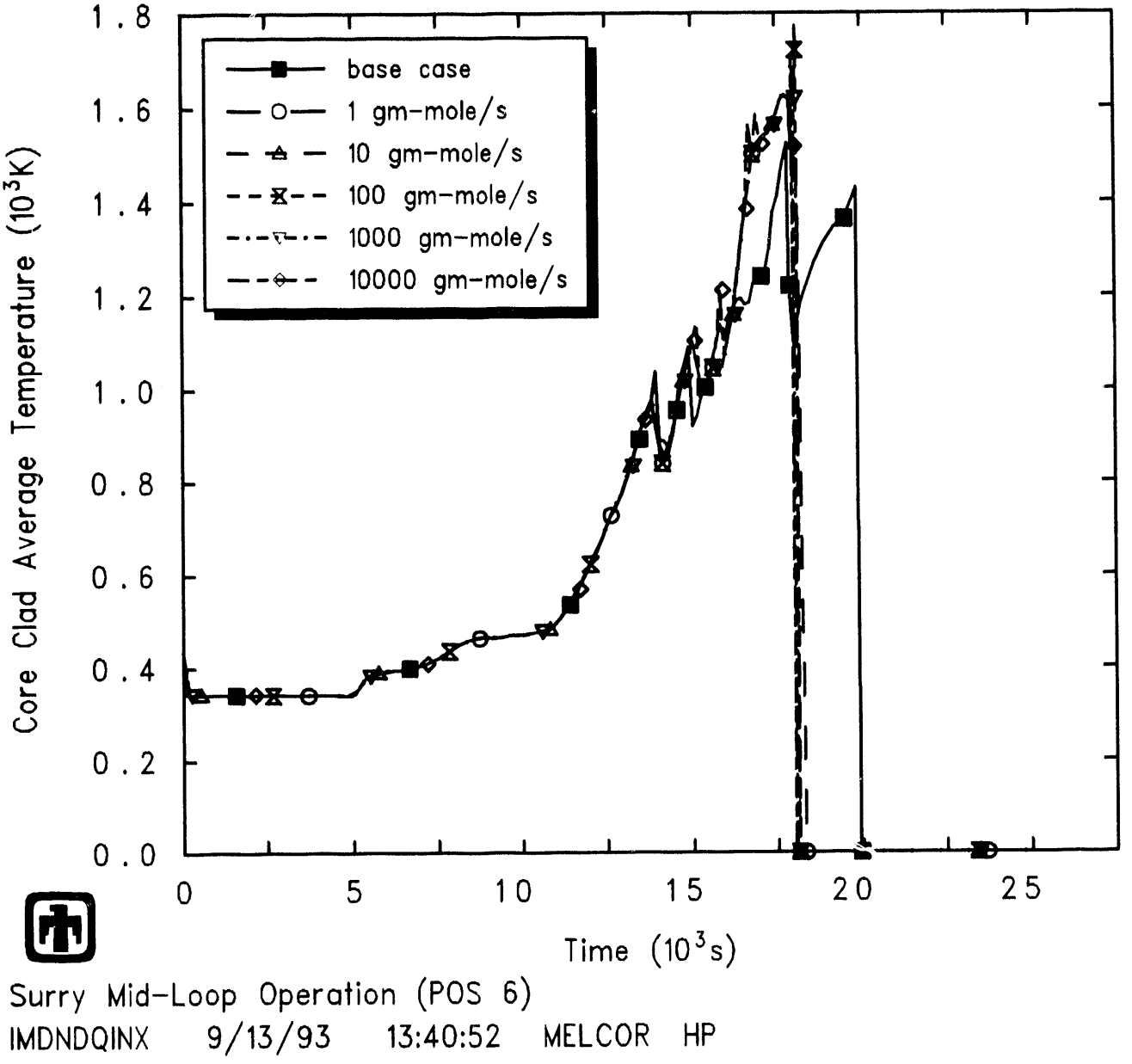

Figure 3.15. Core Average Clad Temperatures in MELCOR Surry Midloop Calculations with Air Ingression

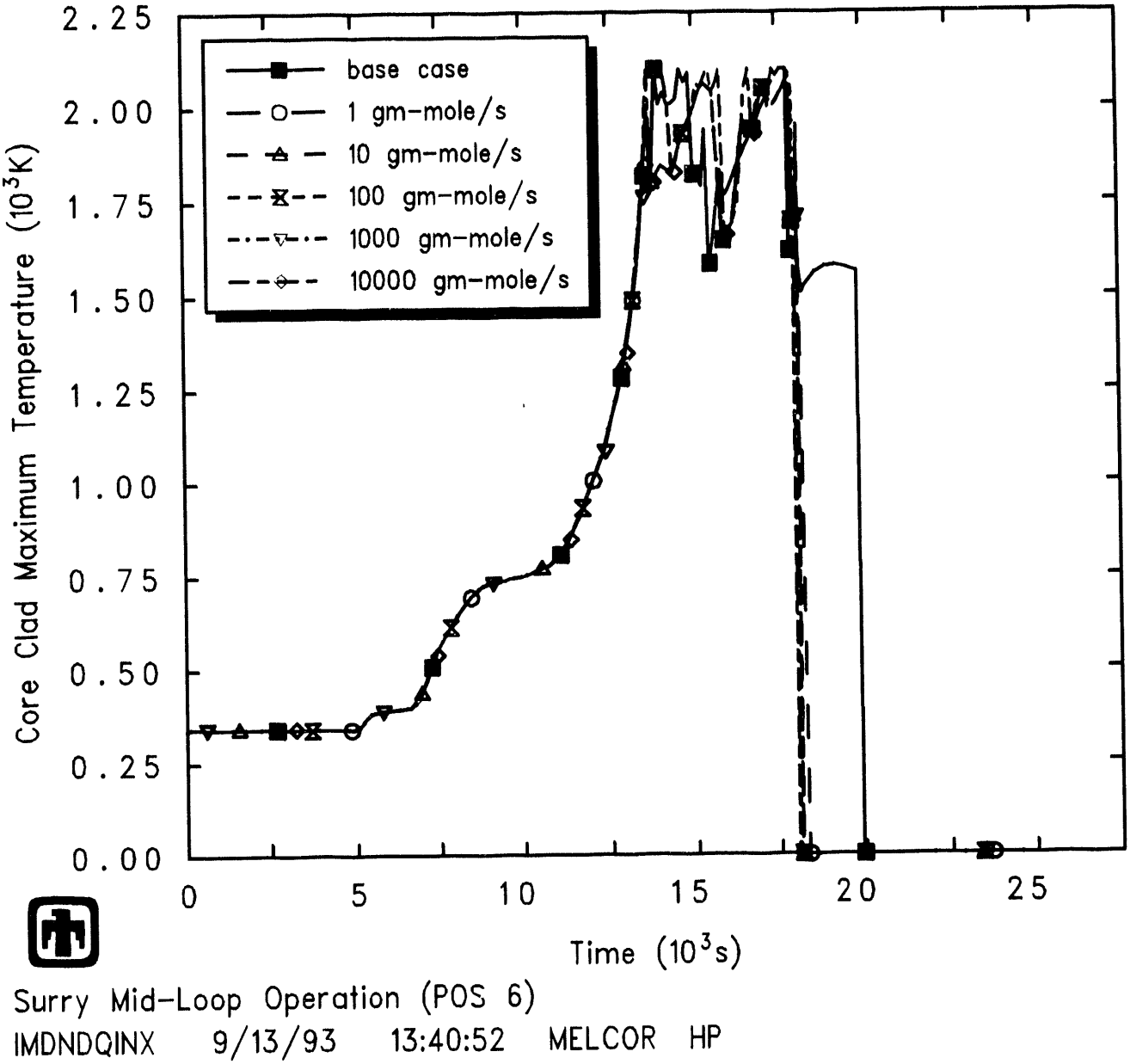

Figure 3.16. Core Maximum Clad Temperatures in MELCOR Surry Midloop Calculations with Air Ingression

almost indistinguishable in the upper core.

Figure 3.19 demonstrates the effect of various amounts of air ingression on the material retention in-vessel *vs* ejection to cavity. All calculations show the same overall behavior, with the majority ($\geq$60%) of the core material ejected immediately upon vessel failure, and most of the remainder ($\leq$40%) of the core material lost to the cavity after some small time delay. The slightly higher late-time temperatures in these midloop-accident calculations with user-specified air ingression into the core, due to the higher energy of reaction for Zircaloy oxidation with air rather than with steam, cause the remainder of the core material to melt, relocate and be lost to the cavity sooner than predicted in the calculation with no user-specified air ingression into the core.

Mass-weighted average core debris temperatures in these calculations with various air ingression rates are presented in Figure 3.20, while Figure 3.21 gives the maximum debris temperatures for these Surry midloop calculations, with and without air ingression. In all cases with any amount of air ingression, the average debris temperatures between $\sim$15,000s and $\sim$17,500s are very similar and are slightly lower than in the basecase analysis with no air ingression. After most material has been ejected from the vessel, at $\sim$18,000s, both the average and maximum debris temperatures decrease as the air ingression rate increases; with increased air ingression rates, very little debris is left in the vessel and that residual debris is being cooled by the increased amounts of relatively cold air being sourced into the core and flowing through the lower plenum and out the vessel breach, as shown in Figure 3.22. (Note that MELCOR does not calculate any oxidation of UO_2 by air.) Debris temperature comparisons in individual cells closely resemble the average and maximum temperature comparisons.

Table 3.2 summarizes the in-vessel ruthenium release fractions, normalized to the initial inventory of class 6 radionuclides (151.1kg in this case). The in-vessel releases are subdivided into releases in the "core" and "lower plenum" regions. The "core" region is the active fuel region, above the core support plate, and includes releases from both intact fuel and from debris still supported by intact core components or by the core support plate; the "lower plenum" release is from debris that has fallen through the core support plate and is being held in the lower plenum on the vessel lower head prior to being lost to the cavity through a lower head failure.

With no air ingression, only trace amounts of ruthenium are released. Note that at 0.032kg/s ($\simeq$1mole/s) of air ingression, there is some slight enhancement of ruthenium release, almost all from debris in the lower plenum. Relatively small rates of air ingression (between $\simeq$1mole/s and $\simeq$10mole/s) cause a qualitative change in the source term, with enhanced ruthenium release in the active fuel region dominating release from debris in the lower plenum. There is a significant increase in ruthenium release as the air ingression is increased from 0.32kg/s ($\simeq$10mole/s) to 3.2kg/s ($\simeq$100mole/s), with $\sim$80% of the release in the core active fuel region and $\sim$20% from debris in the lower plenum. For air ingression rates 32kg/s ($\simeq$1kg-mole/s), almost all the class 6 radionuclide inventory is released in-vessel. These results quantify the amount of air ingression that would be required to significantly enhance ruthenium release during the in vessel core damage phase, one major effect of the air ingression.

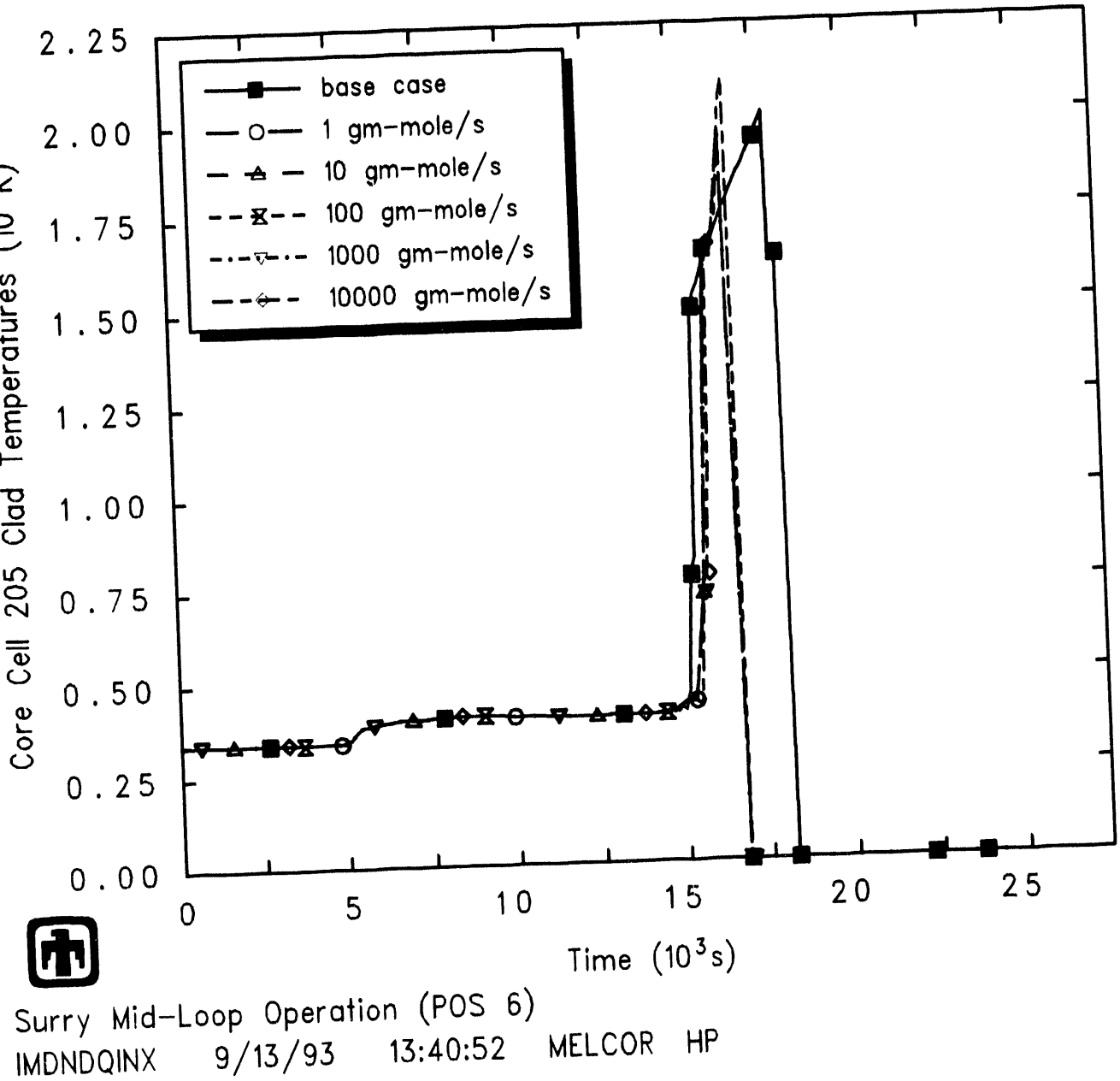

Figure 3.17. Core Ring 2, Level 5 Clad Temperatures in MELCOR Surry Midloop Calculations with Air Ingression

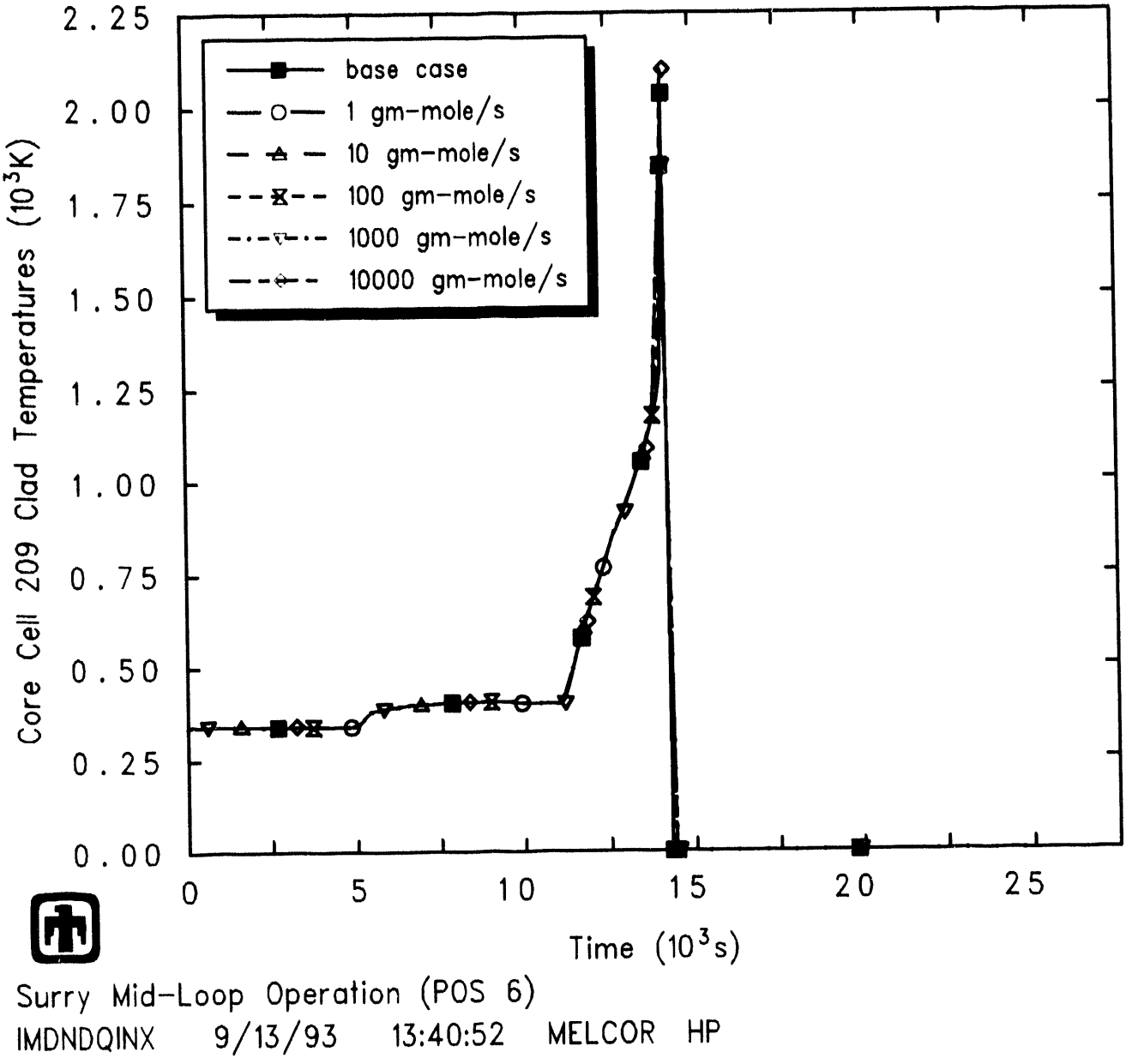

Figure 3.18. Core Ring 2, Level 9 Clad Temperatures in MELCOR Surry Midloop Calculations with Air Ingression

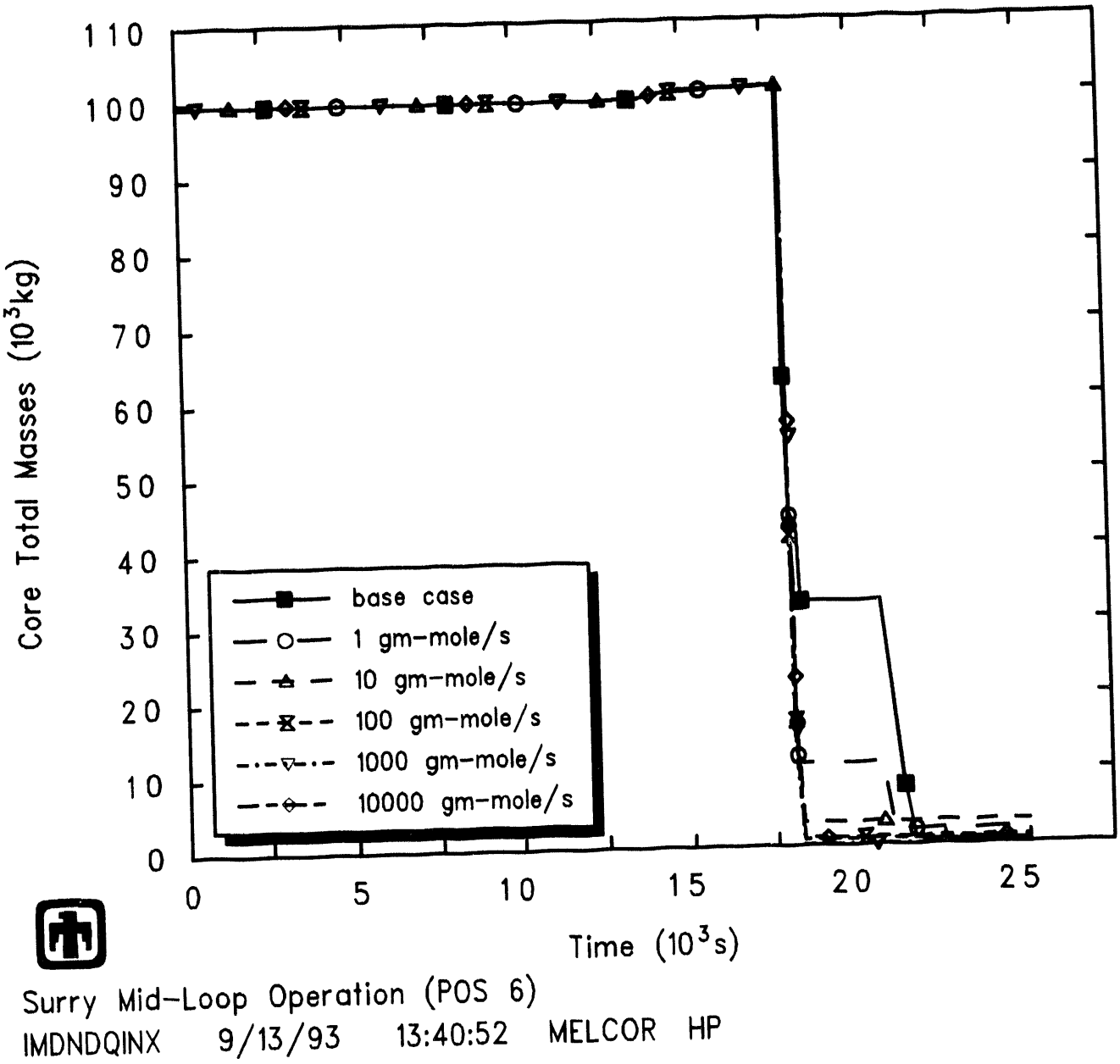

Figure 3.19. Total Core Masses in MELCOR Surry Midloop Calculations with Air Ingression

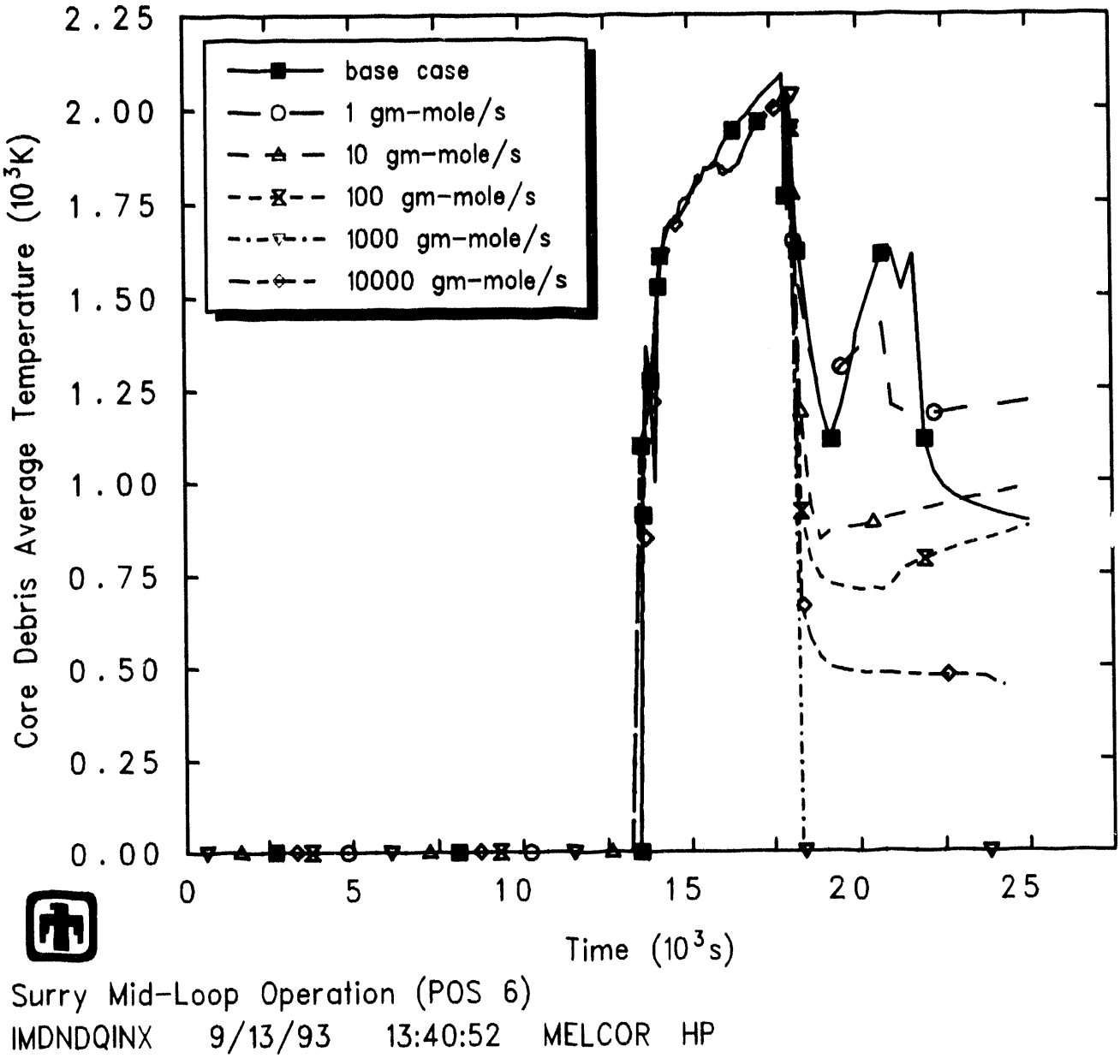

Figure 3.20. Core Average Debris Temperatures in MELCOR Surry Midloop Calculations with Air Ingression

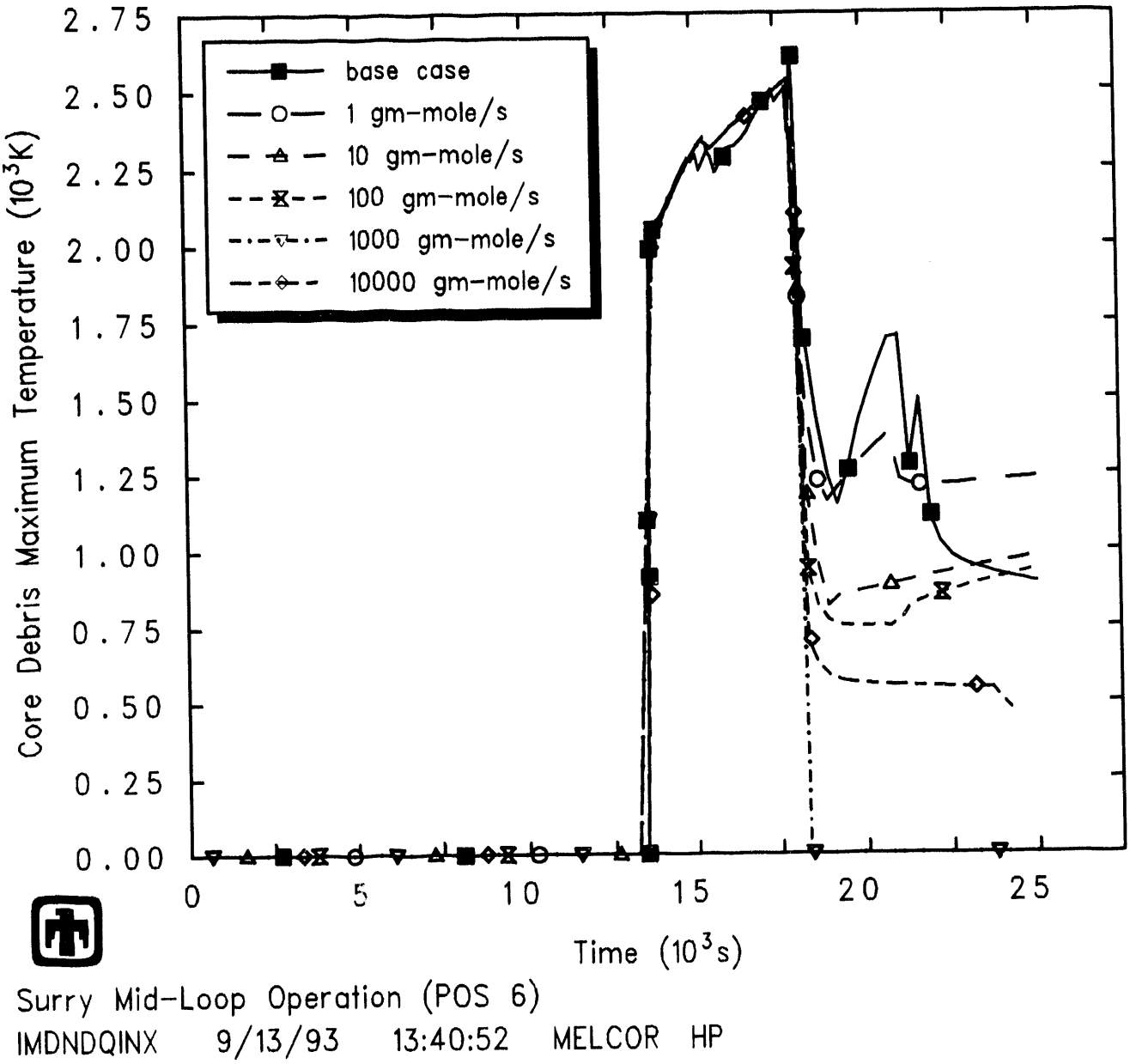

Figure 3.21. Core Maximum Debris Temperatures in MELCOR Surry Midloop Calculations with Air Ingression

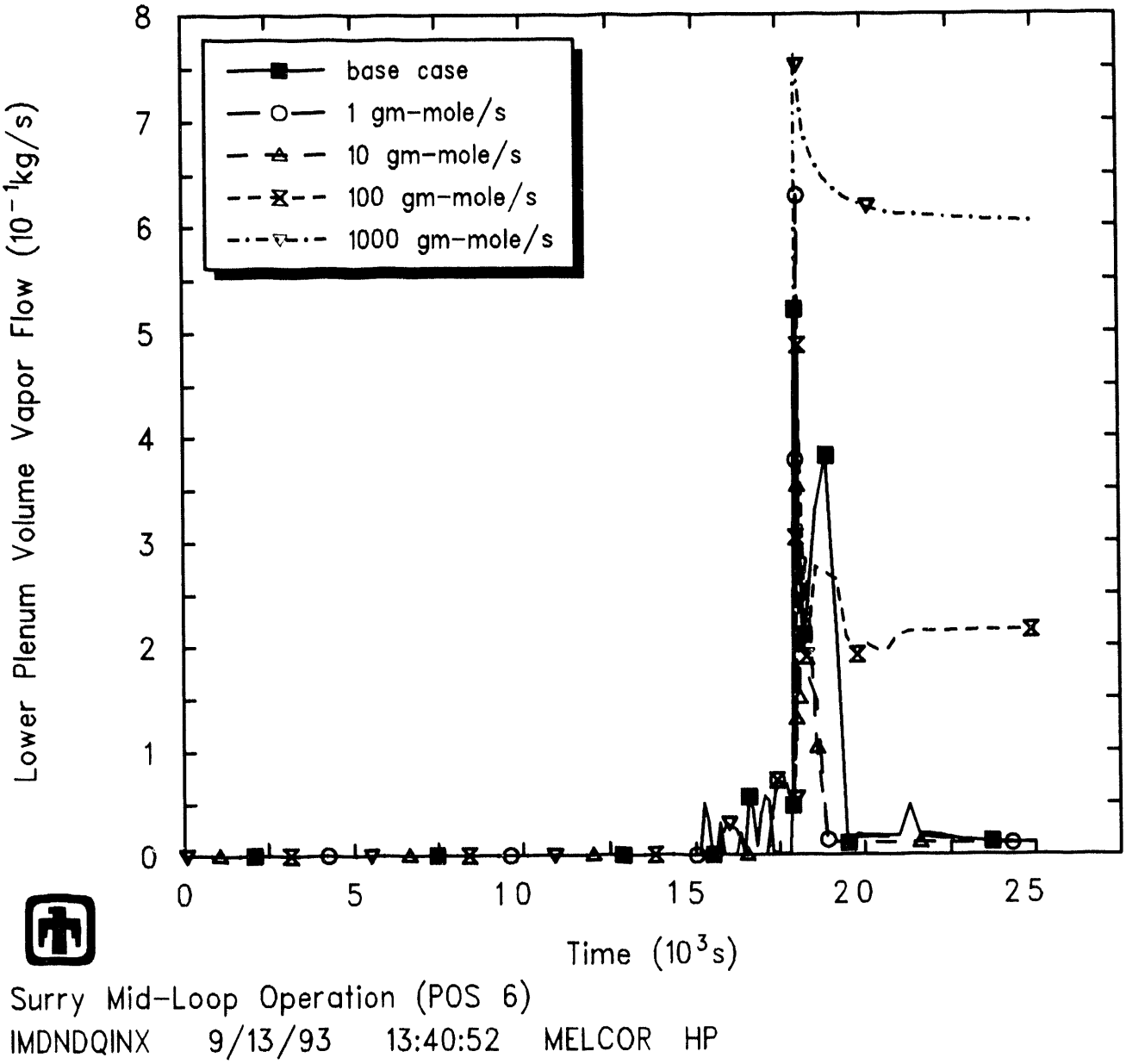

Figure 3.22. Lower Plenum Volume Vapor Flows in MELCOR Surry Midloop Calculations with Air Ingression

Table 3.2. In-Vessel Ruthenium Release in MELCOR Surry Midloop Calculations with Air Ingression

Air Ingression Rate		In-Vessel Release (% Initial Inventory)		
(kg/s)	(mole/s)	Core	Lower Plenum	Total
0	0	1.3×10^{-6}	1.92×10^{-5}	2×10^{-5}
0.032	$\simeq$1	0.07	3.67	3.74
0.32	$\simeq$10	9.24	1.44	10.68
3.2	$\simeq$100	71.64	.003	78.64
32	$\simeq$1,000	78.64	15.31	93.95
320	$\simeq$10,000	79.17	19.57	98.74
3200	$\simeq$100,000	79.23	20.54	99.77

Very little of the oxygen sourced into the core as part of the air ingression is consumed in Zircaloy oxidation. Table 3.3 presents the total amount of oxygen in the air ingression, the amounts of oxygen and steam consumed in-core by oxidation reactions, the amount of hydrogen produced in-vessel (through metal reaction with steam), and the total oxidation energy. The steam consumption and hydrogen production drop only slightly ($\leq$5%) over a wide range of air ingression rates. As would be expected, the oxidation energy rises as more oxygen is consumed, because of the enhanced heat generation from the $Zr+O_2$ reaction vs reaction with steam, but the increase is not very great because so little of the injected oxygen is consumed. Note that the amount of steam consumed in oxidation, the amount of hydrogen produced and the total oxidation energy include Zircaloy oxidation with steam prior to the specified air ingression (in addition to Zircaloy reaction with oxygen during air ingression), as well as oxidation of core and lower plenum structural steel with steam throughout the transient period calculated; there is currently no provision in MELCOR to edit the Zircaloy and steel oxidation reactions separately.

The assumed air ingression has the greatest effect on the ruthenium release, but also a small effect on the release for other radionuclides. Table 3.4 gives the in-vessel releases as a percentage of initial inventory present, calculated for other radionuclide classes. Note that, with the CORSOR-M option used, there is no in-vessel release of Class 7 (the early transition elements, represented by Mo), Class 9 (the trivalents, represented by La) or Class 11 (the more volatile main group elements, represented by Cd). As the rate of air ingression assumed is increased, there is very little change in the release fractions of the volatiles (*i.e.*, the noble gases, the alkali metals represented by Cs and the halogens represented by I). There is also very little change in the release fraction of the chalcogens, represented by Te, and apparently very little holdup in unoxidized Zircaloy clad in any case. Small increases in release fraction are seen for the alkaline earths, represented by Ba, and the less volatile main group elements, represented by Sn;

these two classes are intermediate in release ($\sim$1%) between the volatiles ($\leq$100% release) and the refractories ($\ll$1% release), and the small increases in release probably reflect the enhanced clad/fuel heatup from the $Zr+O_2$ reaction. In contrast, there is a decrease in the trace amounts of refractories released, for both the tetravalents represented by Ce and for uranium, in the calculations with air ingression assumed; this is probably due to the cooling effect of the air ingression on the core debris. There may be other changes in fission product release with air ingression, if other species are also sensitive to the oxygen potential as is ruthenium; however, any such additional effects air could have on the release and transport characteristics of other radionuclides were not modelled for these initial calculations. (For instance, we expect the U releases predicted remain very small because the reaction $UO_2 + 1/2\ O_2 \rightarrow UO_3(g)$ was not modelled; since this reaction generates a gaseous uranium oxide form, it would obviously greatly increase the release of U from the fuel.)

Table 3.3. In-Vessel Oxidation in MELCOR Surry Midloop Calculations with Air Ingression

Air Ingression		Consumed in Oxidation		Produced in Oxidation	
Flow Rate (mole/s)	Total O_2 (kg)	Oxygen (kg)	Steam (kg)	Hydrogen (kg)	Energy (MJ)
0†	0	0.2044	1864	208.6	29,936
≃1†	42.66	3.404	1823	204.0	29,257
≃10†	426.1	9.938	1812	202.8	29,374
≃100†	4,307	46.02	1804	201.8	30,519
≃1,000†	42,380	111.8	1791	200.4	32,428
≃10,000‡	355,500	81.73	1791	200.4	31,396

†run to 25,000s

‡run to 24,222s, to code failure

Table 3.4. In-Vessel Radionuclide Release in MELCOR Surry Midloop Calculations with Air Ingression

Air Ingression (mole/s)	In-Vessel Release (% Initial Inventory)			
	Class 1 (Xe)	Class 2 (Cs)	Class 4 (I)	Class 5 (Te)
0	80.95	80.98	80.94	79.05
≃1	81.40	81.42	81.38	79.65
≃10	81.24	81.27	81.25	79.47
≃100	80.99	80.98	80.98	79.14
≃1,000	80.83	80.83	80.81	78.95
≃10,000	80.59	80.54	80.57	78.67
	Class 3 (Ba)	Class 8 (Ce)	Class 10 (U)	Class 12 (Sn)
0	0.217	8.241×10^{-6}	1.786×10^{-3}	2.646
≃1	0.269	1.840×10^{-6}	1.351×10^{-3}	3.218
≃10	0.269	1.836×10^{-6}	1.348×10^{-3}	3.213
≃100	0.265	1.791×10^{-6}	1.319×10^{-6}	3.173
≃1,000	0.261	1.787×10^{-6}	1.316×10^{-6}	3.164
≃10,000	0.262	1.784×10^{-6}	1.311×10^{-3}	3.144

4 MELCOR Surry TMLB' Calculations with Surge Line Break and Air Ingression

A set of two MELCOR calculations has been completed examining the impact from interaction of air with residual fuel following vessel rupture in the Surry PWR for a station blackout scenario in which a surge line rupture has occurred during the in-core damage phase of the accident. The surge line rupture is expected to create a "chimney-like" flow of air into the core region following vessel breach [1]. While MELCOR can calculate the inflow of gases from the cavity up though the core and out the surge line break in such a situation, it predicts little or no oxygen present in the cavity source region during this period as the original cavity atmosphere is all displaced by steam and noncondensables generated in core-concrete interactions. Either a specific code model for single-phase countercurrent flow or a noding with multiple subdivided flow paths with different elevation differences, flow areas and loss coefficients would be needed to calculate hot cavity gases flowing up into the dome (or out into the basement) simultaneously with colder containment atmosphere flowing down into the cavity. That noding modification was not tried for the calculations in this study. Instead, air was sourced into the core region beginning immediately after vessel failure, at a rate determined from the sensitivity studies described in Section 3 for mid-loop calculations with air ingression.

The deck used was our standard Surry TMLB' deck [18]. A high-pressure station blackout scenario was run with the most recent code version, and the vessel lower head calculated failure time determined to be 11,422s. A surge-line-break flow path was then added to the deck, and the valve controller specified to open the assumed surge-line break at 10,500s, the time selected as ~15min before vessel failure in the high-pressure scenario. At this time, the core is mostly uncovered and the core outlet temperature and most of the clad temperatures are >1273K. (This is similar to the approach taken in previous MELCOR analyses of a Surry station blackout with surge line failure, described in more detail in [22].)

A reference calculation was done with the surge line break and with no air ingression forced, and another calculation was done with ≃100mole/s air ingression; both calculations were run to 30,000s. In the latter case, a flow path was defined going from the containment dome to the core, and a constant velocity flow was specified to start immediately at vessel failure. The containment dome was used as the air source volume instead of the cavity because the cavity air was quickly displaced by steam and/or hydrogen, while the containment dome atmosphere remained mostly ~80%-N_2/~20%-O_2 with less dilution by steam, hydrogen and other noncondensables generated by core-concrete interaction. The velocity needed to obtain desired molar flows was estimated based upon STP conditions, not adjusted for containment pressurization; the ~20% increase between the actual flow obtained using a velocity estimated based on STP conditions and the desired air flow (≃100mole/s) was considered negligible.

There was obviously no change in the transient sequence in these three calculations prior to the surge line failure. Initiating the surge line break interrupted the core heat-up

and degradation process, with core level swell and enhanced steam cooling temporarily driving most of the core back to saturation temperatures. The heatup then resumed, and the vessel lower head failed at 14,555s, $\leq$1hr later than in the high-pressure scenario. Figure 4.1 shows the swollen and collapsed liquid levels in the core for these three calculations, while Figure 4.2 shows the clad temperatures in a cell in the inner core ring, about 1.3m above the core support plate and about 0.3m below the core midplane, a typical response. (The location of that core cell can be found by referring to the MELCOR Surry core nodalization presented in Figure 3.1.)

Results for the two calculations with the surge line break, with and without user-specified air ingression into the core, continued to remain identical until the air ingression specified began at the time of vessel failure. Table 4.1 summarizes the state of the various materials in the core active fuel region, core plate and lower plenum at the time a lower head penetration first fails (*i.e.*, at vessel breach); this state is common to the surge line break calculations done with and without air ingression, because the air ingression is specified to start at vessel breach. Masses of intact components and of debris components are given for each region, together with average temperatures for the debris in the lower plenum, and fractions of Zircaloy and steel oxidized by the time of vessel breach. The fraction of debris molten in each region is estimated from the average debris temperature, which in this case resulted in assuming that most of the Zircaloy, steel, steel oxide and control rod poison in the debris are molten and that UO_2 and ZrO_2 in the debris are solid (*i.e.*, neglecting eutectics mixtures; this assumption is forced by the MELCOR output available to the analyst). Also given is the fraction of material relocated. This is generally larger than the fraction molten because material can melt and relocate, and then subsequently refreeze or quench; also, MELCOR usually relocates UO_2 fuel as a solid, after clad collapse but before fuel melt.

(Note that the total material masses present in the core as shown in this table and in the various plots in this section differ from the corresponding results in for the midloop calculations with air ingression presented in Section 3, because in that input model the $\sim 30 \times 10^3$kg of lower plenum structural steel was modelled using heat structures, which cannot oxidize, melt or relocate, while in these TMLB' calculations with surge line rupture and air ingression that lower plenum structural steel was included in the core package modelling as material that could oxidize, melt and relocate.)

The various materials in the MELCOR "fuel/clad" component just prior to vessel failure, both any intact materials remaining in their original position and candled, refrozen conglomerate debris materials, are shown in Figures 4.3 through 4.5 for the three radial rings in the MELCOR Surry core model. Figures 4.6 through 4.8 show the materials calculated to be in the "particulate debris" component in the three core rings at the same time, while the various materials in the MELCOR "other-structure" component just prior to vessel failure, both intact materials and candled, refrozen conglomerate debris materials, are shown in Figures 4.9 through 4.11 for the three core rings in the MELCOR Surry core model. (Refer to [8] for an explanation of these MELCOR components, if necessary.) The "elevation" used as the ordinate in Figures 4.3 through 4.11 is the same as the core level elevations shown in Figure 3.1, with the core support plate

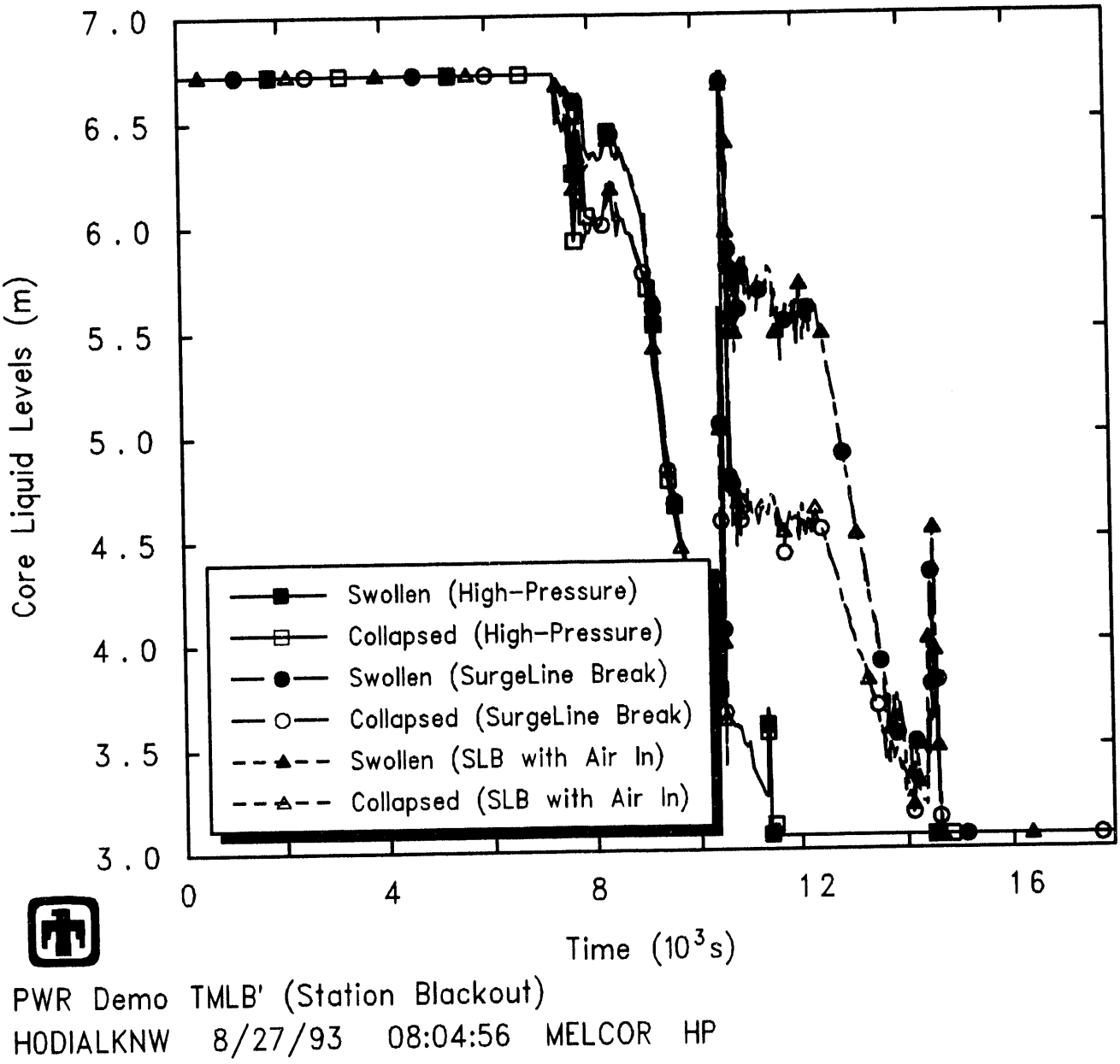

Figure 4.1. Core Liquid Levels in MELCOR Surry TMLB' Calculations with Surge Line Break and Air Ingression

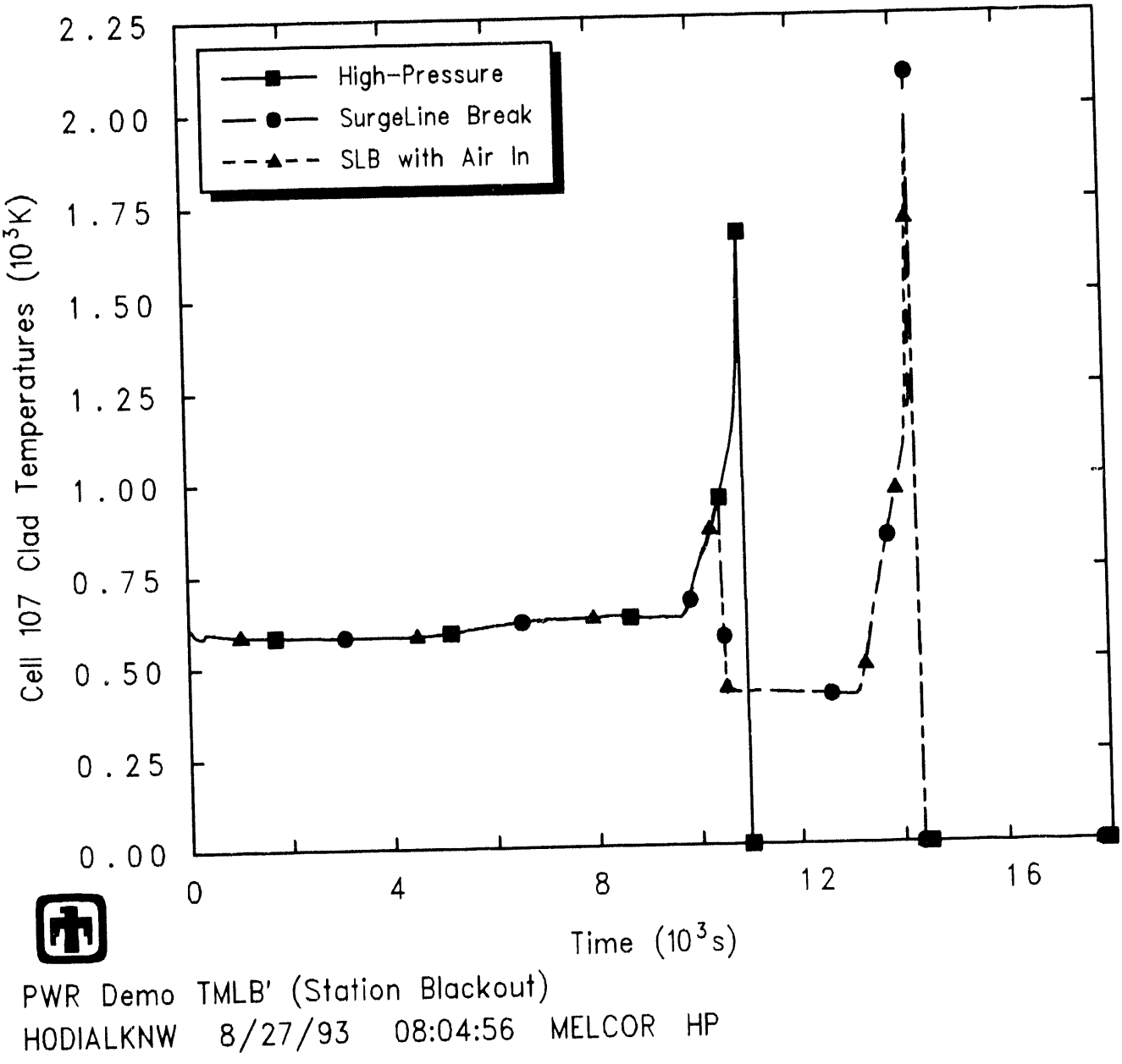

Figure 4.2. Ring 1, Level 7 Clad Temperatures in MELCOR Surry TMLB' Calculations with Surge Line Break and Air Ingression

Table 4.1. Core State at Vessel Failure in MELCOR Surry TMLB' Calculations with Surge Line Failure and Air Ingression

	Intact	Debris
Active Fuel Region Masses (kg)		
UO_2	43,185	1,018
Zircaloy	9,774	41
Zirc Oxide	301	99
Steel	295	0
Steel Oxide	17	0
CRP	1,672	0
Total	55,244	1,158
Core Plate Masses (kg)		
UO_2		946
Zircaloy		51
Zirc Oxide		86
Steel	1,815	1
Steel Oxide	0	2
CRP		0
Total	1,815	1,086
Lower Plenum Masses (kg)		
UO_2		35,563
Zircaloy		4,030
Zirc Oxide		2,453
Steel	32,663	93
Steel Oxide	20	46
CRP		334
Total	32,683	42,519
Average Debris Temperature (K)		
Active Fuel Region		~2340
Core Plate		~2200
Lower Plenum		~2020
Fraction Debris Molten		
Active Fuel Region		~3%
Core Plate		~5%
Lower Plenum		~1%
Fraction Material Relocated	~45%	
Fraction Oxidized	Zircaloy	Steel
	~18.3%	~0.265

at ≥3m, the lower plenum between 0 and ~3m, and the active fuel region from ≥3m to ~6.722m. The fraction of each core cell occupied by any given material is shown. However, recall that the core cells are not equal in the three rings; the innermost, high-powered ring includes ~15% of the core, the middle ring contains ~60% of the core, and the outermost, low-power ring includes the remaining ~25% of the core.

As in the core state at vessel failure for the midloop operation analyses, the innermost ring has no intact structure in the active fuel region at all at the time of vessel failure for these surge-line break calculations (Figure 1.3). However, in this case there is a smaller but still substantial debris bed only in the lower plenum in that first ring (Figure 4.6), with a very small amount of debris still held above the failing core plate. About half of the intact material remains in the active fuel region in the second ring (Figure 4.4), with those intact materials together with the core plate supporting a small amount of particulate debris in the active fuel region (Figure 4.7); note that, unlike the results in the midloop operation core state predicted at vessel failure, a substantial debris bed is found in the lower plenum in the second ring as well as in the first ring in these full-power station blackout with surge line break calculations. Almost all of the intact material remains in place in the active fuel region in the third ring (Figure 4.5); there is little or no particulate debris retained in the active fuel region in the third ring (Figure 4.8), but again a substantial debris bed in the lower plenum. The core plate itself is clearly visible in Figures 4.9 through 4.11 as the very thin structure at ≥3m elevation; the substantial mass of lower plenum structural steel modelled as a core component in these surge line break analyses is also clearly visible in Figures 4.9 through 4.11. Some intact other structure and some candled, refrozen other structure, such as control rod poison and the control rod guide tube material, are visible in the middle of the active fuel region in Figures 4.10 and 4.11. Note that only ≤20% of the Zircaloy (and <1% of the steel) has been oxidized up to this time, either in the intact clad or in the debris bed; most of the Zircaloy remains unoxidized in both the remaining intact clad and in the debris bed at the time of vessel failure and at the specified start of the assumed air ingression.

The air ingression begun at vessel breach does not produce any major changes in the subsequent accident progression, but does affect the core atmosphere, the core materials and the fission product release, directly through air oxidation of the clad and enhanced ruthenium release, and indirectly by slightly changing the later-time core clad and debris temperatures. Figure 4.12 shows the clad temperatures in a cell in the outer core ring, about 2m above the core support plate, with a slightly accelerated heatup of the clad just before melt and failure in the calculation with air ingression, due to the higher energy of reaction with air rather than with steam (a response typical of other core cells).

Figure 4.13 through 4.16 demonstrate the effect of the air ingression on the core mole fractions of steam and of nitrogen, oxygen and hydrogen, respectively. Without any air ingression the core atmosphere consists mostly of steam prior to vessel failure and mostly hydrogen after vessel failure; with air ingression, the core atmosphere is ~35% air and ~60% steam after vessel failure, with very little (≤5%) hydrogen due to the preferential oxidation of Zircaloy clad by reaction with oxygen.

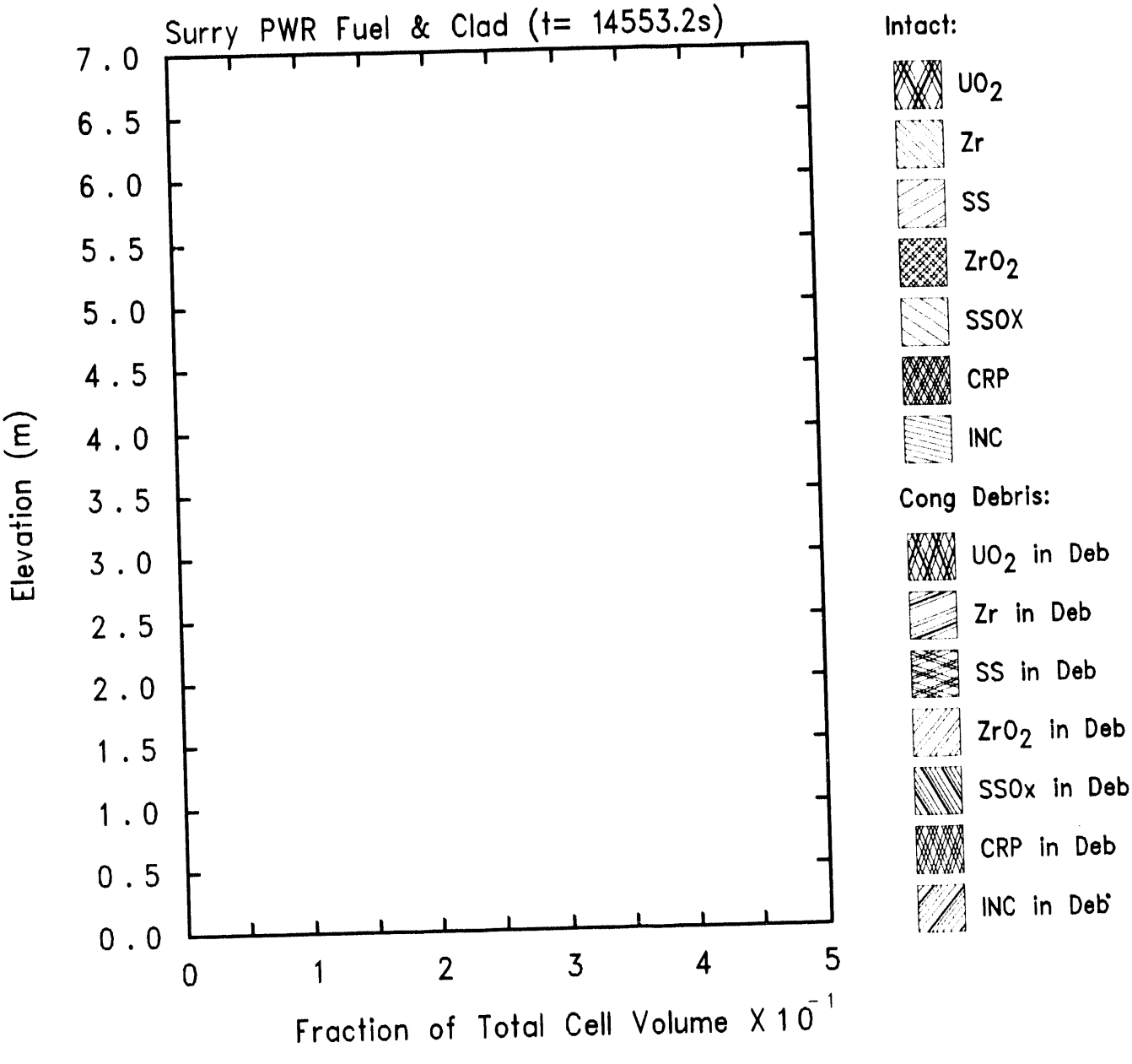

Figure 4.3. Core Ring 1 Fuel/Clad Component Materials at Vessel Failure in MELCOR Surry TMLB' Calculations with Surge Line Failure and Air Ingression

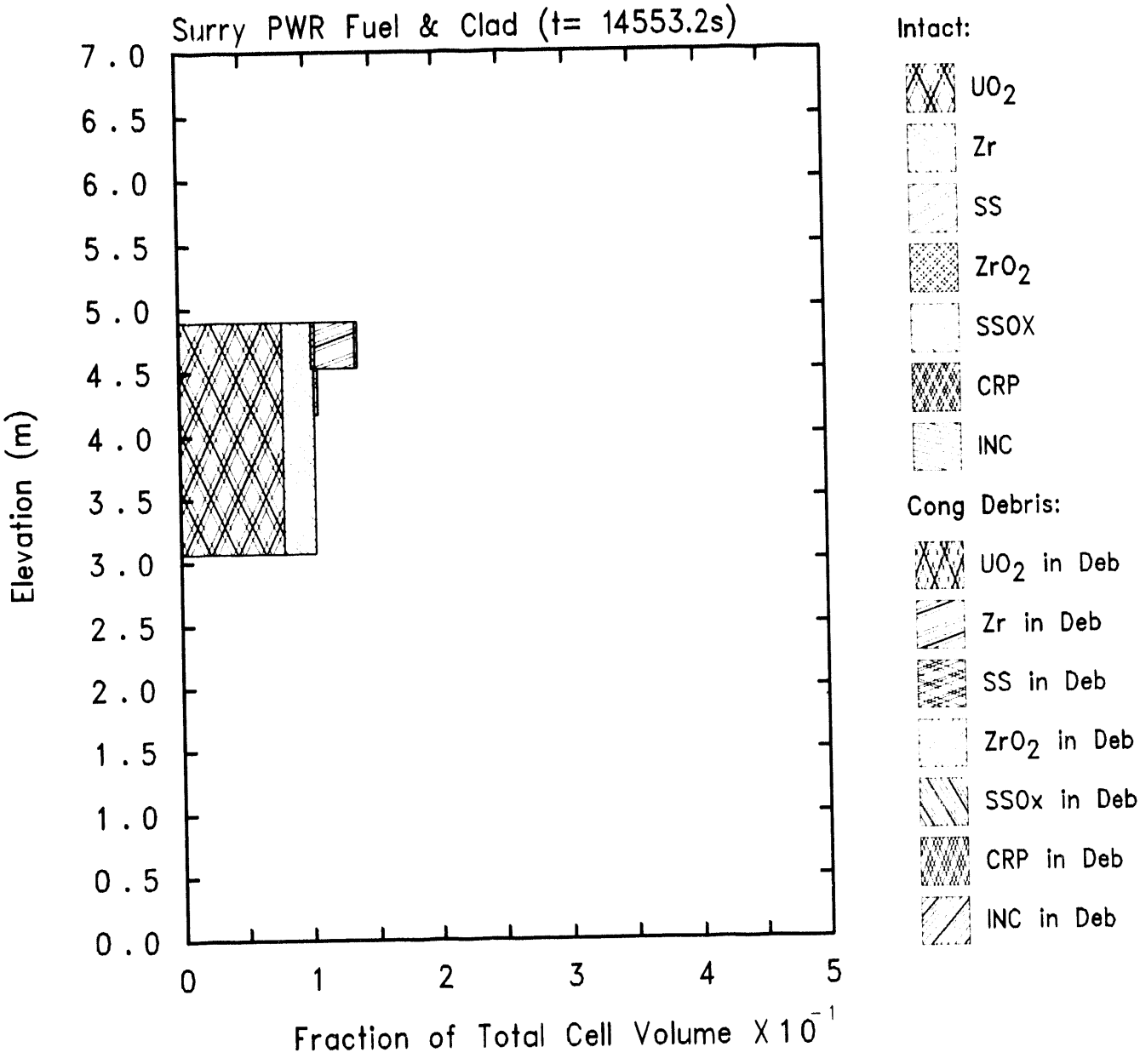

Figure 4.4. Core Ring 2 Fuel/Clad Component Materials at Vessel Failure in MELCOR Surry TMLB' Calculations with Surge Line Failure and Air Ingression

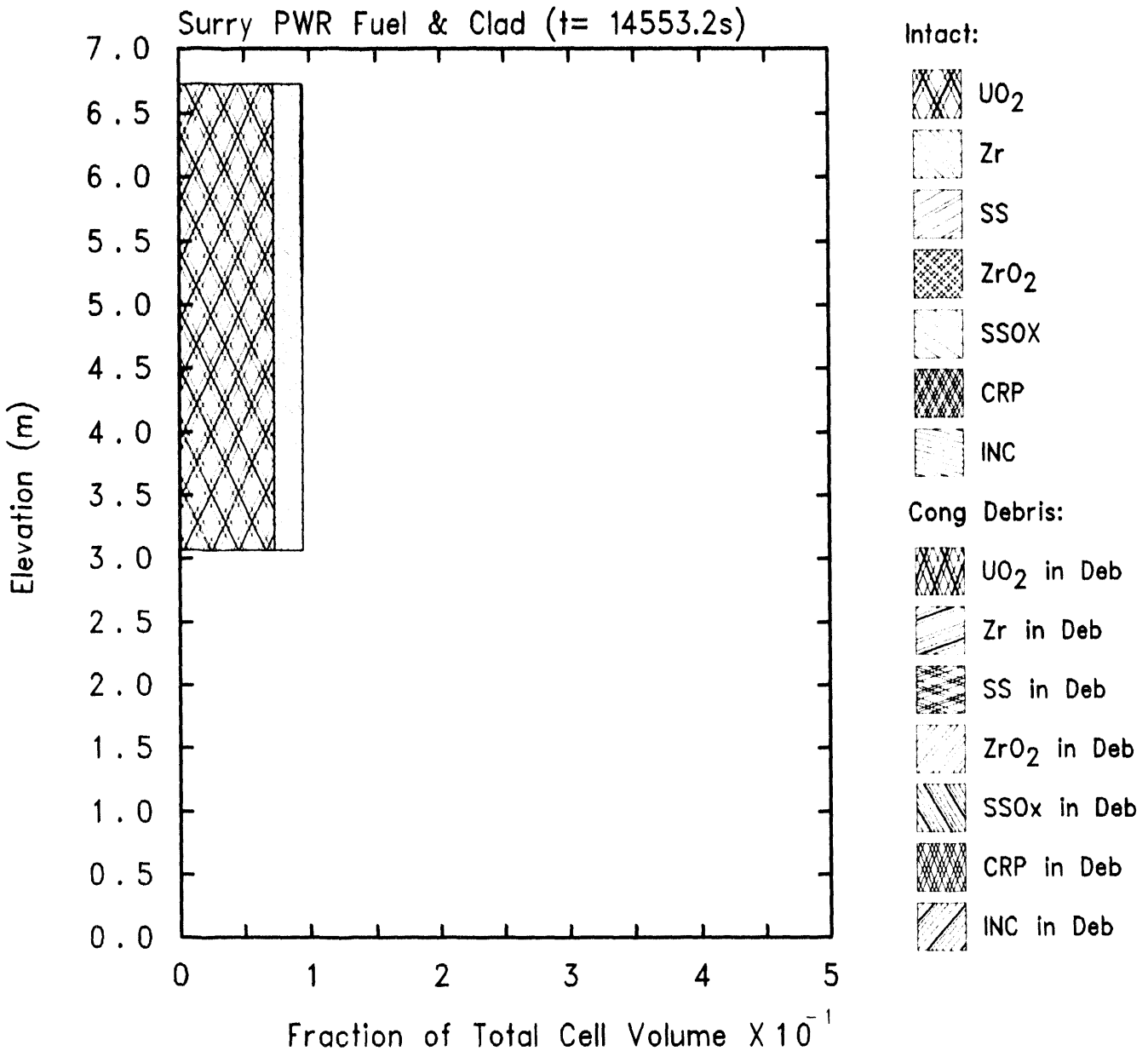

Figure 4.5. Core Ring 3 Fuel/Clad Component Materials at Vessel Failure in MELCOR Surry TMLB' Calculations with Surge Line Failure and Air Ingression

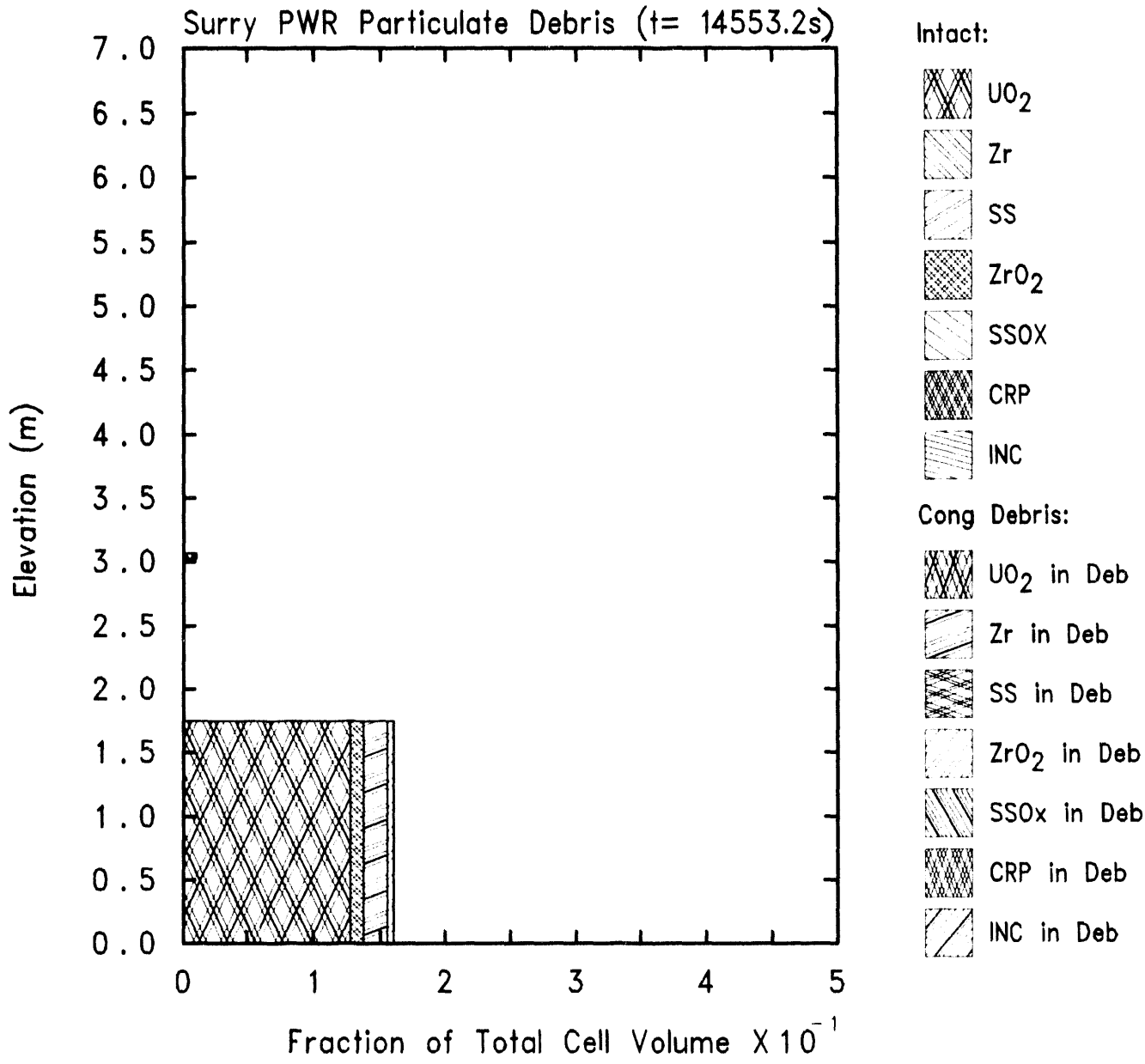

Figure 4.6. Core Ring 1 Particulate Debris Component Materials at Vessel Failure in MELCOR Surry TMLB' Calculations with Surge Line Failure and Air Ingression

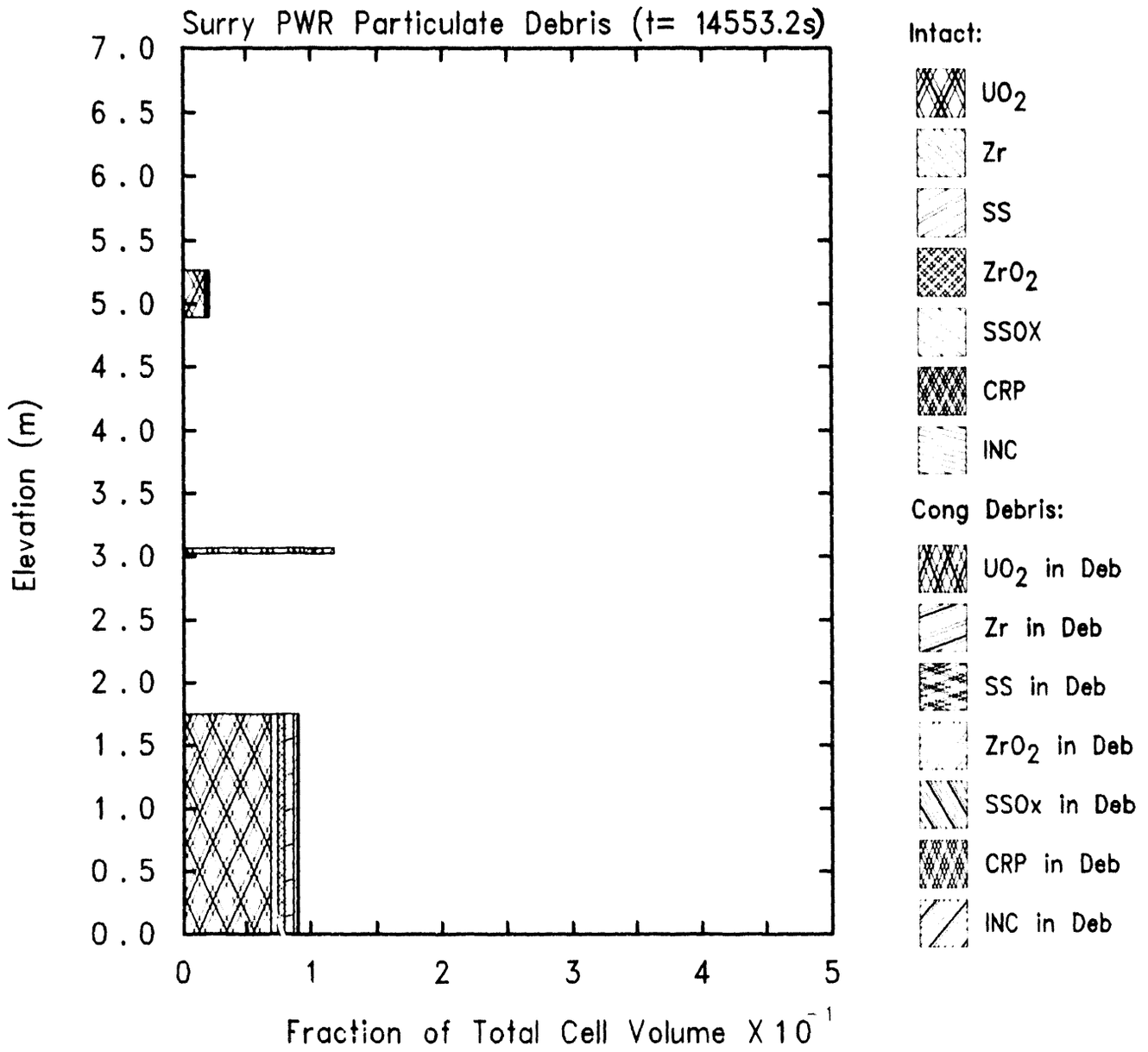

Figure 4.7. Core Ring 2 Particulate Debris Component Materials at Vessel Failure in MELCOR Surry TMLB' Calculations with Surge Line Failure and Air Ingression

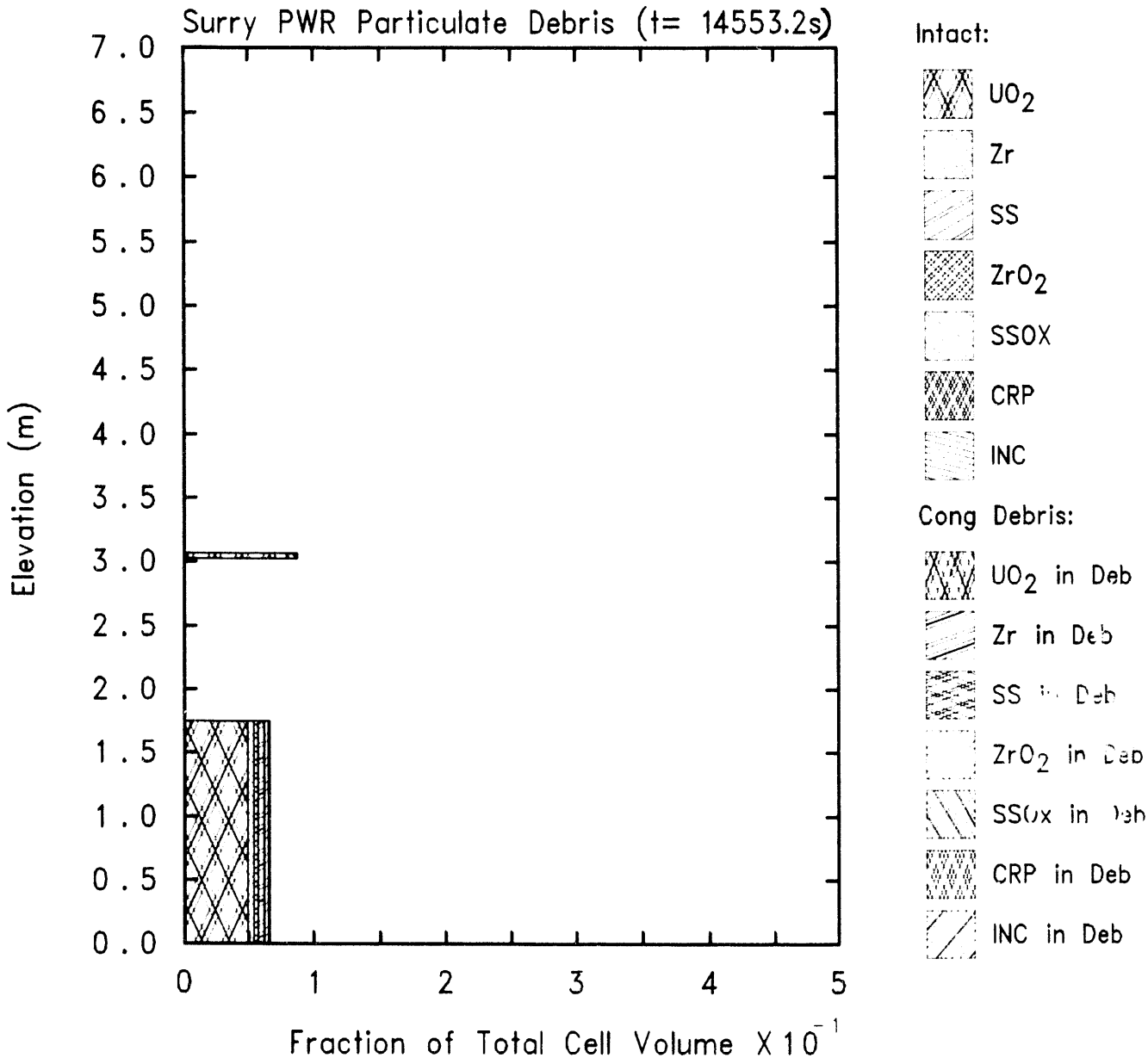

Figure 4.8. Core Ring 3 Particulate Debris Component Materials at Vessel Failure in MELCOR Surry TMLB' Calculations with Surge Line Failure and Air Ingression

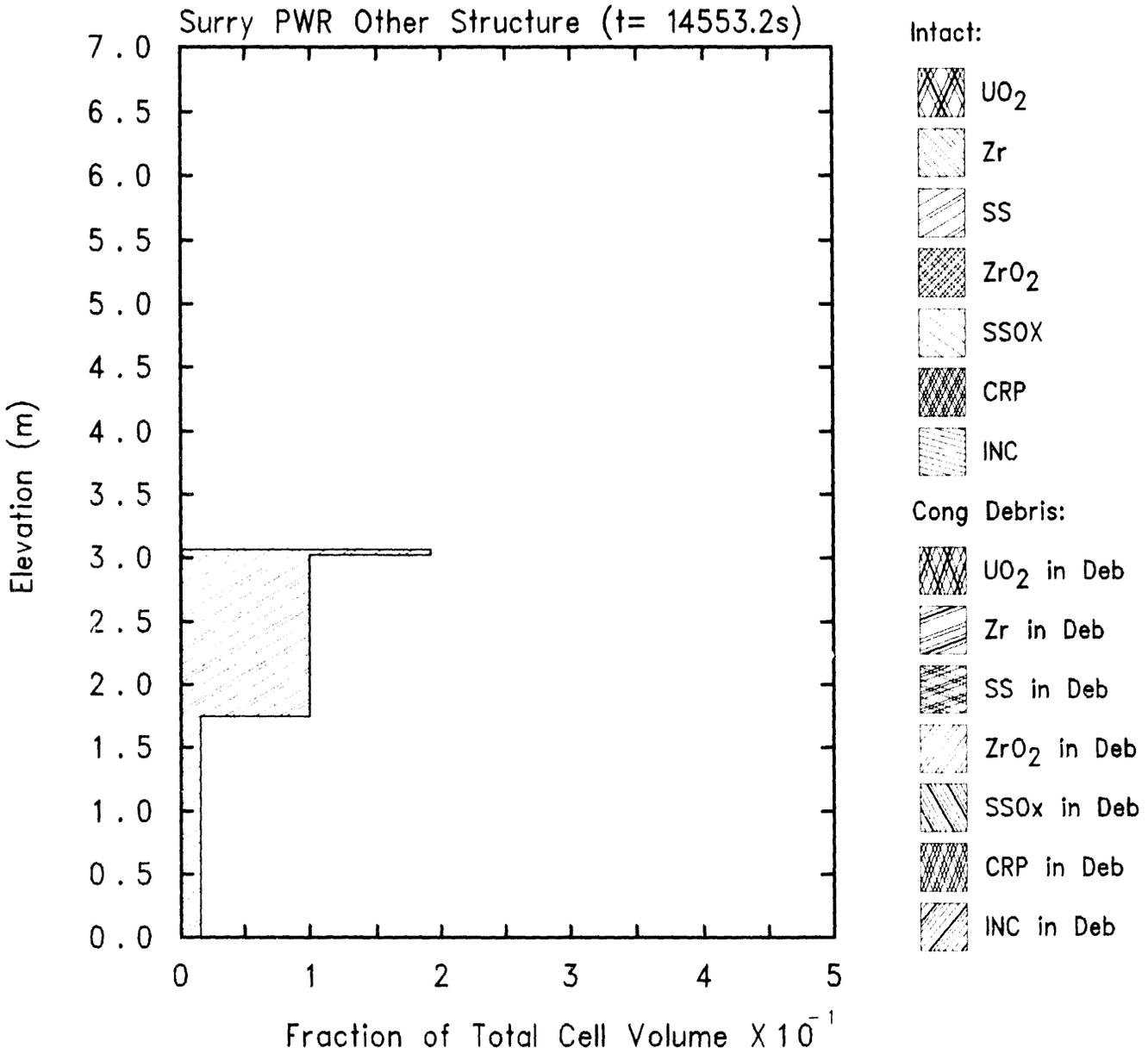

Figure 4.9. Core Ring 1 Other Structure Component Materials at Vessel Failure in MELCOR Surry TMLB' Calculations with Surge Line Failure and Air Ingression

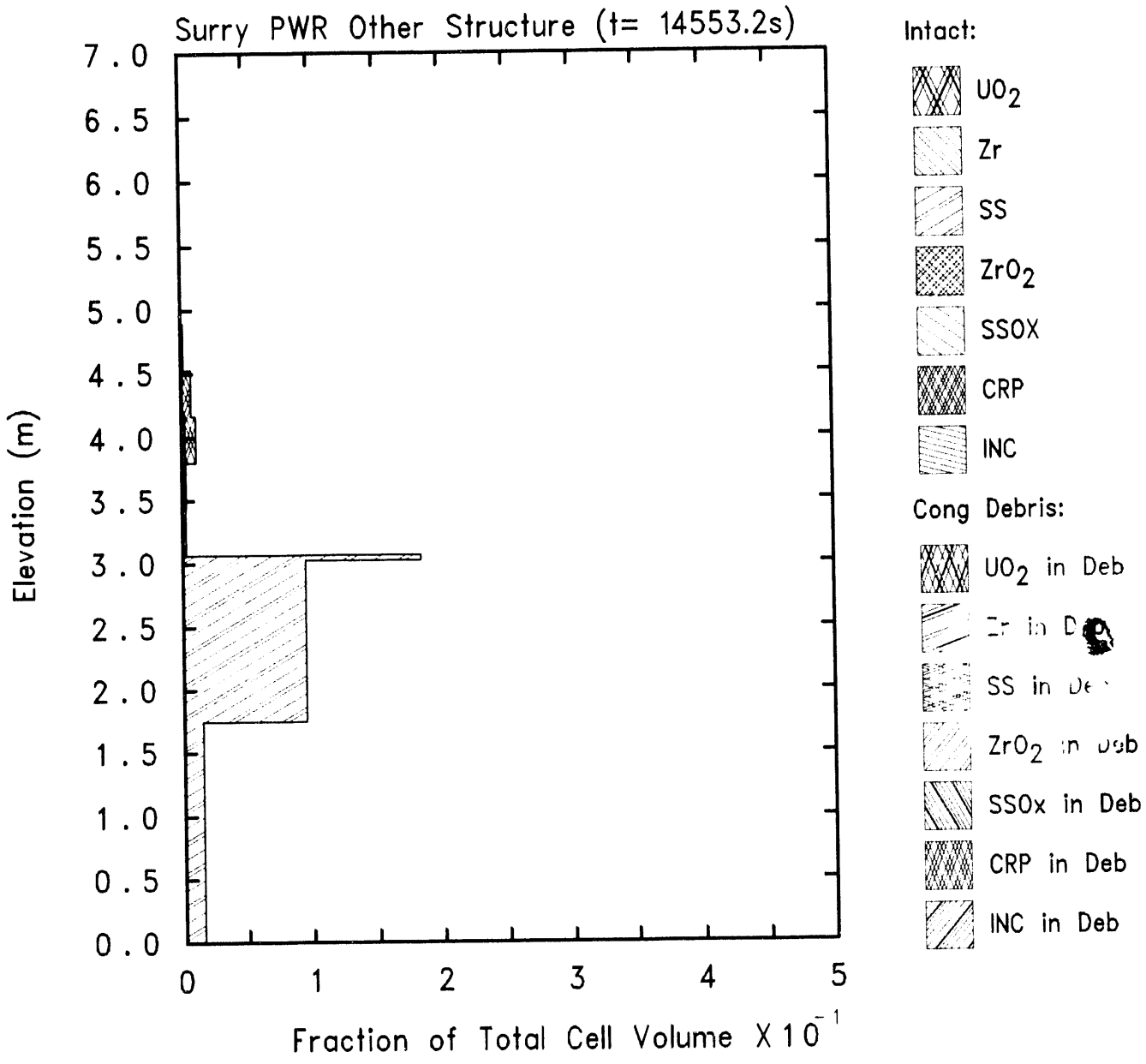

Figure 4.10. Core Ring 2 Other Structure Component Materials at Vessel Failure in MELCOR Surry TMLB' Calculations with Surge Line Failure and Air Ingression

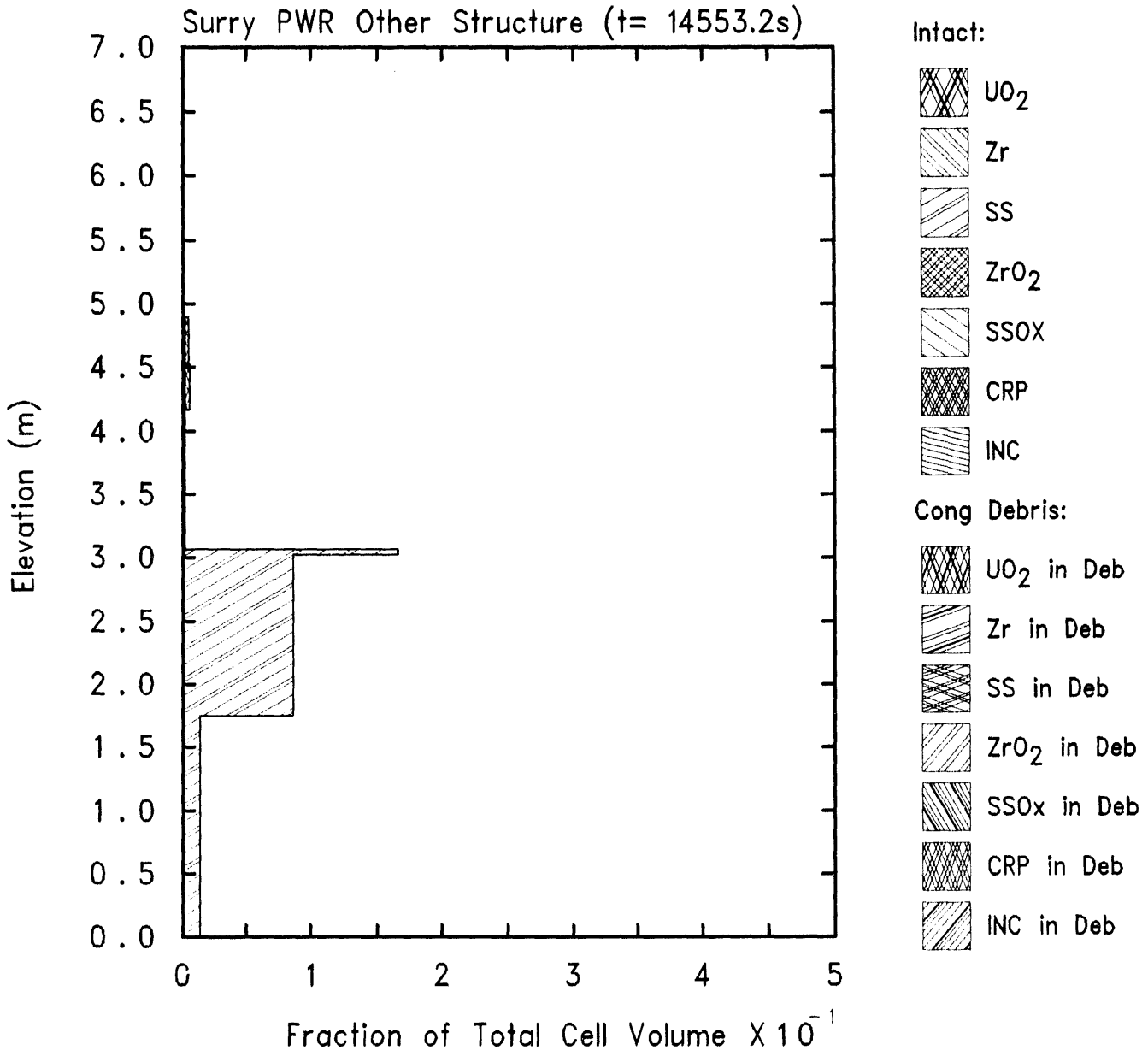

Figure 4.11. Core Ring 3 Other Structure Component Materials at Vessel Failure in MELCOR Surry TMLB' Calculations with Surge Line Failure and Air Ingression

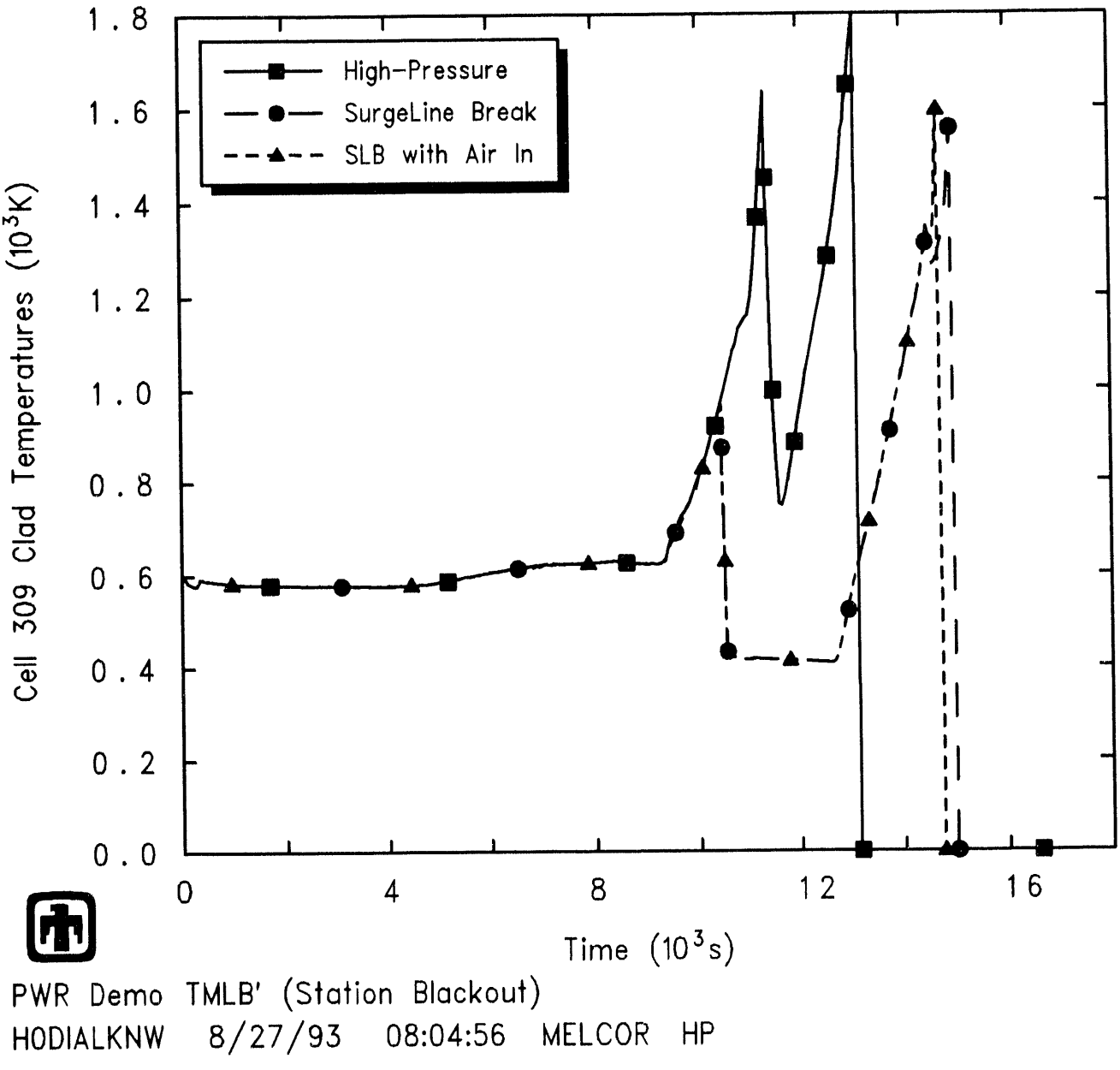

Figure 4.12. Ring 3, Level 9 Clad Temperatures in MELCOR Surry TMLB' Calculations with Surge Line Break and Air Ingression

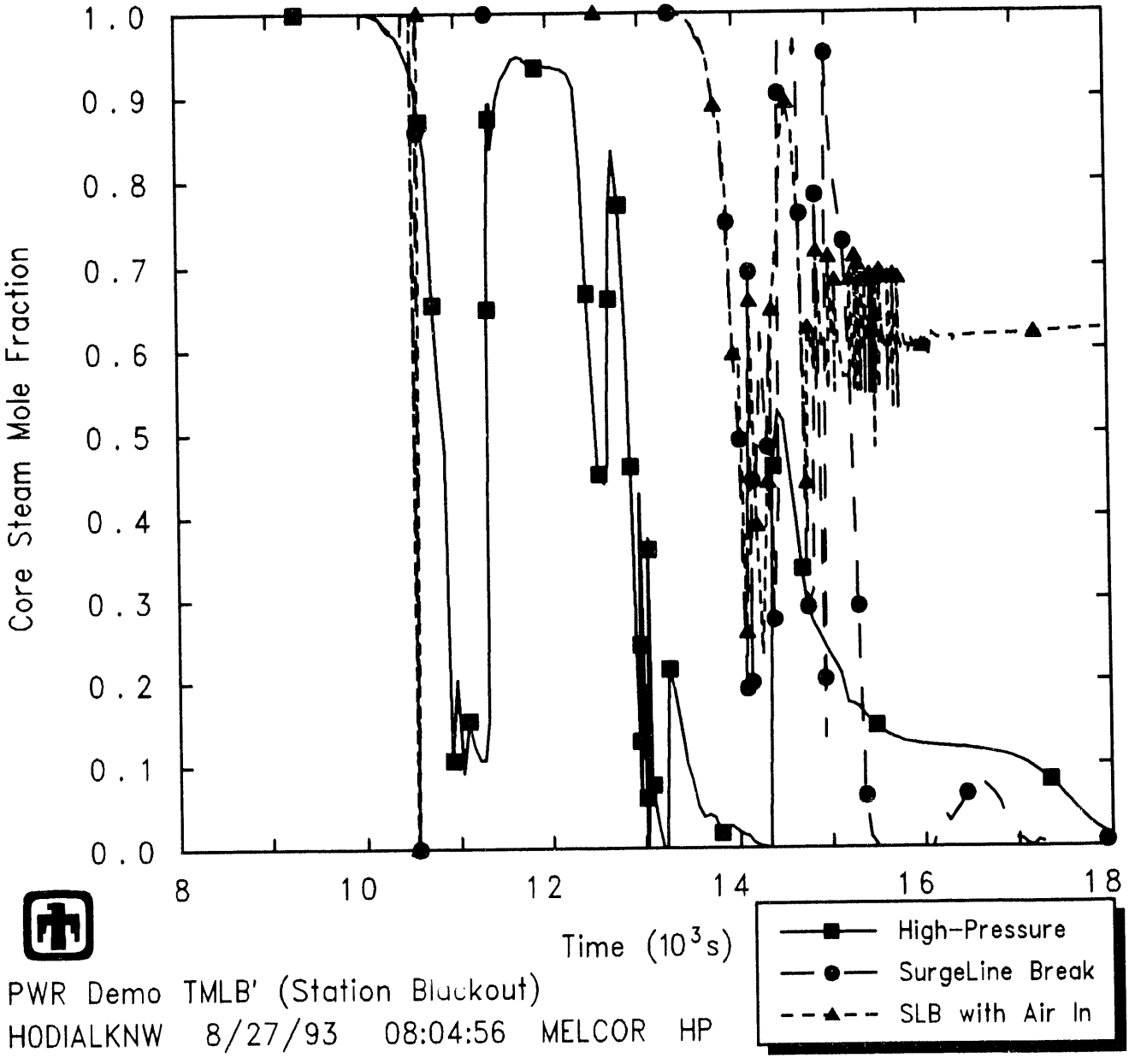

Figure 4.13. Core Active Fuel Region Steam Mole Fractions in MELCOR Surry TMLB' Calculations with Surge Line Break and Air Ingression

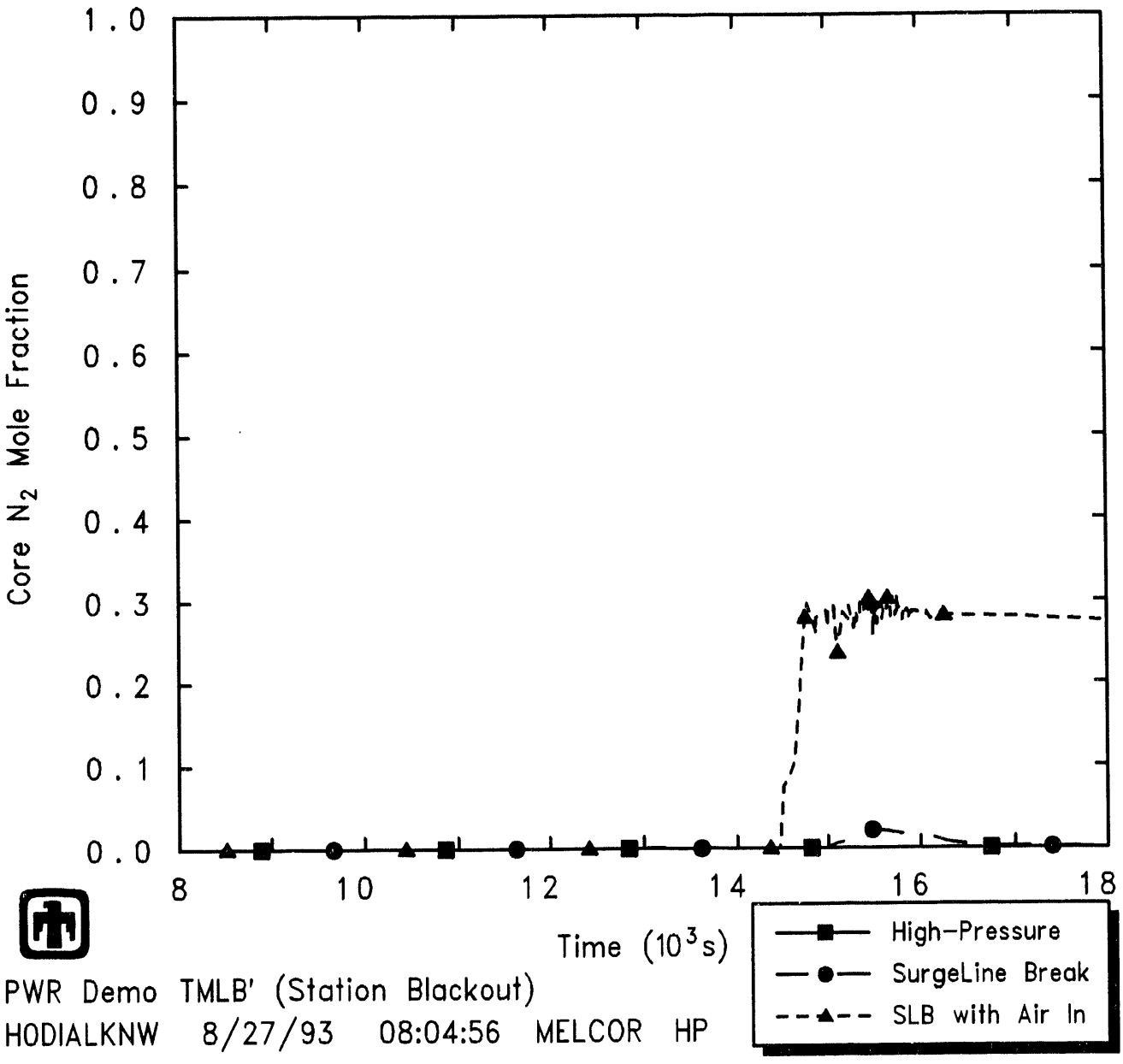

Figure 4.14. Core Active Fuel Region Nitrogen Mole Fractions in MELCOR Surry TMLB' Calculations with Surge Line Break and Air Ingression

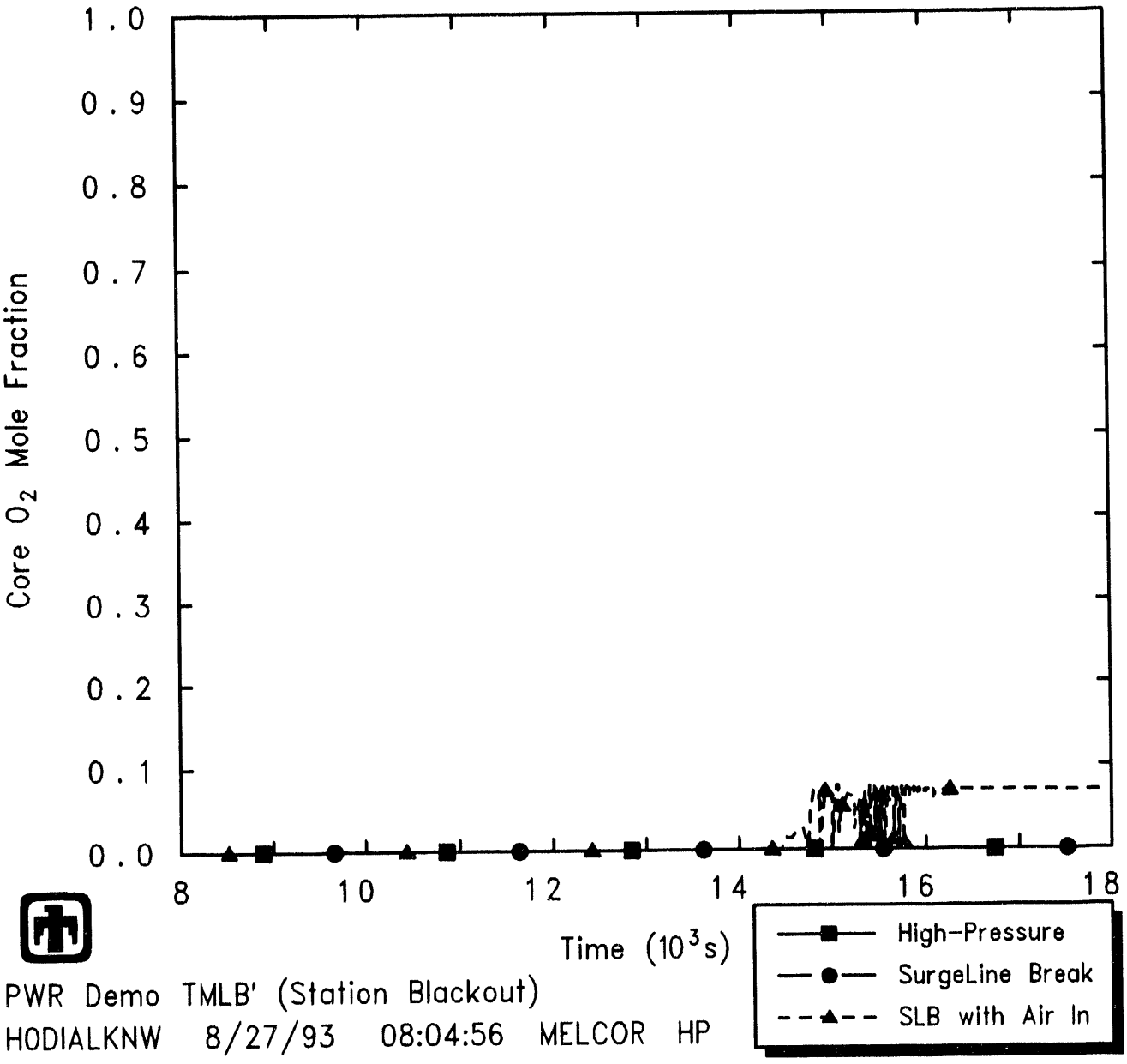

Figure 4.15. Core Active Fuel Region Oxygen Mole Fractions in MELCOR Surry TMLB' Calculations with Surge Line Break and Air Ingression

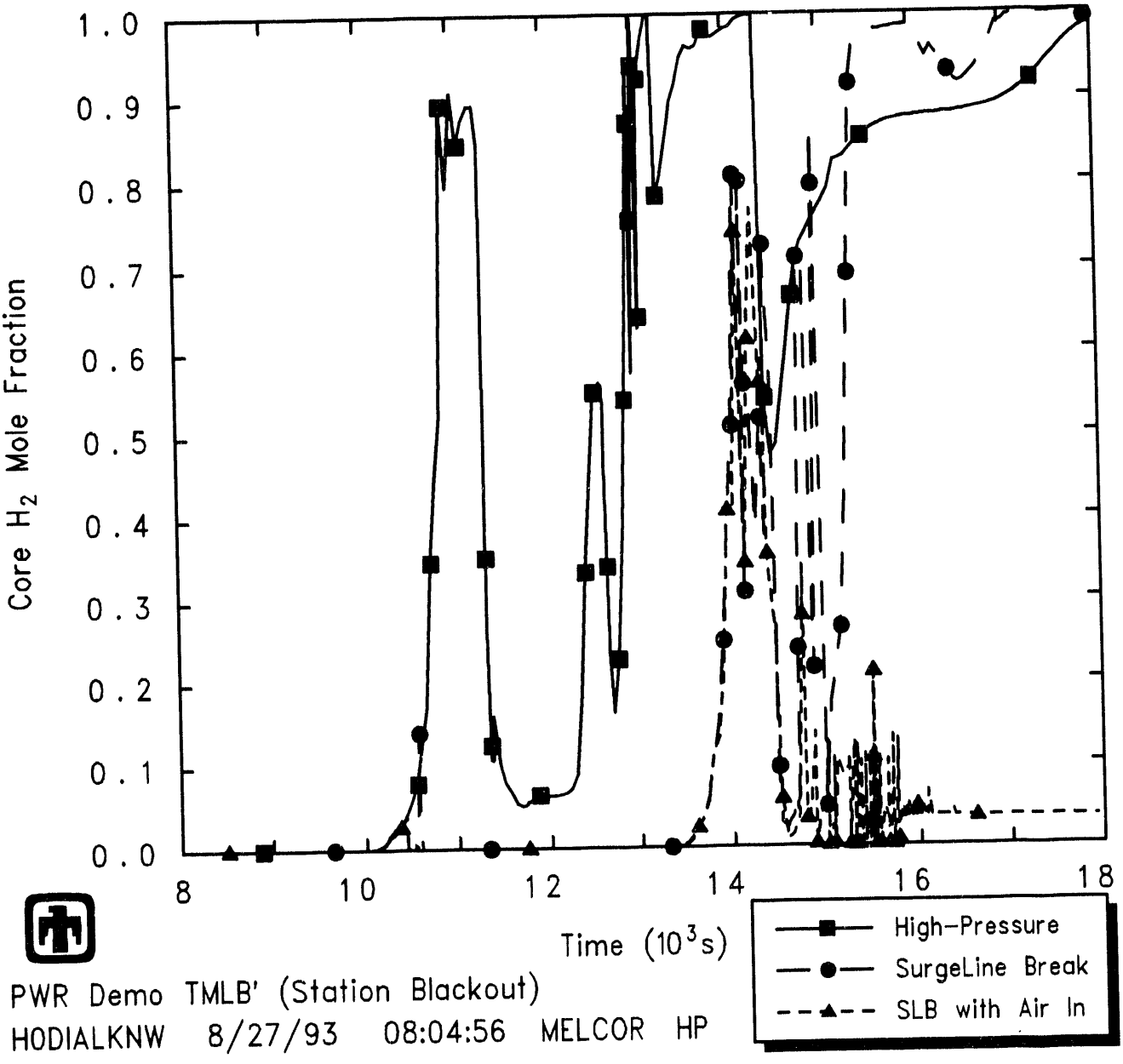

Figure 4.16. Core Active Fuel Region Hydrogen Mole Fractions in MELCOR Surry TMLB' Calculations with Surge Line Break and Air Ingression

The biggest difference in results in the two calculations with the surge line break, with and without user-specified air ingression into the core, is found in the ruthenium fission product releases, as expected. Table 4.2 summarizes the in-vessel ruthenium release fractions, normalized to the initial inventory of class 6 radionuclides (151.1kg). The in-vessel releases are subdivided into releases in the "core" and "lower plenum" regions in this table. The "core" region is the active fuel region, above the core support plate, and includes releases from both intact fuel and from debris still supported by intact core components or by the core support plate; the "lower plenum" release is from debris that has fallen through the core support plate and is being held in the lower plenum on the vessel lower head prior to being lost to the cavity through a lower head failure. There is a significant ruthenium release in-vessel ($\leq$50% of the inventory present) as the air ingression is increased to 3.2kg/s ($\simeq$100mole/s), with $\sim$80% of the release in the lower plenum and $\sim$20% in the core. Note that this is the opposite of the pattern seen in the air-ingression calculations done for a midloop-operation low-power and shutdown accident sequence in Surry; those results (in Table 3.2) also showed enhanced ruthenium release with air ingression, with $\leq$79% of the ruthenium inventory released for $\simeq$100mole/s air flow, but with $\sim$80% of the release in the core and $\sim$20% in the lower plenum. With no air ingression, only trace amounts of ruthenium are released, $\leq 2.7\times10^{-6}$% ex-vessel in the cavity; as in the case with no air ingression, again only trace amounts of ruthenium ($\leq 3.6\times10^{-7}$%) are released ex-vessel in the cavity in the calculation with air ingression assumed.

Figure 4.17 demonstrates that there is a small effect on the material retention in-vessel *vs* ejection to cavity in these calculations. All three calculations show the same overall behavior, with a small fraction ($\sim$10-20%) of the core material ejected immediately upon vessel failure, the majority ($\sim$60-65%) of the core material lost to the cavity after some time delay, and another $\sim$20-25% of the core material, primarily structural steel in the lower plenum, remaining in-vessel. The delay in vessel failure time if surge line rupture occurs is clearly visible. The slightly higher late-time temperatures in the surge-line-break calculation with user-specified air ingression into the core, due to the higher energy of reaction for Zircaloy oxidation with air rather than with steam, causes the majority of the core material to melt, relocate and be lost to the cavity sooner than predicted in the calculation with a surge line break but with no user specified air ingression into the core.

However, while the overall core degradation and ejection are similar, there are differences in detailed response. Figures 4.18 through 4.21 present the total masses of some individual core materials (Zircaloy and ZrO_2, stainless steel and steel oxide) remaining in the vessel. (The individual masses of UO_2 fuel and control rod poison are not given, because they show little or no dependence on air ingression; instead, in all cases the predicted behavior of both the UO_2 and the control rod poison is very similar to the calculated overall mass response given in Figure 4.17, but with no residual retention in-vessel later in the transient.) There is an increase in ZrO_2 mass due to the air oxidation, shown in Figure 4.19, but there is an even greater increase in the steel oxide mass given in Figure 4.20 (even though MELCOR does not consider steel reacting with O_2, only with steam); this represents the increased availability of steam to oxidize the steel because

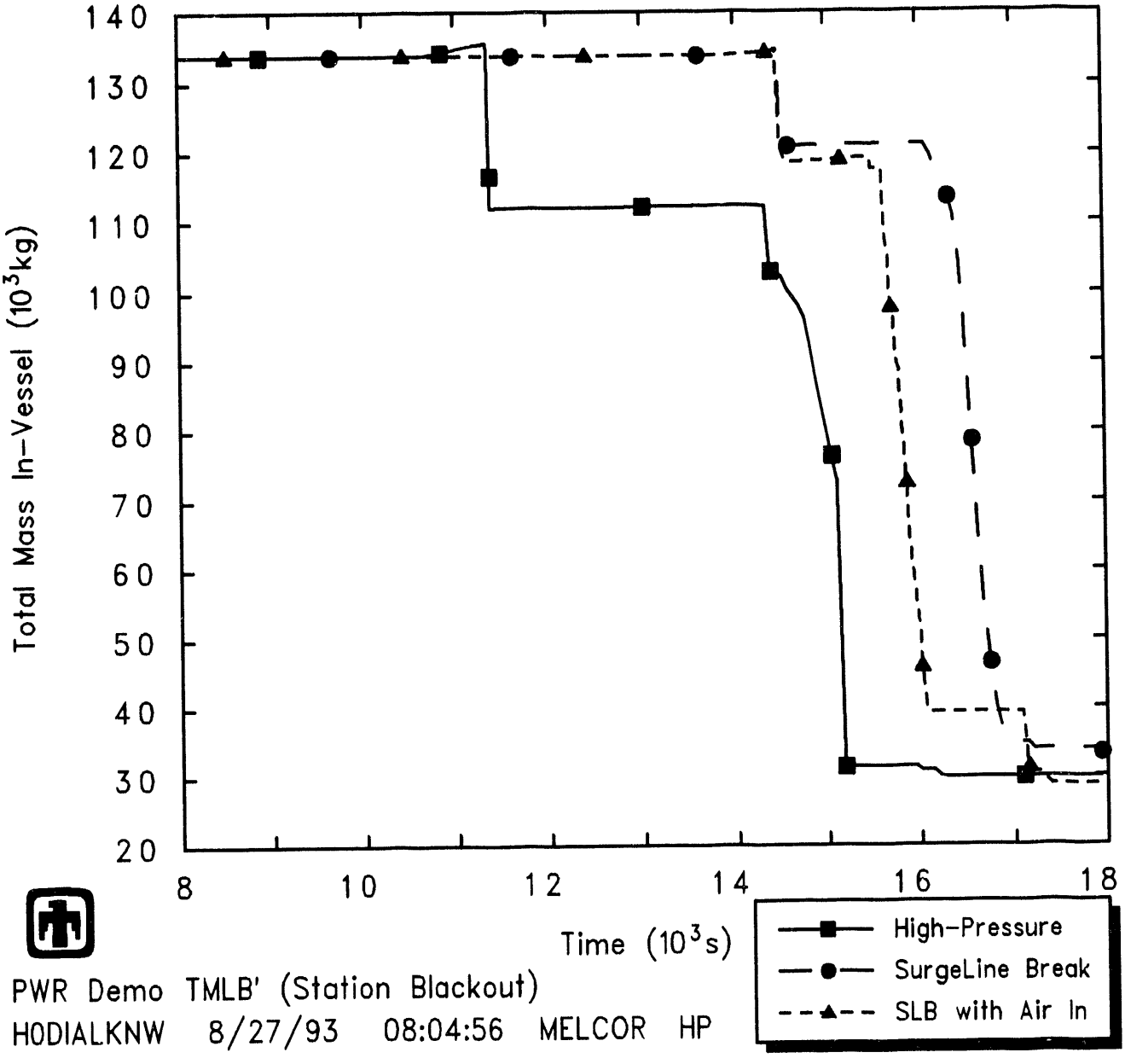

Figure 4.17. Total Core Masses in MELCOR Surry TMLB' Calculations with Surge Line Break and Air Ingression

the Zircaloy is being oxidized preferentially with the oxygen introduced. The increase in Zircaloy oxidation with air ingression into the core is not sustained or significant because of the more rapid loss of Zircaloy from the vessel to the cavity in the surge-line-break calculation with user-specified air ingression into the core, discussed above.

Table 4.3 presents the total amount of oxygen in the air ingression, the amounts of oxygen and steam consumed in-core by oxidation reactions, the amount of hydrogen produced in-vessel through metal reaction with steam, and the total oxidation energy. (Note that the amount of steam consumed in oxidation, the amount of hydrogen produced and the total oxidation energy include Zircaloy oxidation with steam prior to the specified air ingression, in addition to Zircaloy reaction with oxygen, as well as oxidation of core and lower plenum structural steel with steam throughout the transient period calculated; there is currently no provision in MELCOR to edit the Zircaloy and steel oxidation reactions separately.)

Overall, about 15% of the total oxygen sourced into the core as part of the air ingression between $\geq$14,500s and 30,000s is consumed in Zircaloy oxidation; however, since most of the in-vessel oxidation occurs over a much shorter time period ($\sim$14,000s-16,000s), the actual fraction of oxygen available during that period that was consumed in metal-oxidation reactions is much greater ($\geq$75%). As would be expected, the steam consumption and hydrogen production drop and the oxidation energy rises as more oxygen is consumed, because of the enhanced heat generation from the $Zr+O_2$ reaction *vs* reaction with steam.

The assumed air ingression has the greatest effect on the ruthenium release, but also a smaller effect on the release for other radionuclides. Table 4.4 gives the in-vessel releases as a percentage of initial inventory present, calculated for other radionuclide classes. Note that, with the CORSOR-M option used, there is no in-vessel release of Class 7 (the early transition elements, represented by Mo), Class 9 (the trivalents, represented by La) or Class 11 (the more volatile main group elements, represented by Cd). As the rate of air ingression assumed is increased, there is a small increase ($\sim$3%) in the release fractions of the volatiles (*i.e.*, the noble gases, the alkali metals represented by Cs and the halogens represented by I); there is also a similar small increase in the release fraction of the chalcogens, represented by Te, and apparently very little holdup in unoxidized Zircaloy clad in any case. These small increases in release probably reflect the enhanced clad/fuel heatup from the $Zr+O_2$ reaction. In contrast, small decreases in release fraction are seen for the alkaline earths, represented by Ba, and the less volatile main group elements, represented by Sn, both of which are intermediate in release ($\sim$1%) between the volatiles ($\leq$100% release) and the refractories ($\ll$1% release), as well as in the trace amounts of refractories released, for both the tetravalents represented by Ce and for uranium, in the calculations with air ingression assumed; this is probably due to the cooling effect of the air ingression on the core debris.

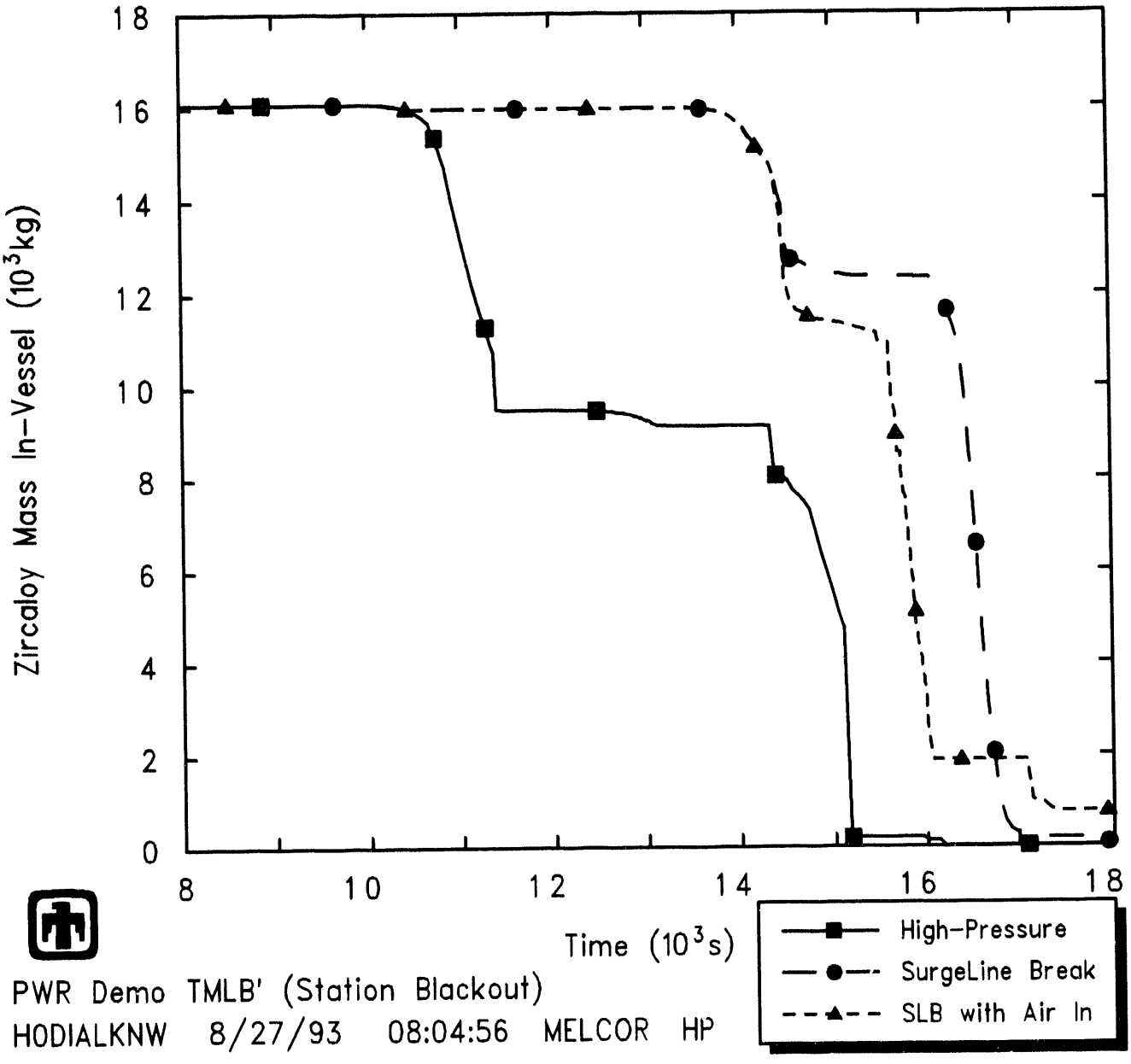

Figure 4.18. Core Zircaloy Masses in MELCOR Surry TMLB' Calculations with Surge Line Break and Air Ingression

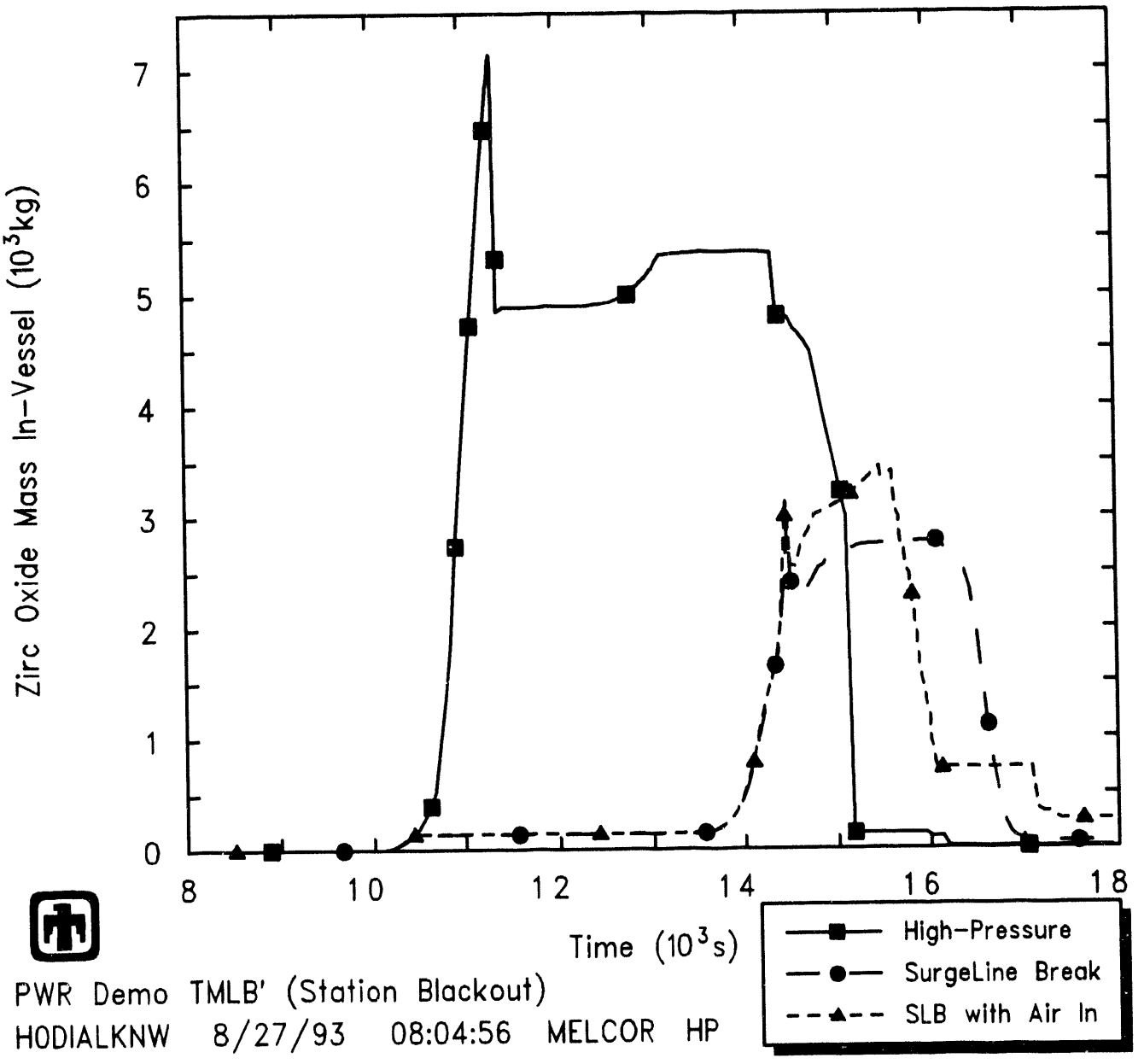

Figure 4.19. Core Zirconium Oxide Masses in MELCOR Surry TMLB' Calculations with Surge Line Break and Air Ingression

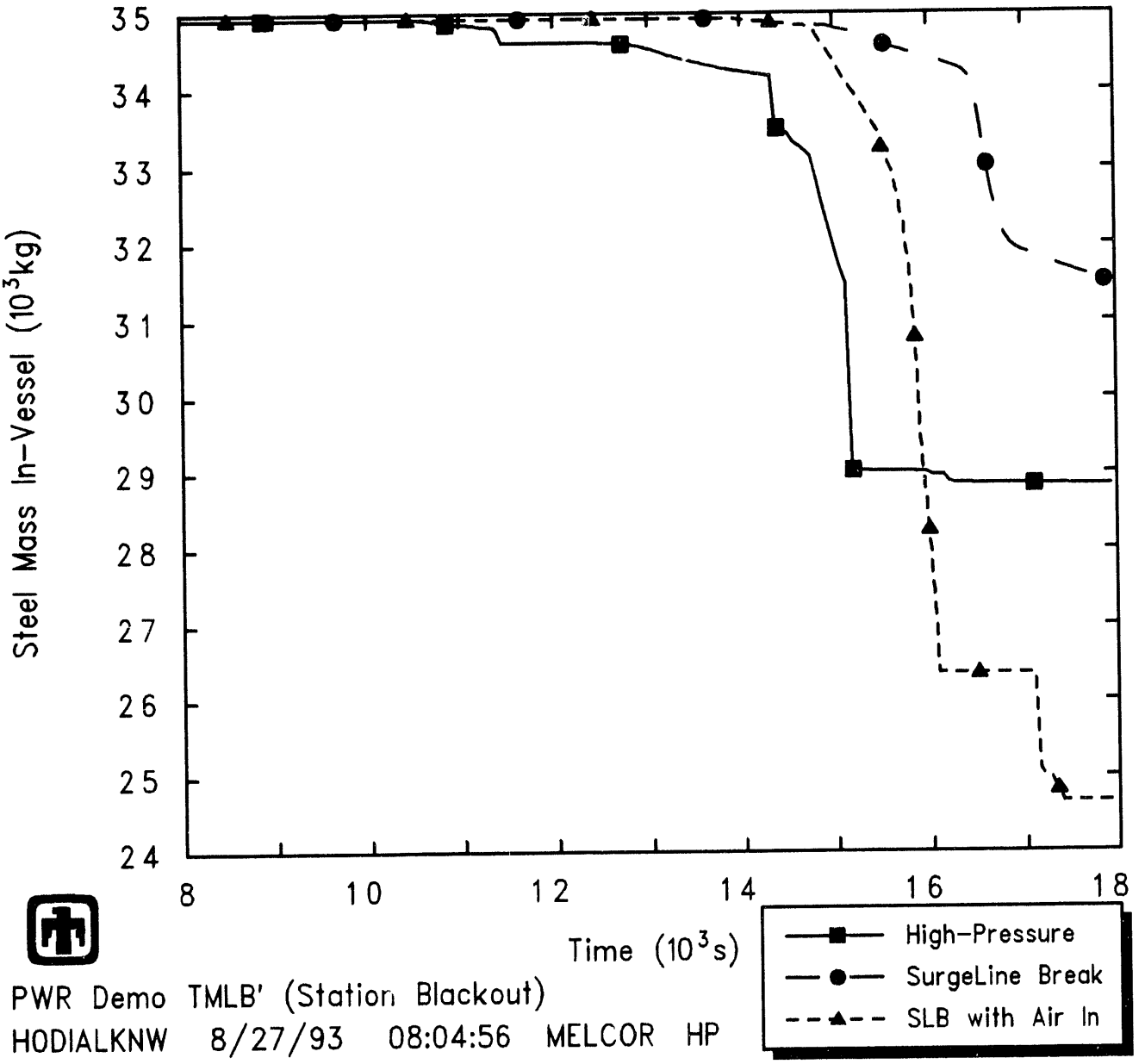

Figure 4.20. Core Steel Masses in MELCOR Surry TMLB' Calculations with Surge Line Break and Air Ingression

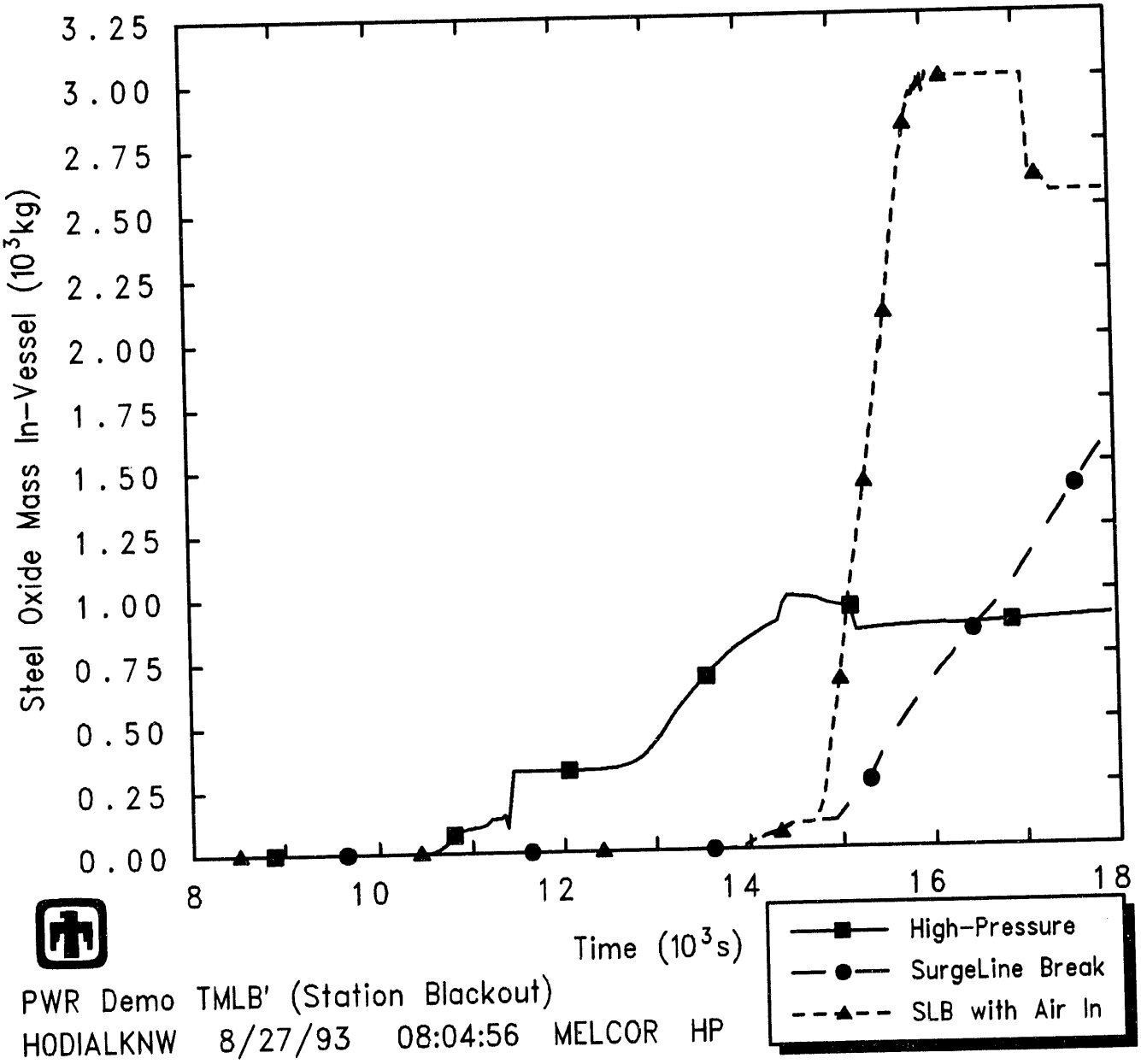

Figure 4.21. Core Steel Oxide Masses in MELCOR Surry TMLB' Calculations with Surge Line Break and Air Ingression

Table 4.2. In-Vessel Ruthenium Release in MELCOR Surry TMLB' Calculations with Surge Line Break and Air Ingression

Air Ingression Rate		In-Vessel Release (% Initial Inventory)		
(kg/s)	(mole/s)	Core	Lower Plenum	Total
0	0	0	0	0
3.2	≃100	9.8	40.1	49.9

Table 4.3. In-Vessel Oxidation in MELCOR Surry TMLB' Calculations with Surge Line Break and Air Ingression

Air Ingression		Consumed in Oxidation		Produced in Oxidation	
Flow Rate (mole/s)	Total O_2 (kg)	Oxygen (kg)	Steam (kg)	Hydrogen (kg)	Energy (MJ)
0	0	18.14	3085	345.2	24,132
≃100	5,833	813.1	2319	259.4	40,288

Table 4.4. In-Vessel Radionuclide Release in MELCOR Surry TMLB' Calculations with Surge Line Break and Air Ingression

Air Ingression (mole/s)	In-Vessel Release (% Initial Inventory)			
	Class 1 (Xe)	Class 2 (Cs)	Class 4 (I)	Class 5 (Te)
0	46.12	46.10	46.09	45.93
≃100	49.14	49.13	49.11	48.97
	Class 3 (Ba)	Class 8 (Ce)	Class 10 (U)	Class 12 (Sn)
0	0.6125	2.544×10^{-4}	2.568×10^{-2}	1.939
≃100	0.1488	1.817×10^{-5}	3.031×10^{-3}	0.848

5 MELCOR Grand Gulf Low-Power/Shutdown Calculations with Air Ingression

As part of a separate, ongoing program providing MELCOR support calculations for the Grand Gulf low-power/shutdown PRA [11], two calculations were done to address concerns about air oxidation and the associated enhanced release of ruthenium expected to occur when irradiated reactor fuel is heated in air. In both, the effect of oxidation with free oxygen in addition to the oxygen in steam was included in the code; in one calculation a constant release rate coefficient was used for Class 6 (Ru), greater than the default CORSOR-M value (Eq. 2.4 in Section 2), while the other calculation used a variable coefficient dependent on the partial pressure of oxygen in the core (Eq. 2.3 in Section 2).

(While these Grand Gulf MELCOR calculations were not done as part of the air ingression analysis effort reported on in this report, they investigated the same issues and evaluated the same accident consequences, and came to basically the same conclusions. Because those calculations will not be formally documented until the completion of that PRA program, the NRC contract monitor for that program has graciously agreed to allow us to include a brief summary of those calculations and results in this report.)

These Grand Gulf air-ingression calculations assume the plant to be in POS6, a condition occurring during the early portion of the refueling mode of operation. This state is the BWR analogue of the POS6 mid-loop operation modelled for the Surry low-power and shutdown air ingression accidents analyzed in Section 3. For a BWR, POS 6 begins when the vessel head is detached and ends when the upper reactor cavity has been filled with water. The earliest the plant enters this mode of operation is typically four days after shutdown. In this POS both the drywell head and the vessel head have been removed and the containment hatch and personnel locks are open; the drywell equipment hatch also is open. Thus, both the vessel and the drywell communicate directly with the containment (*i.e.*, the suppression pool is effectively bypassed) and the containment is open to the auxiliary building. During this POS the steam dryers are removed and the steam lines are plugged. The suppression pool can be either at its normal operating level, partially drained or completely empty. Furthermore, the suppression pool makeup system has been isolated; therefore the suppression pool cannot be used as a continuous supply of water for either core cooling or the containment sprays. [23, 24]

The Grand Gulf low-power/shutdown calculations done predict no oxygen to be drawn into the core until late in the transient, after the core material has fallen into the cavity. To investigate the impact of air oxidation and enhanced ruthenium release, we had to externally introduce oxygen directly into the core control volume. A total of 28,608kg of O_2 (the amount that would be required to oxidize all the clad in the core), was added into the core control volume starting when the core liquid level drops below the top of the active fuel until a lower head penetration first fails (*i.e.*, from 13.04hr to 18.76hr); the oxygen was added at a uniform rate of ~1.4kg/s which is ~44mole/s.

Table 5.1. Oxidation Masses for Grand Gulf Low-Power/Shutdown Calculations with Air Ingression

Material	Total Masses at End of Transient (kg)		
	No Air-Ox	Constant Coeff. (Eq. 2.4)	$P(O_2)$ Coeff. (Eq. 2.3)
In COR Package			
Zircaloy	12356	24551	6848
Zirc Oxide	7211	7890	8784
Stainless Steel	35299	35875	33650
Steel Oxide	1809	1688	3658
Steam Consumed	8750	3078	5738
Oxygen Consumed	–	4862	6291
In CAV Package			
Metal Layer	83959	7746	87965
(Light) Oxide Layer	591150	413250	618710
Hydrogen			
Produced in Vessel	1001	344	642
Produced in Cavity	1280	1019	1159
Total Produced	2281	1363	1801

There is no difference in timing on any events before the extra oxygen is first sourced in. The gap release and the failure of the lower head penetrations in the various rings are predicted to occur somewhat earlier, because of the slightly accelerated core heatup due to more clad oxidation. There are no major differences observable in primary and containment systems pressure histories, or core inventory boiloff. Clad temperature histories in the core level just below the active fuel midplane in one of the six core rings are presented in Figure 5.1, as representative of the overall core response. The two air-oxidation sensitivity study calculations both show more rapid clad heatup due to the increased degree of (exothermic) clad oxidation, resulting in earlier melt, relocation and lower head failure.

The masses of Zircaloy and ZrO_2, stainless steel and steel oxide, steam and oxygen consumed and hydrogen generated by the end of these transient calculations are presented for these air-oxidation sensitivity studies in Table 5.1. With the free oxygen source, 10-20% more Zircaloy and 100% more steel is oxidized in-vessel. Because 30-60% less steam

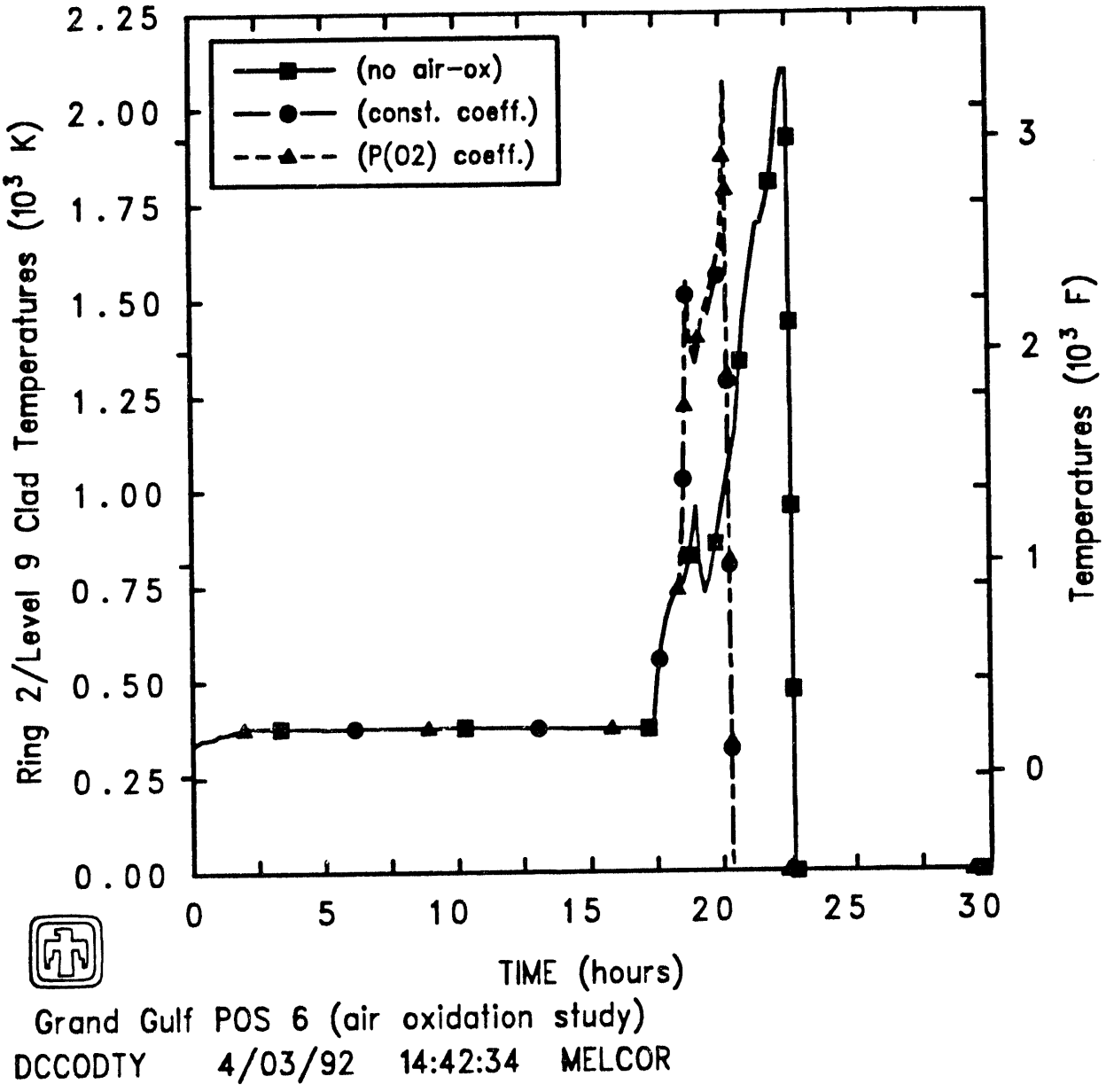

Figure 5.1. Level 9 Clad Temperatures for Grand Gulf Low-Power/Shutdown Calculations with Air Ingression

is consumed, 30-60% less hydrogen is generated in-vessel; with 10-20% less hydrogen generated in the cavity, the total amount of hydrogen generated is 20-40% less in the two air oxidation sensitivity studies. The lower amounts of hydrogen produced in the air oxidation sensitivity studies are primarily a result of sharp differences during the time period the free oxygen is being added, not gradual divergences throughout the remainder of the transient. (Most of the oxygen sourced into the core control volume therefore escapes out through the upper head and vessel breach, to the containment and then the environment, without being consumed in oxidation processes.)

Table 5.2 compares the masses of radionuclides released in this set of MELCOR calculations, when a lower head penetration first fails and at the end of the calculation (*i.e.*, when the cavity is predicted to rupture), normalized to the initial masses of each class. The primary difference is the (as expected) $\simeq$100% release of ruthenium in-vessel in the two air-oxidation sensitivity study analyses, both using a constant release rate coefficient and using a variable coefficient dependent on the partial pressure of oxygen in the core. But there are other differences. Greater amounts of the more refractory classes (Ba, Ce, U and Sn) are released prior to vessel breach in the two air-oxidation sensitivity study calculations; unexpectedly, while more of the more volatile classes (Xe, Cs, I and Te) are released using a constant Ru release rate coefficient, slightly less are released using a variable Ru release coefficient dependent on the partial pressure of oxygen in the core than predicted with no air oxidation at all.

The comparison of released radionuclides by the time of cavity rupture is more confused. The three classes with identically-zero in-vessel releases all show the greatest release fraction for the air-oxidation sensitivity study using a constant release coefficient for Class 6; the other more refractory classes (Ba, Ce, U and Sn) show higher release in the calculation with a variable Ru release coefficient dependent on the partial pressure of oxygen; the volatiles (Xe, Cs, I and Te) all show 90-100% releases with no clear pattern of variation.

The radioactive masses released from the fuel and debris for each class, and the amount released to the environment by the time of cavity rupture (given in terms of the initial inventory) also are summarized in Table 5.2. Most (>50%) of the $\sim$100% ruthenium released in the two air-oxidation sensitivity study analyses escapes to the environment (in the absence of any additional retention in the auxiliary building, not included in these calculations).

Table 5.2. Fission Product Release Masses for Grand Gulf Low-Power/Shutdown Calculations with Air Ingression

Class	Radionuclides Released (% of Initial Inventory)					
	Before Vessel Breach			Before Cavity Rupture		
	No Air	Const. Coeff. (Eq. 2.4)	$P(O_2)$ Coeff. (Eq. 2.3)	No Air	Const. Coeff. (Eq. 2.4)	$P(O_2)$ Coeff. (Eq. 2.3)
1 (Xe)	81.3	93.2	79.5	100.0	97.7	100.0
2 (Cs)	81.7	93.3	79.9	100.0	97.9	100.0
3 (Ba)	2.38	8.65	22.1	42.0	42.7	47.1
4 (I)	81.0	93.1	79.2	95.5	93.4	89.0
5 (Te)	72.5	92.6	76.3	95.2	95.8	92.8
6 (Ru)	0.00002	99.9	100.0	0.0070	100.0	100.0
7 (Mo)	0.0	0.0	0.0	1.61	3.23	1.405
8 (Ce)	0.000003	0.0074	0.1186	0.0037	0.0082	0.1276
9 (La)	0.0	0.0	0.0	0.2170	0.666	0.3588
10 (U)	0.00156	0.520	4.59	1.62	0.522	5.10
11 (Cd)	0.0	0.0	0.0	0.0385	0.0808	0.0763
12 (Sn)	2.866	19.3	28.0	22.5	20.7	34.8

Class	Released Before Cav-Rupture			Escaped to Environment		
	No Air	Const. Coeff. (Eq. 2.4)	$P(O_2)$ Coeff. (Eq. 2.3)	No Air	Const. Coeff. (Eq. 2.4)	$P(O_2)$ Coeff. (Eq. 2.3)
1 (Xe)	100.0	97.7	100.0	100.0	97.5	100.0
2 (Cs)	100.0	97.9	100.0	67.6	62.6	60.7
3 (Ba)	42.0	42.7	47.1	21.3	21.8	16.9
4 (I)	95.5	93.4	89.0	95.5	93.4	88.9
5 (Te)	95.2	95.8	92.8	62.3	60.6	47.0
6 (Ru)	0.0070	100.0	100.0	0.0045	62.2	54.6
7 (Mo)	1.61	3.23	1.405	0.642	1.26	0.487
8 (Ce)	0.0037	0.0082	0.1276	0.00215	0.00467	0.0259
9 (La)	0.2170	0.666	0.3588	0.1024	0.365	0.168
10 (U)	1.62	0.522	5.10	0.212	0.305	1.20
11 (Cd)	0.0385	0.0808	0.0763	0.0189	0.0388	0.040
12 (Sn)	22.5	20.7	34.8	15.5	12.5	14.3

6 Conclusions

Two sets of MELCOR calculations have been completed studying the effects of air ingression on the consequences of various severe accident scenarios. One set of calculations analyzed a station blackout with surge line failure prior to vessel breach, starting from nominal operating conditions; the other set of calculations analyzed a station blackout occurring during shutdown (refueling) conditions. Both sets of analyses were for the Surry plant, a three-loop Westinghouse PWR. For both accident scenarios, a basecase calculation was done, and then repeated with air ingression from containment into the core region following core degradation and vessel failure.

In addition to the two sets of analyses done for this program, a similar air-ingression sensitivity study was done as part of a low-power/shutdown PRA, with results summarized here; that PRA study also analyzed a station blackout occurring during shutdown (refueling) conditions, but for the Grand Gulf plant, a BWR/6 with Mark III containment.

All three studies lead to the same conclusions. For the two major phenomena dependent on air ingression:

1. There is a significant increase in ruthenium release in-vessel, to ~50-80% of initial inventory, assuming moderate air ingression rates of ~10-100mole/s; without any air ingression, only trace amounts of ruthenium are released.

2. There is some increase in clad oxidation degree and energy, but only ~10-20%; most of the oxygen sourced into the core region escapes before it is consumed.

The enhanced ruthenium release with air ingression was expected. The relatively small changes in core temperatures, hydrogen production and steam consumption, and oxidation energy were not expected. The greater oxidation energy due to reaction of Zircaloy with oxygen does cause core temperatures to rise more quickly than for oxidation only with steam, but those higher temperatures then cause the remainder of the core material to melt, relocate and be lost to the cavity sooner than predicted with no air ingression into the core. Oxidation of Zircaloy with air rather than with steam for the relatively short period of time that the clad remains in-vessel does not significantly affect the overall steam consumption and hydrogen production, and the total oxidation energy, because these are dominated by the long-term oxidation of structural stainless steel in the core and especially in the lower plenum.

The assumed air ingression does not significantly affect most of the accident scenario. There are some small effects on fission product releases in general:

1. There is very little change in the release of the volatile species, *i.e.*, noble gases, Cs, I and Te, which are released at lower temperatures ($T \leq 2000$K); most of their initial inventory has been released before vessel breach and air ingression.

2. In most cases, there is a small increase in the releases of those species, *i.e.*, Ba and Sn, requiring somewhat higher temperatures (2000K $\leq T \leq$ 2500K) for release, probably reflecting the increased oxidation energies and temperatures from Zircaloy reacting with air.

3. There is usually a decrease in the release of refractory species, *i.e.*, Ce and U, which are released only at very high temperatures ($T >$ 2500-3000K), possibly due to the cooling effect of sourcing relatively cool containment air into the core region.

These predicted changes in radionuclide release reflect only the effects of air ingression changing the calculated core temperatures and relocation history. There may be other, larger changes in fission product release with air ingression, if other species are also sensitive to the oxygen potential as is ruthenium; however, any such additional effects air could have on the release and transport characteristics of other radionuclides were not modelled for these initial calculations.

These studies help quantify the amount of air that would have to enter the core region to have a significant impact on the severe accident scenario. These calculations demonstrate the potential of air ingression to substantially enhance ruthenium release. These analyses indicate no substantive increases in maximum core temperatures, albeit with modest acceleration of the core degradation process, due to the increased heat of reaction of Zircaloy oxidized by air rather than by steam.

Bibliography

[1] M. Donahue, M. Hazzan, J. Metcalf, E. Warman, "Analysis of Retention/Revaporization in a Mark II Power Plant", Proceedings, International Symposium on Source Term Evaluation for Accident Conditions, Columbus, Ohio, October 28-November 1, 1985 (published by IAEA, Vienna, 1986), pp. 279-292.

[2] A. S. Benjamin, D. J. McCloskey, D. A. Powers, S. A. Dupree, "Spent Fuel Heatup Following Loss of Water During Storage", NUREG/CR-0649, SAND77-1371, Sandia National Laboratory, March 1979.

[3] F. C. Iglesias, C. E. L. Hunt, F. Garisto, D. S. Cox, "Measured Release Kinetics of Ruthenium from Uranium Oxides in Air", Proceedings, International Seminar on Fission Products Transport Processes During Reactor Accidents, Dubrovnik, Yugoslavia, May 1989.

[4] F. Garisto, F. C. Iglesias, C. E. L. Hunt, "A Thermodynamic/Mass-Transport Model for the Release of Ruthenium from Irradiated Fuel", Proceedings, International Seminar on Fission Products Transport Processes During Reactor Accidents, Dubrovnik, Yugoslavia, May 1989.

[5] R. Williamson, S. A. Beetham, "Fission Product Release During the Air Oxidation of Irradiated Uranium Dioxide", Proceedings, International Seminar on Fission Products Transport Processes During Reactor Accidents, Dubrovnik, Yugoslavia, May 1989.

[6] C. J. Shaffer, L. A. Miller, A. C. Payne, Jr., "Integrated Risk Assessment for the LaSalle Unit 2 Nuclear Power Plant: Phenomenology and Risk Uncertainty Evaluation Program (PRUEP); Volume 3: MELCOR Code Calculations", NUREG/CR-5305, SAND90-2765, Sandia National Laboratories, October 1992.

[7] L. N. Kmetyk, L. N. Smith, "Summary of MELCOR 1.8.2 Calculations for Three LOCA Sequences (AG, S2D, and S3D) at the Surry Plant", NUREG/CR-6107, SAND93-2042, Sandia National Laboratories, to be published.

[8] R. M. Summers *et al.*,"MELCOR 1.8.0: A Computer Code for Severe Nuclear Reactor Accident Source Term and Risk Assessment Analyses", NUREG/CR-5531, SAND90-0364, Sandia National Laboratories, January 1991.

[9] W. Krischer, M. C. Rubinstein, "The Phebus Fission Product Project", Elsevier Applied Science ISBN 1 85166 765 2 (1992).

[10] I. Shepherd, A. Jones, C. Gonnier, S. Gaillot, "Phebus-FP: Analysis Programme and Results of Thermalhydraulic Tests", Proceedings, 21st Water Reactor Safety Information Meeting, Bethesda MD, October 25-17, 1993 (to be published).

[11] "Summary Report of: Grand Gulf Low Power and Shutdown Abridged Risk Analysis; POS 6: Early Refueling", Final Letter Report from T. D. Brown, SNL, to C. P. Ryder, NRC, dated October 27, 1993.

[12] R. M. Summers, R. C. Smith, "MELCOR Core (COR) Package Reference Manual", Sandia National Laboratories, draft dated March 17, 1993.

[13] E. A. Boucheron, R. K. Cole, R. C. Smith, S. W. Webb, "Radionuclide (RN) Package Reference Manual", Sandia National Laboratories, draft dated February 25, 1993.

[14] M. R. Kuhlman, D. J. Lehmicke, R. O. Meyer, "CORSOR User's Manual", NUREG/CR-4173, BMI-2122, Battelle Memorial Institute, March 1985.

[15] M. Ramamurthi, M. R. Kuhlman, "Final Report on Refinement of CORSOR – An Empirical In-Vessel Fission Product Release Model", Battelle Memorial Institute, October 31,1990.

[16] "CORSOR Release Coefficients for Ruthenium in Air", Memo from D. A. Powers, SNL, to F. T. Harper, SNL, dated March 30, 1992.

[17] Private communication, B. Holmes, BNL, to L. N. Kmetyk, SNL, May 11, 1993.

[18] L. N. Kmetyk, "MELCOR 1.8.2 Assessment: Surry PWR TMLB' (with a DCH Study)", SAND93-1899, Sandia National Laboratories, to be published.

[19] T.-L. Chu *et al.*, "Status of the Pressurized Water Reactor Low Power and Shutdown Accident Frequencies Program", Proceedings, International Topical Meeting on Probabilistic Safety Assessment, PSA '93, Clearwater Beach, Florida, January 26-29, 1993.

[20] J. Jo *et al.*, "Risk Analyses of Releases from Accidents during Mid-Loop Operation at Surry", Proceedings, International Topical Meeting on Probabilistic Safety Assessment, PSA '93, Clearwater Beach, Florida, January 26-29, 1993.

[21] J. Jo *et al.*, "Analysis of Accidents during Mid-Loop Operating State at a PWR", NUREG/CP-0126, Proceedings, 20th Water Reactor Safety Information Meeting, Bethesda, Maryland, October 21-23, 1992 (published, March 1993)

[22] P. N. Smith, P. L. Mason, "AEA Assessment of MELCOR 1.8.1 Using Calculations for TMLB' Accident Sequences", AEA RS 5484, UK AEA Winfrith Technology Centre, March 1993.

[23] T. D. Brown, L. A. Miller, "Abridged Risk Analysis of a Selected Regime of Shutdown for the Grand Gulf Nuclear Power Plant", Proceedings, International Topical Meeting on Probabilistic Safety Assessment, PSA '93, Clearwater Beach, Florida, January 26-29, 1993.

[24] T. D. Brown, L. A. Miller, L. N. Kmetyk, "Summary of An Abridged Assessment of Shutdown Risk for a Mark III Boiling Water Reactor", NUREG/CP-0126, Proceedings, 20th Water Reactor Safety Information Meeting, Bethesda, Maryland, October 21-23, 1992 (published, March 1993)

External Distribution:

U. S. Nuclear Regulatory Commission (19)
Attn: S. Acharya, NLS-372
Y. S. Chen, NLN-344
M. A. Cunningham, NLS-372
F. Eltawila, NLN-344
R. B. Foulds, NLN-344
C. Gingrich, NLN-344
C. G. Tinkler, NLN-344
S. Basu, NLN-344
A. Behbahani, NLN-344
R. Y. Lee, NLN-344
L. E. Lancaster, NLS-372
R. O. Meyer, NLS-007
J. A. Mitchell, NLS-314
C. P. Ryder, NLS-372
L. Soffer, NLS-324
B. Sheron, NLS-007
J. A. Murphy, NLS-007
L. M. Shotkin, NLN-353
N. Lauben, NLN-353
R. Landry, NLN-344
Washington, DC 20555

U. S. Department of Energy
Attn: P. Worthington, EH-12
19901 Germantown Road
Germantown, MD 20585

S. Y. Chen
Argonne National Laboratory
9700 South Cass Avenue
Argonne, IL 60439

Battelle Columbus Laboratories (3)
Attn: P. Cybulskis
M. Carmel
R. S. Denning
505 King Avenue
Columbus, OH 43201

Battelle Memorial Institute
Attn: C. A. Alexander
505 King Avenue
Columbus, OH 43201

Brookhaven National Laboratory (2)
Attn: I. K. Madni
T. Pratt
Bldg. 130
32 Lewis
Upton, NY 11973

Idaho National Engineering Laboratory (7)
Attn: A. Brown
R. J. Dallman
D. W. Golden
S. E. Reed
G. W. Johnsen
D. Petti
D. Hobbins
EG&G Idaho
P. O. Box 1625
Idaho Falls, ID 83404

D. Jones
EI International
P. O. Box 50736
Idaho Falls, ID 83405

Electric Power Research Institute (3)
Attn: E. Fuller
R. N. Oehlberg
B. R. Sehgal
P. O. Box 10412
Palo Alto, CA 94303

Los Alamos National Laboratory (2)
Attn: B. E. Boyack, K-551
D. R. Liles, K-553
P. O. Box 1663
Los Alamos, NM 87545

Oak Ridge National Laboratory (13)
P. O. Box 2009
Oak Ridge, TN 37831-8057
Attn: S. R. Greene, MS-8057
R. H. Morris, MS-8057
S. E. Fisher, MS-8057
R. Sanders, MS-8057
T. L. Heatherly, MS-8057
S. A. Hodge, MS-8057
C. R. Hyman, MS-8057
B. W. Patton, MS-8057
D. B. Simpson, MS-8057
R. P. Taleyarkhan, MS-8057
M. L. Tobias, MS-8088
T. Kress
A. Wright
P. O. Box 2009
Oak Ridge, TN 37830

Andrzej Drozd
Nuclear Regulatory Commission
OWFN, MS 8E1
11555 Rockville Pike
Rockville, MD 20852

W. P. Barthold
Barthold & Associates
132 Seven Oaks Drive
Knoxville, TN 37922

K. C. Wagner
Science Applications Intl. Corp.
2109 Air Park Rd. SE
Albuquerque, NM 87106

Savannah River Laboratory (2)
Attn: B. DeWald
D. Allison
Westinghouse Savannah River Co.
Bldg. 773-41A
Aiken, SC 29808-0001

Westinghouse Hanford Co. (2)
Attn: D. Ogden
O. Wang
P. O. Box 1970
Richland, WA 99352

General Electric Company (3)
Knolls Atomic Pwer Laboratory
Attn: D. F. McMullan
G. H. Epstein
E. Mennard
Bldg. F3, Room 8
P. O. Box 1072
Schenectady, NY 12301-1072

Bettis Atomic Power Laboratory (3)
Attn: Mark Riley
Jow Semanchik
Vincent Baiamonte
P. O. Box 79
West Mifflin, PA 15122

Mohsen Khatib-Rahbar
Energy Research Inc.
P. O. Box 2034
Rockville, MD 20852

V. K. Dhir
2445 22nd Street
Santa Monica, CA 90403

R. Viskanta
Purdue University
Heat Transfer Laboratory
School of Mechanical Engineering
West Lafayette, IN 47907

Dr. Jim Gieseke
Battelle Memorial Institute
505 King Ave.
Columbus, Ohio 43201

M. A. Kenton
Gabor, Kenton & Associates
770 Pasquinelli Drive
Suite 426
Westmont, IL 60559

University of California (2)
Attn: W. H. Amarasooriya
T. Theofanous
ERC-CRSS
Santa Barbara, CA 93106

F. E. Haskin
University of New Mexico
Department of Chemical and Nuclear Engineering
Albuquerque, NM 87131

University of California, Los Angeles (4)
Nuclear Energy Laboratory
Attn: I. Catton
D. Okrent
W. Kastenberg
G. Apostolakis
405 Hilgaard Avenue
Los Angeles, CA 90024

J. C. Lee
University of Michigan
Dept. of Nuclear Engineering
Cooley Building, North Campus
College of Engineering
Ann Arbor, MI 48109-2104

University of Wisconsin (2)
Dept. of Nuclear Engineering
Attn: M. L. Corradini
G. A. Moses
Engineering Research Building
1500 Johnson Drive
Madison, WI 53706

Ramu K. Sundaram
Manager, LOCA Analysis Group
Nuclear Engineering
Yankee Atomic Electric Company
580 Main Street
Bolton, MA 01740

John Bolin
CEGA
P. O. Box 85608
San Diego, CA 92186-9784

M. Plys
Fauske & Associates
16W070 West 83rd Street
Burr Ridge, IL 60521

Nick Trikouros
GPU Nuclear Corporation
One Upper Pond Road
Parsippany, NJ 07054

B. Raychaudhuri
Nebraska Public Power District
PRA & Engineering Review Group
P. O. Box 499
Columbus, NE 68601

Frank Elia
Stone & Webster Engineering Corp.
245 Summer Street
Boston, MA 02210

Samir S. Girgis
Atomic Energy of Canada Limited
CANDU Operations
Sheridan Park Research Community
Mississagua, Ontario
CANADA L5K1B2

Paul J. Fehrenbach
Chalk River Nuclear Laboratories
Fuel Engineering Branch, RSR Division
Chalk River, Ontario
CANADA KOJ1J0

Dr. Bohumír Kujal
Department of Reactor Technology
Nuclear Research Institute Řež plc
250 68 Řež
CZECH REPUBLIC

Andrej Mitro
Institute of Radioecology and Applied Nuclear Techniques
Garbiarska 2
P. O. Box A-41
040 61 Košice
CHECHOSLOVAKIA

Shih-Kuei Cheng
Institute of Nuclear Energy Research
P. O. Box 3-3
Lung-Tan, Taiwan
REPUBLIC OF CHINA

Technical Research Centre of Finland (3)
Nuclear Engineering Laboratory
Attn: Lasse Mattila
Ilona Lindholm
Esko Pekkarinen
P. O. Box 208 (Tekniikantie 4)
SF-002151 Espoo
FINLAND

Jorma V. Sandberg
Finnish Center Radiation & Nucl. Safety,
Dept. of Nuclear Safety
P. O. Box 268
SF-00101 Helsinki
FINLAND

CEA/Cadarache/Semar (10)
Attn: M. Arnaud
M. Agroguer
M. Mailliat
M. Serre
M. Hidaka
M. Park
Mme. S. Dickinson
M. Dumaz
M. Hueber
M. Wadworth
13108 Saint-Paul-Lez-Durance
FRANCE

CEA/Cadarache/SEA (3)
Attn: M. Clement
M. Gronnier
Mme. Ktorza
13108 Saint-Paul-Lez-Durance
FRANCE

CEA/Cadarache/DRS (3)
Attn: M. R. Zeyen
M. A. Meyer-Heine
M. P. VonderHardt
13108 Saint-Paul-Lez-Durance
FRANCE

CEA/FAR
Attn: Mme. C. Lecomte
60-68 Av. du G. Leclerc - B. P. 6
92265 Fontenay aux Roses Cedex
FRANCE

Dr. Lothar Wolf
Battelle Institute EV
AM Romerhof 35
D-6000
Frankfurt/Main90
GERMANY

Gesellschaft fur Anlagen- und Reaktorsicherheit (3)
Attn: Ulrich Erven
Walter Erdmann
Manfred Firnhaber
Schwertnergasse 1
D-5000 Koln 1
GERMANY

Kernforschungzentrum, Karlsruhe (4)
Attn: P. Hofmann
Werner Scholtyssek
Philipp Schmuck
Dr. Sigfried Hagen
P. O. Box 3640
D-7500 Karlsruhe 1
GERMANY

Udo Brockmeier
University of Bochum
Energietechnik
IB-4-128
D-4630 Bochum
GERMANY

K. D. Hocke
Universtitat Stuttgart IKE
Postfach 180 11 40
D-7000 Stuttgart 80
GERMANY

K. Trambauer
Gesellschaft fur Reaktorsicherheit (GRS) mbH
Forschungsgelande
D-8046 Garching
GERMANY

György Gyenes
Central Research Institute for Physics
Institute for Atomic Energy Research
H-1525 Budapest, P. O. Box 49
HUNGARY

CEC Joint Research Center (4)
Commission of the European Communities
Attn: Alan Jones
Iain Shepherd
Y. Drossinos
J. Capitao
Safety Technology Institute
21020 Ispra (Varese)
ITALY

Giovanni Saponaro
ENEA
Natl. Comm. for R&D of Nuclear Energy
Via Vitaliano Brancati, 48
00144 Rome
ITALY

Japan Atomic Energy Research Institute (4)
Attn: Kunihisa Soda
Jun Sugimoto
Norihiro Yamano
Y. Maruyama
Tokai-mura, Naka-gun, Ibaraki-ken
319-11
JAPAN

Dr. Masayoshi Shiba, Director General
Institute of Nuclear Safety
Nuclear Power Engineering Corporation
Fujita Kankou Toranoman Bldg. 7F
3-17-1, Toranoman
Minato-Ku, Tokyo, 105
JAPAN

Akira Nonaka, Manager
Equipment and Components Department
NUPEC
Nuclear Power Engineering Center
Shuwa-kamigacho Bldg.
3-13, 4-Chome, Toranomon Minato-ku
Tokyo 105
JAPAN

Kenji Takumi
Director and General Manager
Equipment and Components Department
Nuclear Power Engineering Center
Shuwa-kamigacho Bldg.
3-13, 4-Chome, Toranomon Minato-ku
Tokyo 105
JAPAN

Masao Ogino
Mitsubishi Atomic Power Industries
4-1 Shibakoen 2-Chome
Minatoku Tokyo
JAPAN

Hidetoshi Okada
Nuclear Power Engineering Corporation
3-17-1, Toranomon Bldg. 5F
Minato-ku, Tokyo 105
JAPAN

Hirohide Oikawa
Toshiba Corporation
8, Shin-Sugita, Isogo-ku
Yokohama
JAPAN

Korea Atomic Energy Research Inst. (3)
Attn: Kun-Joong Yoo
Song-Won Cho
Dong-Ha Kim
P. O. Box 7, Daeduk Danji
Taejon
SOUTH KOREA 305-353

Jae Hong Park
Safety Assessment Department
Korea Atomic Energy Research Institute
P. O. Box 16, Daeduk-Danji
Taejon
SOUTH KOREA 305-353

Kim, Han Chul, Senior Researcher
Severe Accident Assessment Department
Korea Atomic Energy Research Institute
P. O. Box 16
Kaeduk-Danji
Taejon
SOUTH KOREA 305-606

Netherlands Energy Research Foundation (2)
Attn: Karel J. Brinkmann
E. J. Velema
P. O. Box 1
1755 ZG Petten
THE NETHERLANDS

Dr. Valery F. Strizhov
Russian Academy of Science
Institute of Nuclear Safety
Moscow, G. Tulsky, 52
113191, RUSSIA

Universidad Politecnica de Madrid (2)
Attn: Augustin Alonzo Santos
Francisco Martin
E.T.S. Ingenieros Industriales
Jose Gutierrez Abascal, 2
28006 Madrid
SPAIN

Juan Bagues
Consejo de Seguridad Nuclear
Justo Dorado, 11
28040, Madrid
SPAIN

Oddbjörn Sandervåg
Statens Kärnkraftinspektion
Swedish Nuclear Power Inspectorate
Box 27106 102 52 Stockholm
SWEDEN

L. Hammar, Director
Division of Research
Swedish Nuclear Power Inspectorate
Statens Karnkraftinspektion
Sehlstedtsgatan 11
Box 27106
S-102-50 Stockholm
SWEDEN

Swiss Federal Nuclear Safety Inspectorate (4)
Attn: S. Chakraborty
Sang Lung Chan
U. Schmocker
H. P. Isaak
CH-5232 Villigen-HSK
SWITZERLAND

United Kingdom Atomic Energy Agency (7)
Winfrith Technology Center
Attn: T. Haste
S. R. Kinnersley
D. W. Sweet
A. Nichols, 102/A50
B. Bowsher, 105A/A50
D. Williams, 01/A50
J. Mitchell, 210/A32
Winfrith, Dorchester
Dorset, DT2 8DH, England
UNITED KINGDOM

United Kingdom Atomic Energy Authority (2)
Safety & Reliability Directorate
Attn: M. I. Robertson
C. Wheatley
Wigshaw Lane, Culcheth, Warrington
Cheshire, WA3 4NE
UNITED KINGDOM

Internal Distribution:

MS1328 R. S. Longenbaugh, 6342
MS0736 N. R. Ortiz, 6400
MS0744 W. A. von Riesemann, 6403
MS0744 D. A. Powers, 6404
MS0747 A. L. Camp, 6412
MS0747 S. E. Dingman, 6412
MS0748 F. T. Harper, 6413
MS0742 J. E. Kelly, 6414
MS0745 S. L. Thompson, 6418 (5 copies)
MS0745 R. K. Cole, 6418
MS0745 A. A. Elsbernd, 6418
MS0745 L. N. Kmetyk, 6418 (5 copies)
MS0745 R. C. Smith, 6418
MS0745 D. S. Stuart, 6418
MS0745 R. M. Summers, 6418
MS0745 T. J. Tautges, 6418
MS1137 N. Bixler, 6422
MS1137 T. J. Heames, 6422
MS1139 R. C. Schmidt, 6423
MS0739 K. E. Washington, 6429
MS0899 Technical Library, 7141 (5 copies)
MS0619 Technical Publications, 7151
MS0100 Document Processing for DOE/OSTI, 7613-2 (10 copies)
MS9018 Central Technical Files, 8523-2

*U.S. GOVERNMENT PRINTING OFFICE 1994-0-774-275/80017

DATE FILMED

4 / 14 / 94

END